ELSEVIER

Coordination Chemistry Reviews
77 (1998) 347–414

COORDINATION CHEMISTRY REVIEWS

Applications of functionalized transition metal complexes in photonic and optoelectronic devices

K. Kalyanasundaram *, M. Grätzel

Laboratory for Photonics and Interfaces, Institute of Physical Chemistry, Swiss Federal Institute of Technology, EPFL-Ecublens, CH-1015 Lausanne, Switzerland

Received 16 March 1998; received in revised form 30 June 1998; accepted 16 July 1998

Contents

* Corresponding author. Tel.: +41-21-6933622; Fax: +41-21-6934111; e-mail: kalyan@dcsun1.epfl.ch.

PII: S0010-8545(98)00189-1

Abstract

Transition metal complexes with low lying excited states are finding increasing use as photosensitizers. Major work horses are those derived from polypyridine complexes and metalloporphyrins. The low-lying metal-to-ligand charge transfer (MLCT) and ligand-centered (π–π^*) excited states of these complexes are fairly long-lived to participate in electron transfer processes. The emissive nature and high quantum yields allow development of applications. In this paper we review some of the recent applications of these coordination complexes in photochemical systems for the direct conversion and storage of solar energy. Mesoporous membrane type films with large surface area can be prepared from nanosized colloidal semiconductor dispersions. By suitable molecular engineering, the metal complexes can be readily attached to the surface. These films with anchored complexes are finding increasing use in energy conversion devices such as dye-sensitized photoelectrochemical solar cells, intercalation batteries, optical display and optical sensors. Principles of operation of these optoelectronic devices are reviewed here. Various approaches to anchoring molecules on surfaces are first reviewed followed by an overview of the methods of preparation of mesoporous films. This is followed by a comprehensive discussion of the design details of the

dye-sensitized solar cells and associated mechanistic studies. Principles of operation of electrochromic and photoelectroluminescent devices based on anchored polypyridine complexes of Ru are also indicated.

Keywords: Ruthenium; Nanocrystalline oxides; Photonic; Optoelectronic; Mesoporous films; Solar cells; Polypyridine complexes

1. Introduction

Along with the pursuit for fundamental aspects, scientists have always been interested in designing practical applications of scientific advances in the form of devices. Barring accidental discoveries, progress generally comes about as a result of fruitful interplay of advances in several (sub)disciplines. The focus of this review paper is on photonic and optoelectronic systems where optical excitation of a device leads to useful processes such as light-energy conversion in the form of electricity in solar cells, photochromic and photoelectrochromic systems for digital display, optical sensors for detection of trace quantities of chemicals, smart windows that on one hand can control the amount of light passing through and also assist indirectly in cost-saving measures to mention a few.

Design of these devices requires ability to organize molecules on a nanometric scale, with fine control on their arrangement/distribution, mobility, spectral and redox properties. Several types of heterogeneous/multiphase systems have been proposed and tested [1–7]. Structural organization of these components by controlled molecular engineering allowing synergistic effects is a major feature of these systems. Bard has given the elegant name *integrated chemical systems* (ICS) [8] to such organized structures for efficient execution of specific tasks. Listed below are some examples where different components have been put together in a controlled manner to achieve specific tasks:

1. a heterogeneous catalyst comprising viologen polymerized on silica support and carrying Pt metal particles in the film to mediate H_2 evolution;
2. a photoelectrochemical system for H_2 evolution consisting of either p-GaAs and Pt or particles of CdS and Pt contained in a Nafion matrix and
3. the composite consisting of metallized dye structures used for instant photography.

The idea of using organized molecular structures to achieve special tasks is nothing new. Green plant photosynthesis is a good example of a device for light energy conversion that has evolved over many generations. Progress in the design of efficient systems modeled on this nature-evolved device has been slow due to the lack of knowledge on how to organize molecules on a nanometric scale and to control their reaction efficiencies or directionality. In the last two decades there have been intense efforts in understanding the organization principles of the key apparatus involved, viz. the chloroplast and to mimic in the best possible way the primary reactions of photosynthesis. Isolation, establishment of crystal structure of

reaction centers [9], time-resolved pulsed laser photolysis studies of primary reactions in these and model systems [10,11] and fundamental studies of photo-induced electron transfer [12–18] have aided considerably in establishing a quantitative picture. In artificial systems, the efficiency of light energy conversion in the form of chemical energy stored in charge separated redox products is severely limited by thermodynamically favorable back reaction between the photo-products. Nature achieves this goal Using a highly organized assembly of a chromophore, electron donor and electron acceptor, nature is able to separate photo-produced redox equivalents spatially and to shuttle them further apart through a cascade of energetically downhill electron transfer reactions.

All of the photonic or optoelectronic devices that we will consider involve a photosensitizer (S) that absorbs the light and engages in electron-transfer reaction with suitable electron donors (D) or acceptors (A). Random distribution of these components S, D and A as in a homogeneous solvent clearly is not the way to go. In a first approach the key components can be directly linked with or without spacer units. There have been several studies of linked systems such as porphyrin-quinones, porphyrin-viologens, carotenoid-porphyrin-quinones, Ru-polypyridyl complexes carrying acceptors such as viologens and donors such as phenothiazine) and the resulting molecular dyads or triads examined in solution [19–22]. The term *supramolecular* is often used to represent such an assembly of several molecules and molecular units [23–26]. When the components are dispersed in a homogeneous solution, there is no control over the way the components distribute themselves and diffuse towards one another. To achieve controlled spatial distribution, orientation and mutual diffusion, these key components have to be confined in some host supports or matrices. Spatial confinement of the components in some way (caging in large hosts, anchoring them to surfaces,...) leads to a reduction in the dimensionality. We shall review a possible choice of components, anchoring groups and supports.

In this review paper we will restrict ourselves to semiconductor surfaces as the host matrix/support. Semiconductor host can be present in several forms: as single crystals with well-defined crystallographic faces and dimensions, μm-size particulates, nm-sized colloids or mesoporous films derived from nano-sized colloids. Each of these form has its own advantages and disadvantages. The term *hetero-supramolecular chemistry* [27] is being used to describe such heterogeneous assemblies having anchored redox-active molecules on semiconductor surfaces. For dye-sensitization studies, it is appropriate to use wide-bandgap semiconductors. Those with bandgap energy ≥ 3.0 eV are nearly transparent to major part of the solar spectrum. Bandgap excitation leads to generation of holes in the valence band along with the electrons in the conduction band. The holes being strong oxidants can readily destroy the chemical integrity of the chromophores and redox mediators that are in the immediate vicinity. Redox reactions of the hole with the semiconductor constituents can also lead to loss of integrity of the semiconductor itself, as is the case with most non-oxide semiconductors. Oxides have been widely used for their exceptional stability against photo-corrosion on optical excitation in the bandgap. Table 1 lists some of the commonly used n-type semiconductors along

with indications on the location of flat-band edges (i.e. level of the conduction band in the absence of any band-bending). In chemical terms, the flat/band potentials correspond to chemical potential of the conduction band to serve as an electron acceptor. Table 1 also includes some key references [28–42] related to preparation of nanocrystalline films of these semiconductors.

Major advances in the fields of Colloid and Sol–Gel chemistry in the last two decades [43–49] now allow controlled fabrication of micro- and nano-sized structures using finely divided monodispersed colloidal particles. Monodispersed nm-sized colloids are being used to prepare multilayers with quasi 2-D structures and quasi 1-D structures such as nanowires or clusters in an insulating matrix and to high surface area, porous films. Descriptive procedures are now available for the preparation of nanocrystalline semiconductor films of oxide or chalcogenide particles such as TiO_2, ZnO, Nb_2O_5, WO_3, Ta_2O_5, CdS or CdSe. Nanostructured materials offer many new opportunities to study fundamental processes in a controlled manner and this in turn lead to fabrication of several photonic and optoelectronic devices. The pores of these meso structures can be filled with a semiconducting or a conducting medium, such as a p-type semiconductor, a hole transmitter or an electrolyte, forming a junction of extremely large contact area. In this fashion, the negatively and positively charged contact of the electric cell become inter-digitated of a few nanometers. Dye-sensitized solar cells based on this type of nanocrystalline films have been the subject of several reviews recently [17,50–53].

2. Components for photonic and optoelectronic devices

2.1. Photosensitizers

For applications in photonic and optoelectronic devices, the photoactive component has to meet several stringent requirements. First is the intensity and spectral

Table 1
Bandgap energies and flat-band potentials (conduction band positions) of n-type semiconductors commonly used in dye sensitization studies

Semiconductor (n)	E_{bg} (eV)	E_{fb}/E_{cb} (V) (vs. NHE)	References for the preparation of nanocrystalline films
ZrO_2	5.0	−1.78 V (pH 13)	[28–30]
SnO_2	3.5–3.8	+0.5 (pH 1) −0.1 V (pH 7)	[31–34]
Nb_2O_5	3.4	−0.6 V (pH 7)	[35]
TiO_2 rutile	3.0	−0.05 (pH 2) −0.6 V (pH 12)	[36]
TiO_2 anatase	3.2	−0.28 (pH 2)	[37]
ZnO	3.0–3.2	−0.2 (pH 1) −0.4 (pH 4.8)	[38–40]
WO_3	2.4–2.8	+0.3 (pH 1) −0.15 to +0.05 (pH 9)	[41]
α-Fe_2O_3	2.0–2.2	−0.1 V (pH 13.6) +0.15 (pH 9)	[42]

range of coverage of light absorption in the visible, near-IR and IR regions. Second is the tunability of the absorption band(s). Third is the photophysical properties—types and number of excited states possible, their lifetimes and quantum yields for radiative and non-radiative processes. Fourth is redox properties in the ground and excited states. For redox-sensitizers or redox-mediators, there are further requirements of reversibility and stability of the oxidized or reduced forms. In all of these cases, transition metal complexes derived from polypyridines, porphine or phthalocyanine as ligands come out clearly as the sensitizers of preferred choice [54–60].

These ligands, all nitrogen heterocyclics with a delocalized π or aromatic ring system are capable of complexing with a whole variety of metal ions. The metal complexes have reasonably good solubility in many solvents. The complexes exhibit a variety of low-lying electronically excited states (π–π^*, d–d* and d–π^*/CT). Extensive photophysical studies in the last two decades [61–68] enable comprehensive understanding of the factors that determine the key photophysical parameters. Long-lived luminescent excited states of these sensitizers readily undergo electron-transfer reactions. This in turn has allowed tuning of the redox and photophysical properties required for applications of the type mentioned earlier. The bench-mark systems for polypyridines are mono- and polynuclear complexes based on Ru(II). For metalloporphyrins and metallophthalocyanines the preferred metal ions are those with full or half-filled d-shells such as Zn(II), Mg(II) or Al(III).

2.2. Anchoring groups

Fig. 1 illustrates various ways in which molecular organization can take place on host surfaces: (a) covalent attachment brought about by directly linking groups of interest or via linking agents, (b) electrostatic interactions, brought about via ion exchange, ion-pairing or donor-acceptor interactions, (c) hydrogen bonding, especially important in biological systems, (d) hydrophobic interactions leading to self-assembly of long chain fatty acid derivatives, (e) van der Waals forces involved in physisorption of molecules on solid surfaces, and (f) physical entrapment inside the pores or cavities of hosts such as cyclodextrins, micelles, etc. Most of the functionalized molecules that we consider in this review are of the first kind. Langmuir–Blodgett technique developed largely in the laboratory of Kuhn [69–71] is a powerful method for molecular organization that is based on self-assembly of monolayers of hydrophobic long chain derivatives. When molecules are chemically derivatized onto surfaces, their translational mobility is considerably reduced. This reduction in dimentionality has important consequences in reaction kinetics.

The molecular components have to be structurally modified for attachment to the host matrix. Fig. 2 shows some of the commonly used modes of attaching molecules on oxide and non oxide surfaces. Groups such as silanyl, (–O–Si–), amide (–NH–(C=O)–), carboxyl (–O–(C=O)–), phosphonato (–O–(HPO_2)–) have been shown to form stable linkages. In most of these cases, reactive elements (silanyl,

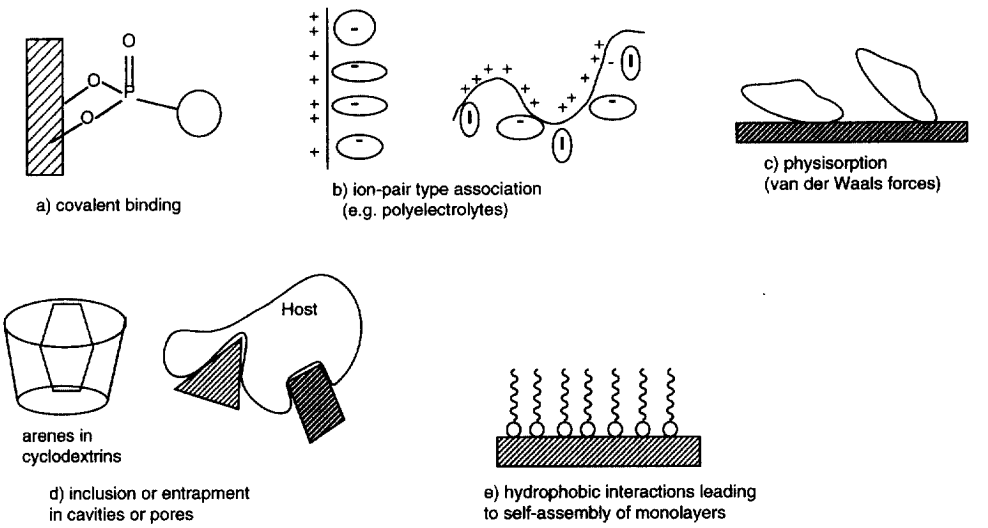

Fig. 1. Schematic presentation of various ways in which molecular organization can take place on host surfaces.

carboxylic acid or phosphonic acid) react spontaneously with surface hydroxyl groups of oxide surfaces to form linkages that exhibit good stability. Trichloro or trialkoxysilanes of various types have been used. Shown below are structures of some of the polypyridine ligands with reactive silanyl units for anchoring to oxide surfaces:

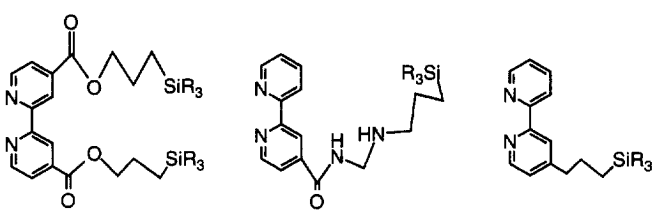

The general procedure is to prepare the activated ligand with the anchor group and the corresponding metal complex attached to the surface of interest. Mallouk et al. [72] have used a cationic silane to modify SnO_2 electrodes in the presence of zeolites and used this functionalized electrode to have selective ion-binding sites for ions such as $Fe(CN)_6^{4-}$, $Os(bpy)_3^{2+}$ and $Fe(phen)_3^{2+}$. Wrighton et al. [73] have made silanyl derivative of the 4,4′-carboxybipyridine (LL–X) and have used to prepare polypyridine carbonyl complexes of Re(I): $[Re(CO)_3(LL–X)(py\text{-}PTH)]^+$, $[Re(CO)_3(LL–X)(py)]^+$ (PTH, phenothiazine—a donor ligand). The Re complexes have been found to attach to high surface area silica gel, glass, indium–tin oxide

(ITO) and Pt electrodes. Spiro, Murray and coworkers [74,75] have elaborated the synthetic details for preparation of the trisilylethyl derivative of 2,2′-bpy and the derivatization of the corresponding Ru complex on electrodes.

Polymerization of polypyridine ligands carrying polymerizable units (e.g. vinyl-bipyridine, vinyl-phenanthroline, pyrrole-bipyridine) on electrode surfaces is another elegant method of anchoring redox components. This method has been exploited by Meyer [76], Spiro [77], Deronzier [78] and others to prepare electrode-confined transition metal polypyridine complexes of various kind. Thiol derivatives (RSH) have been used to anchor molecules on metal electrodes (Au, Ag) and chalcogenide semiconductors such as CdS [79]. Mention can also be made on the efforts of Meyer et al. in the preparation of amino acid-bound redox-active units for anchoring onto the backbone of polypeptides [80]. Lysine-linked sensitizers (Ru, Os-bipyridines), electron donors (phenothiazine) and acceptors (anthracene, viologens) have been prepared and fully characterized. Fox et al. [81] have used cyanuric chloride as organic coupling agent for oxide surfaces. Zirconyl chloride, hydroxy-aluminium ions and acetatohydroxyiron(III) complexes have also been used as inorganic coupling agents.

Carboxylic and phosphonic acid derivatives of photo- and redox-active molecules readily react with oxide surfaces to form the corresponding esters. Table 2 lists some of the polypyridine ligands with different anchoring groups specially prepared for linking onto oxide surfaces ([82–108]a). Amide linkages are obtained via the

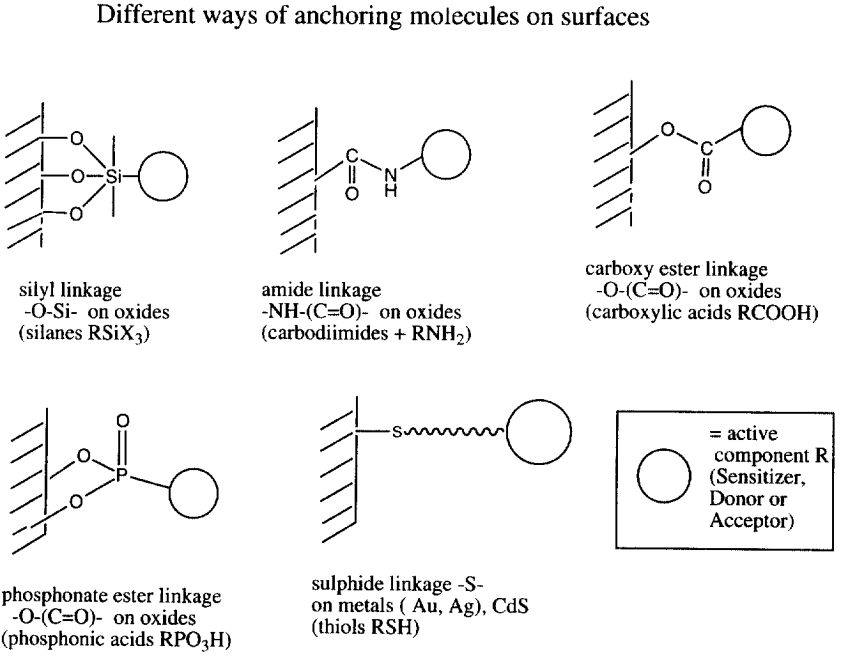

Fig. 2. Some of the commonly used modes of attaching molecules on oxide and non-oxide surfaces.

Table 2
Examples of ligands (bipyridine, terpyridine) derivatives with various anchoring groups (that are being used to prepare sensitizers for use in solar cell studies) and molecular redox-active speices with references to key publications that report synthesis of these ligands

Ligand	Semiconductor	References for synthesis
Carboxylic acid derivatives of polypyridines		
4,4′-Dicarboxy-2,2′-bipyridine	TiO_2	[82–85]
4,4′-(*p*-Dicarboxyphenyl)-2,2′-bpy	TiO_2	[86]
4,4′-Bis(*n*-alkylcarboxy)-2,2′-bpy	SnO_2	[87,88]
4-(Me)-4′-Carboxy)-2,2′-bipyridine	TiO_2	[89]
3-Carboxypropyl-4′-(Me)-2,2′-bpy	TiO_2	[90]
5,5′-Dicarboxy-2,2′-bipyridine	TiO_2	[88]
4,4′,4″-Tricarboxy-2,2′:6′,2″-terpyridine	TiO_2	[91]
4,4′-Dicarboxy-2,2′-biquinoline	TiO_2	[92]
Phosphonic acid derivatives of polypyridines		
4,4′-Bis($CH_2PO(OCH_2CH_3)_2$-2,2′-bpy	TiO_2	[93]
4,4′-Bis(methylphosphonic acid)-2,2′-bpy	TiO_2	[94]
4-(2,2′-Bpy)-phenylphosphonic acid	TiO_2	[95]
2,2′-Bipyridine-4-phosphonic acid	TiO_2	[96,97]
4,4′-Bis(phosphonic acid)-2,2′-bpy	TiO_2	[98]
2,2′:6′,2″-Terpyridine-4-phosphonic acid	TiO_2	[94,99,100]
Silyl derivatives of polypyridines		
4-(Trichlorosilylethyl)-4-Me-2,2′-bpy	TiO_2	[74]
Cyanuric chloride silyl derivative of phen	SnO_2	[101]
4,4′-Di(carboxy-$(CH_2)_2$–SiR_3)-2,2′-bpy	SiO_2, ITO	[73]
Carboxy-derivatives of 4,4′-disubstituted viologens (R_1, R_2-V^{2+})		
(4-Me-4′-Propylcarboxy)-viologen	SnO_2, ...	[102]
4,4′-Di(benzoyl)-viologen	TiO_2	[103]
4,4′-Di(salicylil)-viologen	TiO_2	[103]
(4-Me-4′-Propylphosphonic acid)-viologen	TiO_2	[103]
(4,4′-Di(propylphosphonic acid)-viologen	TiO_2	[103]
Carboxy derivatives of other redox mediators, sensitizers		
10-Phenothiazine-propionic acid	SnO_2	[102]
Perylene tetracarboxylic acid	TiO_2	[104]
Perylene dicarboxylic acid carboximide	TiO_2	[104]
Perylene phosphonate	TiO_2	[105]
Anthracene carboxylic acid	TiO_2	[106,107]
Aryl carboxylic acids	TiO_2	[108]

reaction of amine derivatives (RNH_2) and dicyclohexyl carbodiimide (R–N=C=N–R) on oxides. In aqueous medium the stability of some of linkages can be limited to a certain pH range due to associated protolytic equilibria e.g. carboxy-esters to $pH \leq 4.5$ and phosphonato-esters to $pH \leq 8.5$. In aqueous solutions of higher pH values, hydrolysis and de-chelation of the anchoring group from the surface can occur. Most often equilibration of the surface hydroxyl place takes place rather slow (even hours) that de-chelation shows in limited long-term stability tests. The

pH range where the devices can be used in aqueous media is rather limited for this reason. The known affinity of Au, Ag surfaces to sulfur compounds have been used to anchor long chain thiols (RSH) on these electrode surfaces. Yamada et al. ([108]b) recently studied photoelectrochemical responses of Au electrodes co-modified with sulfur-containing tris(2,2′-bipyridine)ruthenium(II) and viologen derivatives.

2.3. Titanium dioxide (TiO_2)

Amongst oxide semiconductors, titanium dioxide (TiO_2), a white pigment, is by far the most commonly used. With current world-wide annual consumption of ca. 3 million tons, global TiO_2 industry is worth more than 5.5 billion US$. In the present era of ecological and environmental consciousness, preferences are for inert, non-toxic compounds and TiO_2 meets adequately this requirement. Its extensive usage in paint industry comes from its high refractive index and ease of preparation of particles of very small size (leading to large surface area). As a cheap, readily available material, TiO_2 serves as an attractive candidate for many industrial applications (paints, paper, coatings, plastics, fibers, cosmetics, etc.). Thin films of TiO_2 have been prepared by many different physical and chemical techniques such as thermal oxidation, sputtering or chemical vapor deposition [109–118]. Such films are of interest in anti-reflection coatings, dielectric materials, sensors and wave-guides. It is a wide bandgap semiconductor with E_{bg} being ca. 3.2 eV. Interests of chemists on the use of TiO_2 for light energy conversion can be traced to the early 1970s with the reports of Fujishima and Honda [119], on the possible use of TiO_2 as a photoelectrode to decompose water to oxygen.

Rutile, anatase and brookite are the three common crystalline polymorphs of TiO_2. Rutile is the thermodynamically most stable modification (ca. 1.2–2.8 kcal mol^{-1} more stable than anatase). Rutile to anatase transformation occurs in the temperature range 700–1000°C depending on the crystallite size and impurity content. The bandgap energies for anatase and rutile have been estimated to be 3.2 and 3.0 eV, respectively. The flat-band potential fits the equation

$$U_{fb} = U_o - 0.06\text{pH (V vs. SCE)} \quad (1)$$

where U_o is -0.2 and -0.4 V for rutile and anatase, respectively. In view of the cathodic disposition of U_{fb} of anatase with respect to NHE, reduction of water to H_2 by photogenerated conduction band electrons proceeds spontaneously. Photoelectrolysis of water is possible on rutile only with additional potential bias! The smaller bandgap of rutile however implies that a higher fraction of the solar radiation can induce bandgap excitation (3-fold increase in photocurrents).

3. Earlier generations of photoelectrochemical solar cells

Before we take up an in-depth review of the present generation of dye-sensitized solar cells based on nanocrystalline films, it is useful to briefly review the outcome

of earlier attempts directed towards direct conversion of sunlight to electricity. There have been several approaches to light-energy conversion spanning nearly five decades [120–125]. We will confine ourselves to very brief review of some select ones: photogalvanic cells, photography, regenerative or liquid-junction solar cells based on semiconductor electrodes as light absorbers and dye-sensitization of semiconductor electrodes. Most of the key components and processes cited earlier for dye-sensitized solar cell are present in these model systems. It is only through extensive studies of such model system that it has been possible to identify (and control) factors associated with the efficient functioning of a dye-sensitized solar cell based on semiconducting oxides as electron acceptor/mediators.

3.1. Photogalvanic cells

Photogalvanic cells are the simplest form of solar cells involving photo-induced electron transfer following light absorption by dye molecules [126–128]:

$$Ru(bpy)_3^{2+} + Fe^{3+} Ru(bpy)_3^{3+} + Fe^{2+} \quad (2)$$

$$Ru(bpy)_3^{3+} + e^- \rightarrow Ru(bpy)_3^{2+} \text{ (electrode 1)} \quad (3)$$

$$Fe^{2+} \rightarrow Fe^{3+} + e^- \text{ (electrode 2)} \quad (4)$$

The dye and the redox mediator are dispersed in homogeneous solution. The reverse of electron transfer Reaction 2 is kinetically very slow (two to three orders of magnitude) and strongly dependent on the solvent and counter-ions), leading to a net conversion of $\geq 25\%$ of the Ru complex to Ru(III) species under steady state conditions. The photoproducts are subsequently reduced/oxidized at suitable metal or catalytic electrodes. The light-to-electrical conversion efficiencies obtainable with these conceptually simple solar cells however is very poor ($< 0.5\%$).

There are two principal reasons for the poor performance of photogalvanic cells. Firstly, kinetics of electron transfer reactions at the electrodes are much slower as compared to forward and back electron transfer steps of photo-induced processes. Hence reasonable photocurrents can be obtained if, and only if, large differences in the forward and back electron transfer steps exist. If the electron transfer products do not live long, then only the light absorbed in the vicinity of the electrode is processed and most of the light absorbed in the bulk of the solution is lost. If the back electron transfer is 100 times slower than in the forward direction, then the equilibrium under steady state conditions will shift towards products by few percent and under such conditions even sluggish electrodes can intervene. For charge collection at high efficiencies the system must have several orders of magnitude difference between the forward and back electron transfer rates.

Secondly, efficient performance of the photogalvanic cell requires high selectivity on the part of the electrodes (to carry out only the reactions as indicated in Reactions 2 and 3 and not to respond to other redox products present). If the electrodes are not selective, they only function as additional recombination centers for photogenerated products. Electrochemists addressed this problem using modified electrodes but only with very limited success. Attempts to increase

performance by thick coating of the dye on the electrode yielded poor results. Thicker layers of the dye lead to efficient intermolecular quenching of the excited states (process known as concentration quenching) and inner filter effects in competition with the desired electron transfer steps. Overall studies on the photogalvanic cell system clearly showed the need to look for efficient ways of processing photoredox reactions. Key steps such as charge separation, rates of forward and back electron transfer and charge transport to the collector electrodes need to be controlled microscopically.

3.2. Photoelectrochemical solar cells using semiconductors as light absorbers

A photoelectrochemical solar cell is closely related to a battery, fuel cell or other type of electrochemical system, in that it is composed of two electrodes and an electrolyte. Unlike batteries or fuel cells where the energy is stored in the reactants and is then released through the electrical discharge during the formation of chemical reaction products, photoelectrochemical cells utilize the input optical energy to drive electrochemical reactions. Optical sensitivity is introduced by replacement of one of the conventional electrode by a semiconductor electrode or via dyes adsorbed onto these semiconductor electrodes. Light absorbed either by the semiconductor itself [17,121,122,129,130] or by adsorbed dyes produces a current through the cell, which results in the production of chemical fuels and/or electrical energy by the device.

3.3. Dye-sensitized photoelectrochemical solar cell

3.3.1. Principles of operation

A dye-sensitized solar cell can be considered as a hybrid version of photogalvanic cells and solar cells based on semiconductor electrodes. The cell consists of a dye-coated semiconductor electrode and a counter electrode arranged in a sandwich configuration and the inter-electrode space is filled with an electrolyte containing a redox mediator (A/A^-). In our studies we have often used a polypyridine complex of Ru as the dye, TiO_2 as the semiconductor and (I_2/I_3^-) as the redox mediator. The key reactions taking place in a dye-sensitized photoelectrochemical solar cell are shown schematically in Fig. 3. Optical excitation of the dye with visible light leads to excitation of the dye to an electronically excited state that undergoes electron-transfer quenching, injecting electrons into the conduction band of the semiconductor:

$$S^* \rightarrow S^- + e_{cb}^- \tag{5}$$

The oxidized dye is subsequently reduced back to the ground state (S) by the electron donor (A^-) present in the electrolyte filling the pores:

$$S^+ + A^- \rightarrow S + A \tag{6}$$

The electrons in the conduction band collect at the back collector electrode and subsequently pass through the external circuit to arrive at the counter electrode where they effect the reverse reaction of the redox mediator:

$$A + e^- \rightarrow A^- \text{ (at the counter electrode)} \quad (7)$$

The net effect of visible light irradiation is regeneration of the dye, the redox mediator and the driving of electron through the external circuit. The process thus leads to direct conversion of sunlight to electricity. If above cited reactions alone take place, the solar cell will be stable, delivering photocurrents indefinitely. The maximum photovoltage obtainable will be the difference between the Fermi level (conduction band) of the semiconductor under illumination and the redox potential of the mediating redox couple. The photocurrent obtainable is a complex entity depending on the spectral, redox properties of the dye, efficiency of charge injection and structural properties of the semiconductor electrode to collect and channel the electrons through the external circuit.

3.3.1.1. Quantitative measurements on solar cell performance. Quantitative assessment of the solar cell performance is given by two key parameters: the incident photon-to-current conversion efficiency (IPCE) for monochromatic radiation and overall white light-to-electrical conversion efficiency η_{eff}. The IPCE value is the ratio of the observed photocurrent divided by the incident photon flux, uncorrected for reflective losses during optical excitation through the conducting glass electrode:

$$\text{IPCE} = \frac{\text{no. of electrons flowing through the external circuit}}{\text{no. of photons incident}} \quad (8)$$

The IPCE value can be considered as the effective quantum yield of the device. It is the product of three key factors: (a) light harvesting efficiency LHE (λ) (depend on the spectral and photophysical properties of the dye), (b) the charge injection

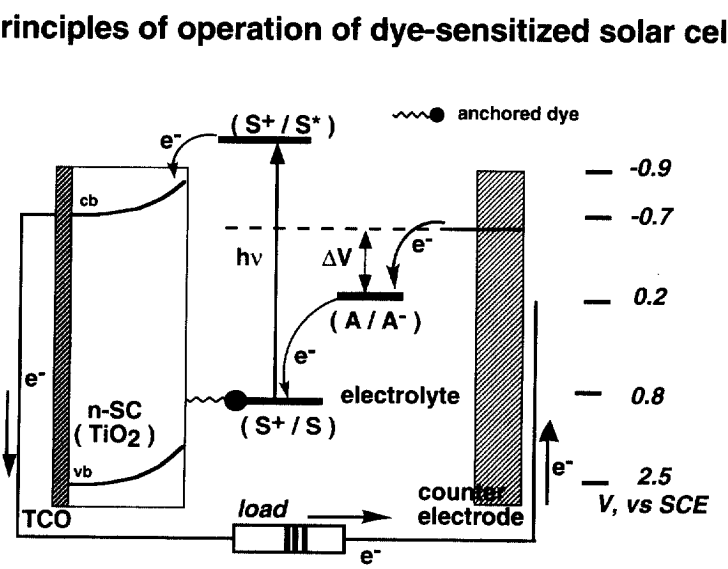

Fig. 3. A schematic presentation of key reactions taking place in a dye-sensitized solar cell.

yield ϕ_{inj} (depend on the excited state redox potential and the lifetime), and (c) the charge collection efficiency η_{el} (depend on the structure and morphology of the TiO_2 layer):

$$IPCE = (LHE_l)(\phi_{inj})(\eta_{el}) \tag{9}$$

The overall efficiency (η_{global}) of the photovoltaic cell can be obtained as a product of the integral photocurrent density (i_{ph}), the open-circuit photovoltage (V_{oc}), the fill factor (ff) and the intensity of the incident light (I_s):

$$\eta_{global} = \{i_{ph} V_{oc} ff\}/I_s \tag{10}$$

The measured photocurrent density is given by the overlap integral of the monochromatic photocurrent yield and the solar spectrum for incident radiation. Tabulated data are available for the wavelength dependent photon flux distribution of solar radiation incident on earth at various incident angles. AM 0 (air-mass zero) corresponds to absence of any atmosphere between the sun (outer space) and the device, and AM 1.5 has the sun at an angle of 48.19° to the device normal. The global spectrum has two components: direct and diffuse. Once the photons enter the atmosphere, they are prone to scattering and absorption, leaving gaps or bands in the spectrum due to H_2O, H_2, CO_2, O_3 and other species. For this reason, solar spectra at various grazing angles such as AM 1.5 has several sharp spikes, particularly in the red, IR region. Solar simulators are now commercially available for indoor experiments with simulated sunlight.

3.3.2. Early studies of dye sensitization of semiconductor electrodes

Sensitization of wide-bandgap semiconductors using dyes has a long (century-old) history, dating back to early days of photography [131]. The report of Putzeiko and Terenin [132] on sensitization of pressed ZnO disks by adsorbed rhodamine B, eosin, erythrosin and cyanine dyes appeared in 1949. Systematic mechanistic studies started only in the late sixties with the work of dye-sensitization process on ZnO and SnO_2 electrodes carried out by Gerischer [133], Terenin [134], Memming [135] and Hauffe [136] and their coworkers. Only then did the basic framework for quantitative analysis of electron-transfer processes involving semiconductors started emerging. Tsubomura, Honda, Goodenough, Bard and many others [137–140] have extended these studies to these and other electrodes. The dyes were deposited simply by immersing the electrode in the dye solution for a short period and subsequent drying in air. The extent of coverage (loading) was empirically controlled by varying the concentration of the dye stock solution. Natural forces (chemical and thermodynamic properties) controlled the way the molecules aligned themselves at the surface.

Most of these early studies were fundamental in nature, aimed at understanding of electron-transfer processes involving valence and conduction bands of a semiconductor immersed in a redox electrolyte. The validity of the underlying principles of dye-sensitized solar cells (whether they use single crystals, sintered disks or high-surface area porous films) illustrated earlier in Fig. 3 indeed come from these early pioneering studies. Without citing specific cases, we summarize here the key

observations. The similarity between the photocurrent action spectrum and the absorption spectrum was taken to indicate the direct involvement of the dye excited state in the observed photocurrent. In the absence of electron donors, the dye after excited state electron transfer remains in the oxidized state and the photocurrent steadily decreased with time. Cations of organic dyes particularly of the xanthene family (and some metalloporphyrins) are very reactive and undergo structural re-organization, resulting in rapid loss of chemical integrity. For sustained observation of photocurrent, electron donors need to be added to the electrolyte solution. Hydroquinones and iodides were employed as electron donors and the process was labeled as *super- or hyper-sensitization.*

It was very quickly realized that, as in photogalvanic cells, only those dye molecules that are in the immediate vicinity of the electrode contributed to photocurrent. Reasonably high IPCE values were obtained only in cases where there is a mono- or sub-monolayer of the dye present on the semiconductor surface. Also most often, the photocurrent saturated at relatively low dye concentration. Several reasons have been identified as the source for the low efficiency. With organic dyes employed in majority of these studies, dye-aggregation occurs even at relatively low concentration of the solution ($\leq 10^{-5}$ M). Only in the exceptional case of special form of aggregates (J-type) of cyanine dyes, charge injection process was efficient (in cases where the aggregates also participated in the charge injection process, concentration dependence of photocurrent showed a maximum different from that seen in the excited state quenching measurements!). The reasons for the low quantum efficiency are not fully understood and several explanations have been proposed: (i) concentration quenching of the excited state via fast energy transfer amongst the dyes or pre-formed dimers (static quenching), (ii) insulating nature of thick dye layers, and (iii) fast electron trapping and back reaction occurring between excited dye molecules and surface traps not subject to electric field of the semiconductor space charge region.

Searches began soon on alternative methods of depositing dyes on the electrode surface. Tsubomura et al. showed that, by using porous sintered ZnO electrodes, it is possible to increase the performance of the solar cell. Using Rose Bengal as the sensitizer and (I^-/I_3^-) as the redox mediator, they obtained IPCE values of 0.2 in the visible region, leading to overall white light conversion of 1.5%. Fromherz and Arden [71] demonstrated the utility of monolayers. Monolayer assemblies of long chain derivatives of cyanine diluted with arachidic acid were shown to give a 4-fold increase in IPCE: 0.8 from 0.2 obtained for dyes distributed by the classical dip–dry coating procedures.

3.3.3. Silver halide photography

Historically the earliest and industrially most important example of dye sensitization is with color photography where a mixture of several organic dyes are used to extend the spectral range of silver halide grains [141–144]. Exposure of the photographic emulsion to light leads to electron transfer from the cyanine dyes to

AgX. The reduced Ag atoms are rapidly stabilized, leading to formation of latent images. The efficiency of development of this latent image, i.e. the optical density of the developed film is often used as a measure of ϕ_{et}. A measure of ϕ_{et}, termed ϕ_{rel} has been devised to measure the efficiency of sensitizing dyes adsorbed on the silver halide grains that are used in photographic films. The optimized efficiency of spectral sensitization of silver halide grains is very high. In view of the strong similarity in the principles of operation of silver halide photography and dye-sensitized solar cells it is useful to review some of the key features of the former process.

Cyanine and related dyes are known to aggregate in solution but in photography, this process is taken to advantage In addition to conventional dimers, photographic dyes associate in large numbers (few hundred to a million) to form the so-called J- and H-aggregates. In J-aggregates the transition dipoles for optical transition are parallel to the molecular plane and this in turn leads to a red-shift of the absorption maximum with respect to that of the monomer. In stacked H-aggregates the transition dipole is oriented perpendicular to the molecular plane and an associated blue shift (J-aggregate > monomer > dimer > H-aggregate). It is well known in photography that J-aggregates function efficiently as photosensitizers while the presence of H-aggregates is to be avoided at all cost. J-aggregates themselves are of several kind—smaller sized (several hundred nm^2) meso-type consisting of up to a thousand monomers and larger size macro-aggregates ($> 5 \times 10^4$ monomers).

The dye distribution on the silver halide microcrystals is a key factor that controls the sensitivity of the resulting emulsion. In the commonly used procedure, the dye dissolved in a solvent is applied over the microcrystal and the natural forces are utilised to control the distribution and orientation of dyes on the silver halide surfaces (random organization). It turns out that this method (fast non-activated physisorption) does produce a satisfactory distribution consisting of small and large domains. J-aggregates are present even at very low surface coverages (ϑ values). For maximum spectral response to the visible light, a mixture of dyes are often employed. Efficient excitation energy transfer occurs between dyes with high energy excited states to those with lower energy ones. The excitation energy migrates efficiently amongst the dye molecules adsorbed on the surfaces as excitons over large distances within a short span of time that, even at a loading of 0.1% of acceptors amongst the donors, can effectively reduce the donor emission lifetime to one-fifth of the unquenched value. While the model system/mechanistic studies are carried out at low surface coverages ($\vartheta \leq 0.01$), the coverage employed in photographic emulsions is much higher (ϑ in the range 0.2–0.3). Nüesch et al. [145] have used nanocrystalline films of TiO_2, Al_2O_3 and ZrO_2 as hosts for the merocyanine, 3-acetyl-5(2-(3-ethyl-2-benzothiazolidinylene)ethylidene)rhodanine to scrutinize templating effects in the accommodation of the dye within the porous network. Conditions that favor formation of J-aggregates in preference to H-type have been identified.

As a result of such efficient exciton migration amongst the dye molecules the photosensitivity decreases at high surface coverages of the dye. At high coverages, there is invariably an increase in the trap (hole) sites. Fassler et al. ([146]a) have indeed found that on silver halides, the charge injection efficiency decreases at high coverages due to increased dye–dye interactions at the surface. Kavassalis and Spitler ([146]b) observed similar behavior in the measures of photooxidation yields of cyanine dyes at ZnO electrodes. Internal reflection spectroscopy has also been used to probe the sensitization of ZnO single crystals by J-aggregates of cyanine dyes ([146]c). Recently it has been found that, with better control over the molecular organization of dyes on the surfaces it is possible to increase even the response time. Procedures have been developed to selectively adsorb the dye molecules at the physical surface defects (atomic surface steps, edges or corners), chemical surface defects (surface iodides) or controlled nucleated growth.

Studies of excited state decay of various cyanine dyes on AgBr crystals have clearly shown the effect of adsorption on excited state decay dynamics ([146]c). For many cyanine dyes in solution, the rate constants for internal conversion and intersystem crossing are so large that the fluorescence lifetimes is often reduced to < 50 ps. These fast pathways for decay require a torsional motion about the polymethine chain of the dye, a motion which has also been found to be prerequisite for intersystem crossing and which is strongly hindered when the dye is in a medium of high viscosity or adsorbed on the surface in a planar orientation. Such a restriction of torsional motion can also be effected through rigidisation of the polymethine chain through bridging groups on the cyanine molecule. This rigidisation can increase the quantum yield for fluorescence from < 0.05 to > 0.7.

3.3.4. Polypyridine complexes as sensitizers

Returning to the topic of sensitization of wide-bandgap semiconductors by metal complexes, Memming and coworkers [147] were the first to explore polypyridyl complexes of Ru on SnO_2 electrodes. These studies were followed by similar experiments on $Ru(bpy)_3^{2+}$ and related complexes by several others on TiO_2, $SrTiO_3$ and ZnO electrodes [148–150]. Anodic photocurrents corresponding to charge injection from the excited Ru complex to the conduction band of the semiconductor was observed for excitation with photons of energy less than that of the bandgap. Interestingly slow rise time cathodic photocurrent was obtained in addition to the fast risetime anodic photocurrent. Copper(I) complexes of phenyl-substituted 1,10-phenanthrolines have also been found to sensitize semiconducting ZnO electrodes [151]. Following reports of possible catalytic water oxidation to molecular oxygen by $Ru(bpy)_3^{3+}$ and their surfactant derivatives [152], several authors examined photosensitized oxidation of water using long-chain/surfactant derivatives of $Ru(bpy)_3^{2+}$ adsorbed on to semiconductor electrodes such as SnO_2, TiO_2 and $SrTiO_3$ [153,154]. In aqueous media, the lifetime of the dye cation formed following excited state charge injection, $Ru(bpy)_3^{3+}$ decreases rapidly with increasing pH values.

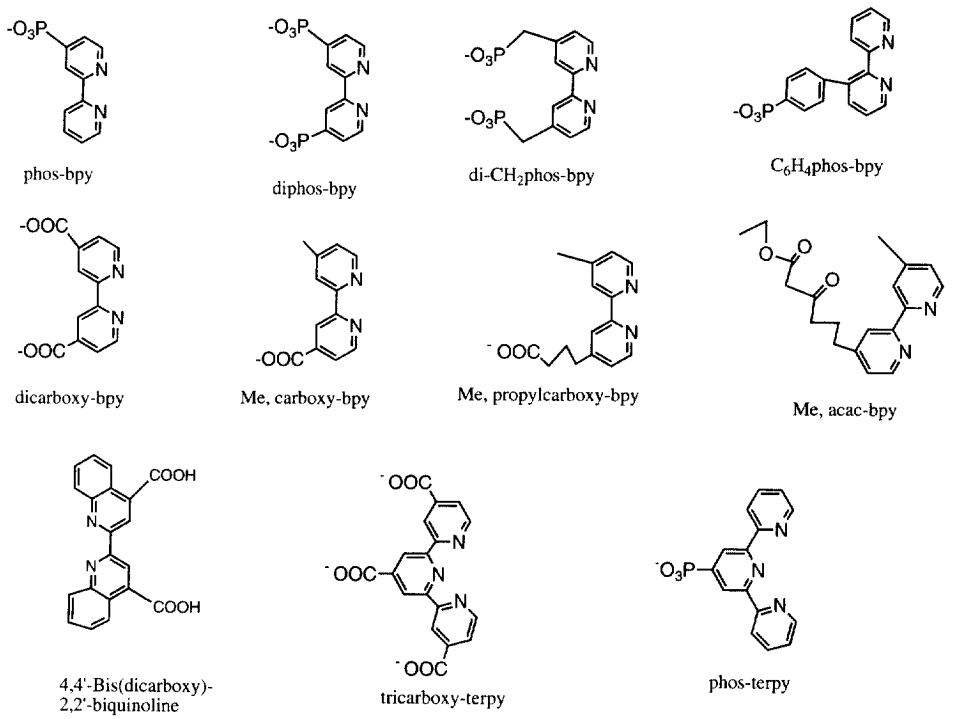

Fig. 4. Various types of polypyridine ligands with carboxyl or phosphonato groups that are being used in solar cell studies.

3.3.5. Surface chelation of the sensitizer

The deactivation of electronically excited state of dyes is generally rapid. Typical rate constant for the process (k_{eff}) is in the range of 10^8–10^9 s^{-1}. For dyes that are homogeneously dispersed in solution, the diffusion length (L) is ca. 250 Å for an excited state lifetime of 500 ns. To achieve high quantum yield for the excited state electron-transfer process, the rate constant (k_q) for the quenching process should be at least two orders of magnitude greater than k_{eff} ($k_q \geq 10^{11}$ s^{-1}), or the probability of the dye to be found in the immediate vicinity of the acceptor (in this case the semiconducting oxide) is considerably high. For these reasons, dyes are preferably adsorbed or chemically bound to the surface by some form of derivatization using appropriate anchoring groups.

Soon after the realization in mid 1970s that intimate contact between the semiconductor acceptor and the dye molecule is necessary to obtain high efficiencies, there have been many studies of dyes covalently bound to semiconductor surfaces. Fujihira, Tsubomura and coworkers [70,138] showed that rhodamine B can be attached to the surface by esterification or by using a $SiCH_2CH_2CH_2NHCO$-dye linkage. Fig. 4 shows some of the polypyridine-derived ligands with different anchoring groups that have been employed for surface derivation of Ru–polypyridyl complexes. Goodenough and coworkers [155] examined the photosensitization of TiO_2, $SrTiO_3$ single crystal electrodes and SnO_2 films by the mixed

ligand complex $[Ru(bpy)_2(dcbpy)]$ chemically attached via the ester linkages. The electrode surface was derivatized by two different chemical routes, both involving reaction with electrode surface sites that react like hydroxyl groups: the surface was either reacted with the mixed ligand complex in the presence of dicyclohexylcarbodiimide in a one-step process or with 2,2′-bpy-4,4′-di(carbonylchloride), followed by *cis*-$[Ru(bpy)Cl_2]$ in a two-step process. The quantum efficiency for electron injection was found to be quite low (η is ca. 0.25%). Murray, Spiro and coworkers [156,157] demonstrated covalent binding of carboxy ester derivatives of Ru–bpy complex on to TiO_2 using silanyl groups.

3.3.6. Porphyrins and phthalocyanine as sensitizers

One of the very early investigations exploring the photosensitization capacity of porphyrins is the work of Tributsch and Calvin [158] when they examined in 1971 chlorophylls on ZnO electrodes. Although quantum efficiencies up to 0.125 e^- per absorption photon were observed in the presence of phenylhydrazine as the sacrificial electron donor, the measured photocurrents were extremely small (ca. 5 $\mu A\ cm^{-2}$ for monochromatic excitation) due to very small light harvesting efficiency of a monolayer of the dye on semiconductor single crystal. Honda, Fujishima and coworkers [159] examined the effect of various metal ions in monolayers of chlorophyll derivatives on SnO_2 electrodes deposited using a Langmuir–Blodgett procedure. Quantum efficiencies of the order of 0.3 were obtained.

Due to a more extended π-system compared to porphyrins, phthalocyanines show farther red-shifted absorption, with the lowest energy band occurring in the near-IR region. Hence they are ideally suited for red-light harvesting in solar cells. But major problems with the metallophthalocyanines are their extremely low solubility in solvents of choice for electrochemical studies and the tendency to aggregate even at concentrations ≤ 1 μM. Sensitization properties of thin films (100–250 Å) of several metallophthalocyanines MPcs (M = Mg, Zn, Al(Cl), TiO, Fe and H_2) deposited on TiO_2 and WO_3 single crystal electrodes have been studied ([160]a–d). Anodic photocurrents corresponding to an IPCE range of 0.001–0.1 were found for visible light irradiation in the presence of donors such as hydroquinone ([160]a,b). Phthalocyanines behave as p-type semiconductors and for this reason, cathodic photocurrents can also be observed at negative potentials and in the presence of suitable electron acceptor molecules. Fujishima et al. ([160]c) recently studied the dye-sensitizing effect of TiO–Pc thin film on the $\langle 001 \rangle$ surface of TiO_2 single crystals.

4. Nanocrystalline oxide film-based solar cells

4.1. A description of the nanocrystalline oxide based solar cell

The use of mesoporous nanocrystalline films of the semiconductor in place of compact signal increases considerably the effective surface area for dye adsorption. For this reason recent studies of dye-sensitized solar cells use invariably such

nanocrystalline films. Advances in the photophysics and photoredox chemistry of transition metal complexes have led to identification of numerous examples of coordination complexes as efficient photosensitizers. Fig. 5 presents a cartoon of the make-up of the present generation of dye-sensitized photoelectrochemical cells based on nanocrystalline films of TiO_2. The early reports [161–164] of high efficiencies obtained by the Lausanne group (using tris- and mixed ligands) bipyridine complexes attached to these porous electrodes have been confirmed and extended to a number of Ru complexes [165–188]. While major emphasis is still on optimising the performance of solar cells based on TiO_2 films (white light conversion efficiency, stability, etc.), there have also been exploratory studies on nanoporous films of other semiconducting oxides, particularly on ZnO [189–191] and SnO_2 [192–197].

The solar cell consists of two conducting glass electrodes in a sandwich configuration, with a redox electrolyte separating the two. On one of these electrodes, a few micron-thick layer of TiO_2 is deposited using a colloidal preparation of monodispersed particles of TiO_2. The compact layer is porous with a high surface area, allowing monomolecular distribution of dye molecules. After appropriate heat treatment to reduce the resistivity of the film, the electrode with the oxide layer is immersed in the dye solution of interest (typically 2×10^{-4} M in alcohol) for several hours. The porous oxide layer acts like a sponge and there is very efficient uptake of the dye, leading to intense coloration of the film. Molar absorbances of 3 and above are readily obtained within the micron-thick layer with a number of Ru–polypyridyl complexes. The dye-coated electrode is then put together with another conducting glass electrode and the intervening space is filled with an organic electrolyte (generally a nitrile) containing a redox electrolyte (I^-/I_3^-). A

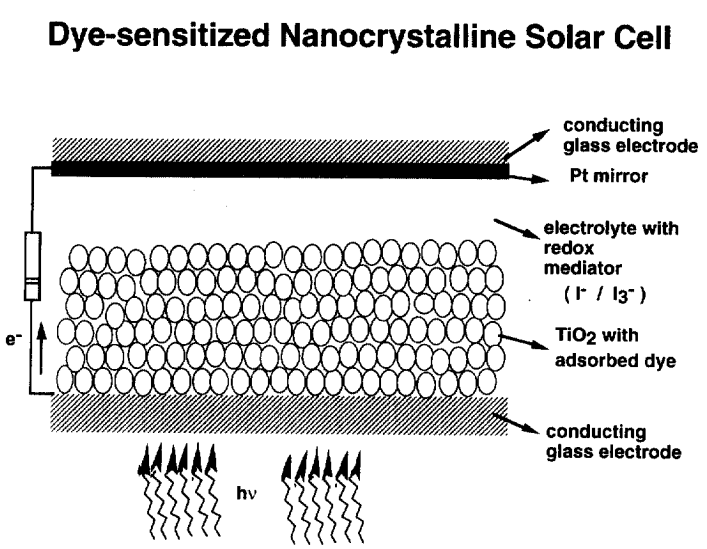

Fig. 5. A cartoon of the make-up of the present generation of dye-sensitized photoelectrochemical cells.

small amount of Pt (5–10 μg cm^{-2}) is deposited to the counter-electrode to catalyze the cathodic reduction of triiodide to iodide. After making provisions for electrical contact with the two electrodes, the assembly is sealed.

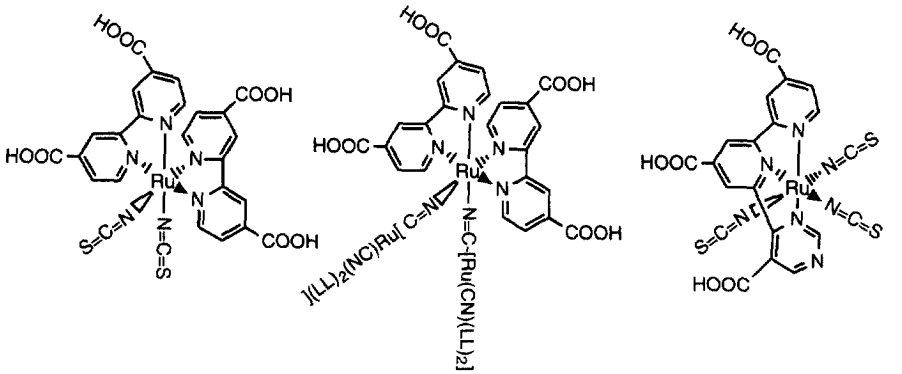

$[Ru(dc\text{-}bpyH_2)_2(NCS)_2]$ $[Ru(dc\text{-}bpyH_2)_2\{(CN)_2Ru(LL)_2\}_2]$ $[Ru(tc\text{-}terpyH_3)(NCS)_3]$

Fig. 6 presents photocurrent action spectra obtained using simulated sunlight (AM 1.5) in above type of dye-sensitized solar cells using three representative Ru–polypyridyl complexes: $[(CN)(bpy)_2Ru\text{–}CN\text{–}Ru(dcbpy)_2\text{–}NCRu(bpy)_2]$, $[Ru(4,4\text{-bis(carboxy)-bpy})_2(NCS)_2]$ and $[Ru(2,2',2''\text{-}(COOH)_3\text{-terpy})(NCS)_3]$. The curves represent in some sense the evolution in the increased performance of the

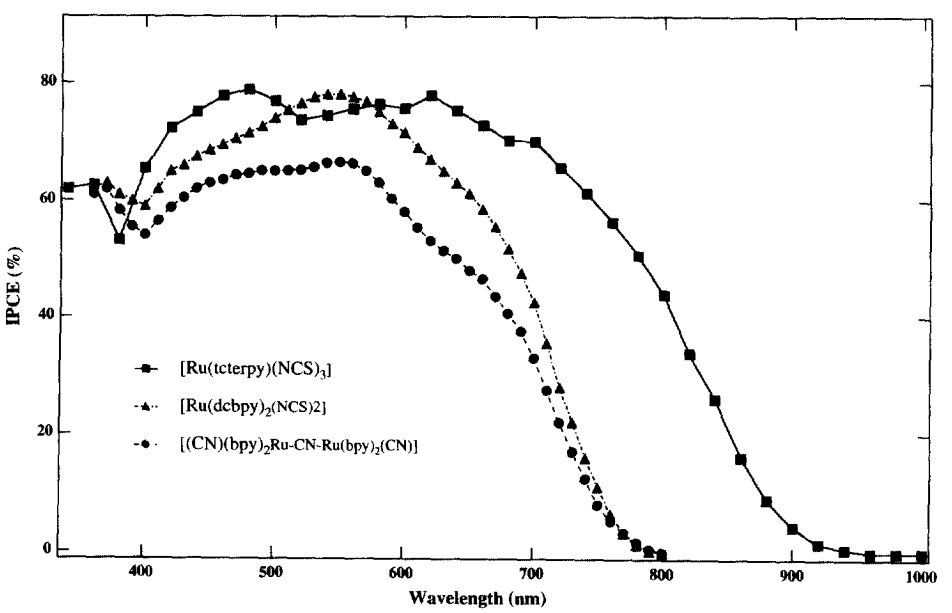

Fig. 6. Photocurrent action spectrum for three efficient photosensitizers $[Ru(tcterpy)(NCS)_3]$, $[Ru(dcbpy)_2(NCS)_2]$ and $[(CN)(bpy)_2Ru\text{–}CN\text{–}Ru(bpy)_2(CN)]$ measured on nanocrystalline TiO_2 solar cells.

cells with evolving series of photosensitizers. The spectra are based on incident photon flux and are not corrected for transmittance of the conductive glass substrate and reflective and other losses. Hence photocurrent reaching constant values around 80% represent near-quantitative conversion of sunlight energy into electrical energy. The bis(carboxy)bipyridine complex is used routinely as a standard in many laboratories, including our own. It was mentioned earlier that carboxylic esters are susceptible to facile hydrolysis in view of their low pK_a. Phosphonate esters are preferred choices in this context, particularly for studies in aqueous media. The photosensitizer [Ru(PO_3-terpy)(Me_2bpy)(NCS)] is an example of a sensitizer that adheres to the TiO_2 surface firmly and shows monochromatic and overall light to electrical conversion efficiency comparable to dcbpy-based complexes [169,173]. Currently the best spectral response is with the triscarboxy-terpyridine Ru complex, [Ru(2,2′,2″-$(COOH)_3$-terpy)$(NCS)_3$]. With absorption covering the entire visible range, the dye appears nearly black. With this complex as the photosensitizer in a standard nanocrystalline solar cell and one sun irradiation level the photocurrent corresponds to an i_{sc} of ca. 18–22 mA cm^{-2} and photovoltages V_{oc} of ca. 0.65 V with a fill factor of 0.7. These figures translate to visible light to electrical conversion efficiency of nearly 10%.

4.2. Key components of the solar cell

Understandably in a multi-component device, the overall performance of the solar cell depends critically on the individual properties of the constituent components and processes. The structure, morphology, optical and electrical properties of the nanoporous oxide layer; chemical, redox and photophysical and photochemical properties of the dye; visco–elastic and electrical properties of the electrolyte carrying the redox mediator; redox and optical properties of the redox mediator, electrical and optical properties of the counter electrode are some of the major ones we need to deal with in the design of solar cells. Regarding key processes one can cite: light absorption, charge injection from the excited state of the dye; regeneration of the oxidized dye; electron percolation within the oxide film; dark currents and counter-electrode performance. For devices targeted for commercialization, there are additional factors to consider such as: long term stability and material cost. Optimal performance is obtainable only when we can understand the factors that control each of these components and our ability to tune to the required configuration. On one hand with involvement of so many parameters, these solar cells are extremely delicate devices to fabricate in a reproducible manner. On the other hand these parameters allow total flexibility in tuning to specific applications. Indoor applications in electronic gadgets such as watches, calculators, bathroom balances, etc., require higher photovoltage output at relatively low photocurrent levels upon ambient light exposure to small electrode surfaces. The cells work at ambient temperatures. Outdoor applications employ large area panels composed of modules (typically 10×10 cm). Maximum power conversion is envisaged under conditions where the operating temperature and incident solar flux span a wide range.

4.2.1. Nanoporous TiO_2 layer

It was mentioned earlier that the performance of the solar cell is intimately linked to the material content, chemical composition, structure and morphology of the nanoporous oxide layer. Fortunately colloid chemistry has advanced tremendously in the last two decades that, it is now possible to control the processing parameters such as precursor chemistry, hydrothermal growth temperature, binder addition and sintering conditions and optimize the key parameters of the film, viz. porosity, pore size distribution, light scattering and electron percolation. On the material content, two crystalline forms of TiO_2 are important, the anatase and rutile (the third form brookite is difficult to obtain). Anatase is the low-temperature stable form (appears in the form of pyramid-like crystals) and rutile (needle-like) is the dominant form in high temperature preparations, including single crystals. The reduced density of anatase as compared to rutile (3.89 vs. 4.26 g cm^{-3}) leads to significant differences in many physical properties. Rutile has non-negligible absorption in the near-UV region (350–400 nm), ca. 4% of the solar radiation incident. Excitation within the bandgap leads to generation of holes, a strong oxidant causing long term instability of the solar cell.

For efficient dye distribution, the surface area of the membrane film must be large. It is known that smaller the particle size, larger will be the surface area of the film. It was mentioned earlier that on flat surfaces of single crystal electrodes only a few monolayers of the dye can efficiently participate in the excited state charge injection process. The light harvesting from a planar electrode is poor due to the small absorption cross section of monolayer of the dye. In highly porous nanotextured films, the available surface area for dye adsorption can be enormous (with surface roughness factor over 500), leading to near extinction of incident light within film which is a few microns thick.

Porosity is another factor that needs to be optimized. For the fast regeneration of the oxidized dye and charge transport, the redox electrolyte must be able to penetrate the pores efficiently and be present in places where the dye penetrates. Larger the particle size, the larger will be the porosity of the layer. Larger particles also scatter the incident radiation more effectively and this has been found to be a positive factor in enhancing the red-light response of the sensitizer. So the preparation procedure must be optimized so as to provide an optimal particle size, porosity features. Sintering of the particles that form the film is another important step related to electron percolation within the film and reducing of dark currents. Sintering produces low resistance ohmic contacts between the particles. Thus the electrons injected anywhere within the network of particles can hop through several particles and reach the back contact without being lost (trapped) within the oxide layer.

The injected electron has to be transported across a large number of colloidal particles and grain boundaries. There will be an increased probability of recombination with increased film thickness. Thus there exists an optimal thickness to obtain maximum photocurrent. Another loss mechanism due to increasing film thickness is a resistance loss leading to a decrease in photovoltage and fill factor.

4.2.1.1. Preparation of nanocrystalline TiO_2 layer electrodes. Preparation of nanocrystalline semiconductor films consists of two steps: preparation of a colloidal solution containing monodispersed nanosized particles of the semiconductor and preparation of a few micron-thick film with good electrical conduction properties using this colloidal solution. Various steps involved in the preparation of a stock solution of the TiO_2 colloid are:

1. precipitation (hydrolysis of Ti-alkoxides using 0.1 M HNO_3),
2. peptization (heating at 80°C for 8 h) followed by filtering,
3. hydrothermal growth/autoclaving (12 h, 200–250°C),
4. sonication (ultrasonic bath, 400 W, 15×2 s),
5. concentration (45°C, 30 mbar), and
6. binder addition (carboxowax/PEG, M_w 20 000).

Layers are then deposited on conducting glass substrate either using doctor blade technique or screen printing, followed by sintering (450°C for 30 min) to burn out the binder. Several publications from our group providing a detailed description of these steps and their influence on the performance of the solar cell are available [109–118]. There have been several other studies of preparation and electronic processes in nanocrystalline TiO_2 electrodes [198–209]. Hence we will only briefly review the key results.

Precipitation process involve controlled hydrolysis of a Ti(IV) salt, usually an alkoxide such as Ti-isopropoxide or a chloride followed by peptization. In order to obtain monodispersed particles of desired size, the hydrolysis and condensation kinetics must be controlled. Ti-alkoxides with bulky groups such as butoxy hydrolyze slowly, allowing slow condensation rates. It has been found that, Ti-propoxide suitably modified with acetic acid or acetyl acetonate, give colloids of higher surface area ($\geq 200\ m^2\ g^{-1}$) and small particle diameter (5–7 nm). Peptization step involves heating of the precipitate for ca. 8 h at 80°C. The process leads to segregation of the agglomerates to primary particles. In view of electrostatic factors that control colloid stability, peptization occurs more effectively at pHs farther away from the isoelectric point. Particle growth has also been observed to some extent. The precipitate is then filtered through a glass frit to remove larger agglomerates and water added to the filtrate to reach a sol concentration of ca. 5% (w/w).

Autoclaving of these sols (heating at 200–250°C for 12 h) allow controlled growth of the primary particles and also to some extent the crystallinity. During this hydrothermal growth smaller particles dissolve and fuse to large particles by a process known as *Ostwald ripening*. The higher the autoclaving pH, the more effective the Ostwald ripening is. Aggregation is less efficient at low autoclaving temperatures. The pore size distribution of the film depend on the aggregate size and distribution. Average aggregate sizes of 100, 270 and 440 nm, for example, gives rise to average pore sizes of 10, 15 and 20 nm, respectively. At higher autoclaving temperatures, more rutile formation occurs, particularly at temperatures above 240°C. Electrodes prepared using colloids autoclaved at or below 230°C are transparent while those made from colloids autoclaved at higher temperatures are translucent or opaque. Each of these have their own advantages. Solar cells are

usually made on a 240–250°C autoclaved colloidal solution with a film thickness of 10 μm, whereas for electrochromic display applications, it is desirable to use a solution autoclaved at 200°C giving a transparent 3–4 μm thick film. Sedimentation takes place to some extent during the hydrothermal growth procedure and the precipitates are redispersed using a Ti-ultrasonic horn (15 × 2 s pulses at 400 W). The sol is then concentrated at 45°C on a rotary evaporator to reach a final concentration of ca. 11%. An increase in the porosity of the film can be obtained by adding a binder such as polyethylene glycol (M_w 20 000) to the above sol.

The sol is now ready for deposition on the conducting glass substrate. In our laboratory, we use F-doped SnO_2 glass from NSG (Nippon sheet glass, $R = 8–10$ Ω per square) and the sol is deposited by the doctor blade technique to get a film thickness of 100 μm. In routine work, a piece of Scotch tape at the edges of the support determined the thickness of the film. Commercial powders of TiO_2, such as P-25 and F387 (both Degussa) have also been used in place of the hydrolyzates of titanium alkoxides (P-25 is formed by the hydrolysis of $TiCl_4$ in a hot flame. The relatively short residence time necessary for the conversion of $TiCl_4$ to TiO_2 gives a product which has high surface area (ca. 50 $m^2\ g^{-1}$) and is a mixture of ca. 4:1 anatase to rutile. With such sample sources, the TiO_2 powder was dispersed by grinding with water and particle stabilizers (such as acetylacetone or HNO_3) and wetting agents such as non-ionic surfactant Triton X-100 and spread on the support as with the sols.

The films are then dried in air and then fired at 450°C in air for 30 min. The film thickness was typically 5–10 μm and the film mass about 1–2 mg cm^{-2}. Analysis of the porous films (carbon content) indicate that the binder is totally burnt out. Increase of the firing temperature leads to sintering and pore coarsening. Small pores (≤ 10 nm) decrease substantially and average pore size increases from 15 (400°C) to 20 nm at 550°C. Sintering at 350–450°C produces electronic contact not only between the particles and the support but also between all the particles constituting the film. Thus a sponge-like structure is obtained and the colloidal TiO_2 film is porous (typically a porosity of 50% is achieved) from the outer layers to the ITO contact. The pores between the colloidal particles are interconnected and can be filled with an electrolyte. A roughness factor, defined as the ratio between the real and the projected surface of these films, of about 1000 has been estimated for a 10 μm thick TiO_2 film.

Studies have shown that deposition of a secondary oxide layer to the nanotextured film improves significantly the cell performance. In one procedure the film is impregnated with $TiCl_4$ by immersing the film in a solution in ice water (conc. 0.2 M) followed by firing at 450°C for 30 min. Electrochemical deposition of TiO_2 on the nanotextured film can also be carried out by anodic oxidative hydrolysis of $TiCl_3$. Typically 0.1–0.35 mg cm^{-2} (projected area) of TiO_2 was deposited galvanostatically on top of TiO_2 layer on ITO or Ti sheet. One possible effect of the secondary layer is to increase the electron percolation in the film.

4.2.1.2. Dye uptake and the spectral response in the low-energy region. The morphology of the oxide layer also affects the dye uptake and also the spectral response in

the low energy region. In high surface area films composed of very small TiO_2 particles, the pore size can limit the dye uptake particularly for large size molecules. Feeble coloration is obtained due to low dye uptake that occurs with supramolecular molecules. So tuning of the pore size is necessary in these cases. The absorption of light by a monolayer of the dye adsorbed on to a flat semiconductor surface is weak due to the fact that the area occupied by one molecule is much larger than its optical cross section for light capture. High photovoltaic efficiency cannot be obtained in such a configuration. When the light penetrates the spongy semiconductor in the porous films, it crosses several hundreds of adsorbed dye monolayers. Thus the mesoscopic films fulfill a function similar to the thylakoid membranes of green leaves.

Secondly the photoresponse in the low energy region depend on the scattering properties of the film. As shown in Fig. 6, the IPCE values obtained in the red region is much higher than what is indicated by the absorption spectrum of the dye. At 700 nm, for example, the absorption of the bisthiocyanato complex is hardly 5% of the maximum value corresponding to 530 nm. Yet the IPCE value at 700 is nearly half the maximumum value. Normally the photocurrent action spectrum reproduces the solution absorption spectrum, except for small changes caused by the derivatization of the dye on the electrode. In the wavelength region where the dye absorption is maximal, the high absorbance values (>2) leads to total extinction of the light within the film. In the low energy side, a significant part of the incident radiation penetrates the layer. Multiple reflections of the light in highly scattering films results in increased light absorption and hence increased photoresponse than what the solution absorption spectrum indicates. This dependence of the red light response indeed has been verified by incorporation of added scattering centers during the preparation of the nanocrystalline TiO_2 film. In fact, in current efforts of dye design, particular attention is being paid to small but definitive absorption tail extending further into the red/near-IR region.

4.3. Molecular engineering of photosensitizers

4.3.1. General considerations

Based on the collective experience of ours and several other groups engaged in the molecular engineering of the dyes, we can cite several key criteria that are preferably met for the dyes to serve as efficient photosensitizers in solar cells. Fig. 7 shows schematically the influence of some of the key components in the distribution of the dyes on the semiconductor surface.

4.3.1.1. Spectral properties so as to ensure maximal visible light absorption. Obviously one would like to use a dye that has near black body absorption, i.e. a dye that absorbs all of the visible, near-IR photons of the sunlight incident on earth. Fortunately transition metal complexes derived using three ligand systems mentioned earlier all exhibit strong absorption bands in the spectral region of interest. Dominant electronic transitions contributing to molar absorbances are MLCT for polypyridines and $\pi-\pi^*$ transitions for the porphyrins and phthalocyanines. Suffi-

cient knowledge is available to modulate the energies and intensities of the low-lying excited states. Some examples of design strategies leading to identification of photosensitizers are elaborated below, using Ru–polypyridyl complexes as model candidates. Most of these considerations apply to metalloporphyrins and metallophthalocyanines as well.

For dyes that are adsorbed or covalently bound to the oxide surface, the light-induced electron transfer is non-diffusional. Hence it suffices to have the excited state lifetime to be in the order of tens of ns. Where there are several forms of excited state available, kinetics and thermodynamics decide if charge injection occurs from some or all of them. When the excited state charge injection is kinetically slow, other processes in the excited state manifold such as non-radiative decay, cross-over to metal-centered excited states (can lead to photosubstitution) becomes important in determining the efficiency of charge injection and stability of the dye. We shall return to more detailed discussions later on.

4.3.1.2. Redox properties in the ground and excited state. These are used to ensure fast charge injection and regeneration of the oxidized dye. Efficient charge injection

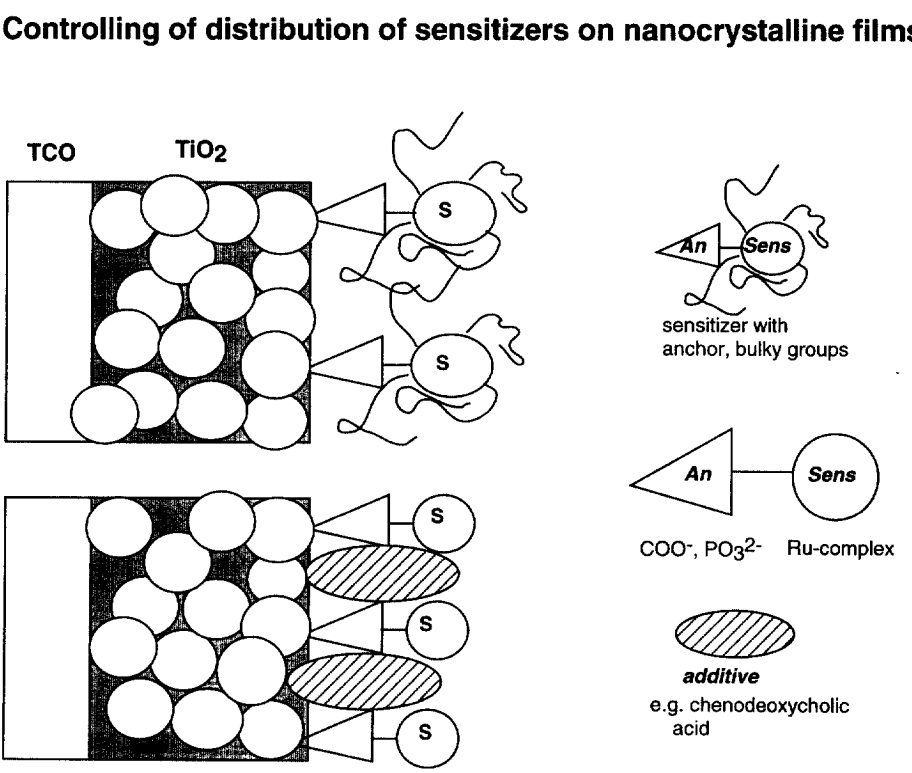

Fig. 7. Different ways of controlling the distribution of dyes on surfaces. Top: using sensitizers with long chain or bulky peripheral substituents. Bottom: using bulky additives such as chenodeoxycholic acids.

from the electronically excited state of the dye into the conduction band of TiO_2 depend on the redox potential of the dye in the excited state $E(S^+/S^*)$. In cases where the reorganization energy for the formation of oxidized dye is small (as is often the case with polypyridine and porphyrin complexes), the excited state reduction potential, $E(S^+/S^*)$ is given by:

$$E(S^+/S^*) = E(S^+/S) + E(S^*) \tag{11}$$

where $E(S^*)$ and $E(S^+/S^*)$ represent the excited state energy and the oxidation potential of the dye in the ground state, respectively. Electron transfer reactions involving semiconductor valence and/or conduction bands have been described by the same Marcus-type formalisms used for electron-transfer reactions of solution redox species, particularly for the rate dependence on the driving force associated with respective electron transfer steps. Strictly speaking the above approach assumes the redox partners to be vibrationally relaxed. Reverse electron transfer reactions most often are kinetically slow to adequately meet the above requirement. But for forward electron-transfer/charge injection step, if it occurs ultra fast i.e. in ps (as has been observed in several cases) the approximations may not be valid (see later).

Obviously one would like to use a dye that absorbs nearly all the sunlight incident on earth, like a black-body absorber. It is interesting to speculate on threshold wavelength if any for optimal light harvesting. The solar spectrum has its maximal intensity in the IR region (ca. 1200 nm) and so it is desirable to shift this threshold to as low energy as possible. The energy content of the photon however decreases as we move further into the IR region. There are two key electron transfer steps (primary charge injection and regeneration of the dye) that must occur very rapidly for solar cells to have high quantum efficiency and long term stability (turnovers). Studies have shown that one needs to provide at least ca. 200 mV driving force for each of these reactions to take place with optimal efficiency. In view of this, for a cell that uses a single photon to drive a single electron through the external circuit (as the present case), an optimal threshold for maximum power conversion would be around 850 nm (ca. 1.45 eV). Solar cells using low energy photons can deliver higher currents but only low photovoltages (vice versa for high energy case). There are many applications that demand higher voltage output at low light flux. The possibility to design efficient solar cells that work in the blue, green or red part of the solar spectrum opens up interesting applications as in fashion watches where the photoactive element embedded in the disk can have different colors.

4.3.1.3. Introduction of anchoring groups. These are employed to ensure uniform (monomolecular) distribution of the dyes on the oxide surface and to promote electronic coupling of the donor levels of the dye with the acceptor levels of the semiconductor: Fig. 7 shows different ways of controlling the distribution of polypyridine-derived sensitizers using different anchoring groups and additives.

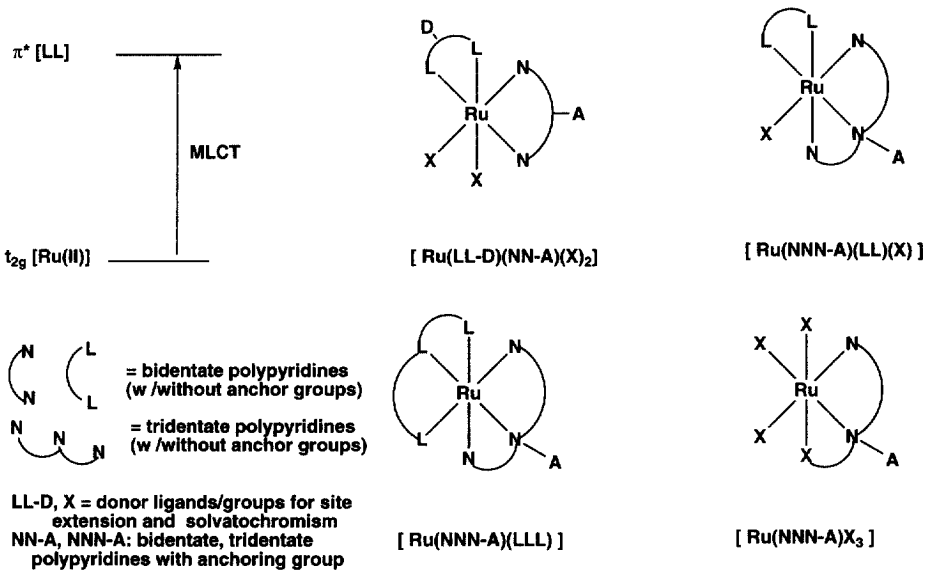

Fig. 8. Molecular design of photosensitizers for use in dye-sensitized solar cells. LL, NN refer to bidentate polypyridines such as 2,2′-bpy, 1,10-phen. NNN refer to tridentate polypyridine such as terpyridines. A and D refer to anchoring and donor groups (peripheral substituents).

4.3.1.4. Choice of counterions and degree of protonation (overall charge). Counterions and degree of protonation (overall charge) are selected to ensure sufficient solubility in organic, aqueous solvents and control of proton and water content in the pores during the loading of the dye.

4.3.1.5. Choice of peripheral groups. Peripheral groups (axial ligands, long chain substituents, etc.) that can lead to considerable reduction in the tendency of the dye to aggregate or stack in solution or on the surface are chosen.

4.3.1.6. Choice of amphidentate ligands. Amphidentate ligands or sites where further metal chelation can take place leading to further tuning of spectral response (e.g. via solvatochromism) are chosen.

4.3.2. Polypyridyl complexes as photosensitizers

As far as choice of sensitizers concerned, major emphasis has been on polypyridyl complexes of transition metals, particularly Ru(II). In the last two decades a vast amount of literature has grown on the photophysics and photochemical properties of these complexes [54,63–68]. Quantitative analysis of the spectral, electrochemical and photophysical properties of several hundred complexes have led to clear understanding of the CT transitions, that it is now feasible to tailor-make complexes with desired properties. In polypyridine complexes of Ru(II), the MLCT transitions account for nearly all the visible light absorption. The MLCT transition

corresponds to promotion of an electron from a molecular orbital (MO) that is largely Ru(II) based (filled t_{2g} level) to a MO that is largely ligand based (empty π^* orbital of the bipyridine ligand) (Fig. 8). Thus the smaller the energy gap, the more red-shifted is the related MLCT transition.

The basic principles of molecular engineering that we have chosen to use in the design of photosensitizers can be outlined as follows. Given the above requirements it is logical to go for systematic design of a mixed ligand complex with different constituent groups each for a specific task. It has been found that, in high surface area, porous, nanocrystalline films it is easy to achieve absorbances of 2.0 for a few micron thick film, particularly with moderate size Ru–polypyridine complexes. In polypyridine complexes of Ru(II), the metal center (a d^6 ion in a strong ligand field) has a coordination number of six. Contribution of a single bipyridine ligand to the molar absorbance of the associated MLCT band in the visible region is ca. 4000–5000 M^{-1} cm^{-1}. Fig. 8 also shows some of the complex structures that have been examined recently. Hence the coordination shell can be filled by a combination of mono-, bi- and tri-dentate ligands in mixed ligand complexes of the type $[M(LL–A)_3]$, $[M(NN)(LL–A)(X)_2]$, $[M(LL)_2(NN–A)(X)]$, $[M(LL–A)(LL1)(LL)_2]$, $[M(LLL–A)(NN)(X)]$, $[M(LLL–A)(NNN)]$, $[M(LLL–A)(X)_3]$,... where LL–A stand for a bidentate ligand with the anchoring group (e.g. phosphonato-bpy), NN, a bidentate donor ligand (e.g. dimethyl-bpy), LLL–A a tridentate with the anchoring group (e.g. phosphonato-terpyridine) and X, a monodentate ligand. Cyanato (CN–) and thiocyanato (–SCN) ligands have been widely used in view of their amphidentate character (they can chelate through both the N– and C–/S–ends) and solvatochromic sensitivity. Table 3 lists examples of mixed ligand complexes that have been examined recently on nanocrystalline oxide electrodes.

4.3.3. Tuning of t_{2g} and π^* levels in polypyridine complexes

Numerous spectro- and electrochemical studies of polypyridine complexes have clearly established that the first oxidation and reduction potentials are good indicators of the electronic levels of the donor and acceptor MOs. The MLCT transition energy can be reduced either by tuning of the metal-based MO (t_{2g} tuning) or by tuning the polypyridine acceptor based MO (π^* tuning). The energy level of t_{2g} is determined largely by the electron density at the metal center. Hence electron-donating substituents (such as $-NMe_2$ or $-OMe$) on the polypyridine raise this level and thereby decrease the energy associated with the MLCT transition. Electron-withdrawing groups (such as –COO–) lower the level. Many of the mixed ligand complexes cited later as efficient photosensitizers are the outcome of this type of molecular engineering of the composition of the complex.

This tuning of redox levels concept can be demonstrated with a graded series of metal complexes with different peripheral substituents. Consider, for example, the spectral and redox properties in a series of mixed ligand complexes of the type $[Ru(dcbpy)_2(X)(Y)]$, where X and Y are electron-rich monodentate non-chromophoric ligands or bidentate polypyridine ligands [210]. The dicarboxy-bipyridine ligand was chosen as the anchoring ligand and also to ensure sufficient visible light absorption. In all these complexes, the lowest excited state is Ru → dcbpy CT. The

auxiliary ligands allow tuning of the energy of the Ru → dcbpy CT transition by increasing the charge density at the metal centre. Increasing the charge density at Ru raises the energy of the donor (t_{2g}) level, thereby decreasing the energy of the associated MLCT transition. If we take three representative cases of $Ru(dcbpy)_3$,

Table 3
Examples of Ru–polypyridine complexes that have been examined as photosensitizers in nanocrystalline TiO_2-based solar cells[a]

Ru complex	λ_{max} (ε, mM) in EtOH	References
M(LL)$_3$ type		
$Ru(bpy)_3$		[161]
$Ru(dcbpy)_2(H_2O)_2$	500 (11.9)[b]	[162]
$Ru(dcbpy)_3$		[84]
M(LL)$_2$ (NN) type		
[Ru(dmbpy)$_2$(dcbpy)]	462 (11.7)	[180]
[Ru(dmbpy)$_2$(CH_2)$_3$-cbpy)]	462 (10.4)	[180]
[Ru(dmbpy)$_2$(acac-bpy)]	462 (12.2)	[180]
[M(LL–A)$_2$(X)$_2$]		
$Ru(dcbpy)_2(Cl)_2$	534 (9.6)	[166]
$Ru(dcbpy)_2(Br)_2$	530 (8.4)	[166]
$Ru(dcbpy)_2(I)_2$	536 (6.8)	[166]
$Ru(dcbpy)_2(NCS)_2$	534 (14.2)	[166]
$Ru(dcbpy)_2(H_2O)_2$	500 (11.9)	[166]
$Ru(dcbpy)_2(CN)_2$	493 (14.5)	[166]
$Ru(dcbpy)_2(CN)_2$		[177]
$Os(dcbpy)_2(CN)_2$		[177]
$Ru(dcbpy)_2(H_2O)_2$	500 (11.9)	[166]
[M(LLL)(LL–A)(X)]		
Ru(bmipy)(dcbpy)($N(CN)_2$)	492(13.8)	[172]
Ru(bmipy)(dcbpy)(Cl_3-pcyd)	502 (13.0)	[172]
Ru(bmipy)(dcbpy)(H-pcyd)	506 (12.6)	[172]
Ru(bmipy)(dcbpy)(4Cl-pcyd)	506 (12.7)	[172]
Ru(bmipy)(dcbpy)(2Cl-pcyd)	506 (12.7)	[172]
Ru(bmipy)(dcbpy)(2Cl-pcyd)	506 (12.7)	[172]
Ru(bmipy)(4PO_3H-bpy)(NCS)	496(11.3)	[172]
Ru(bmipy)(Hdcbpy)(OH)	528 (10.5)	[171]
Ru(bmipy)(Hdcbpy)(NCS)	502 (14.0)	[171]
Ru(bmipy)(Hdcbpy)(CN)	486 (13.5)	[171]
Ru(bhipy)(Hdcbpy)(NCS)	500 (1.3)	[171]
Ru(bmipy)(Hdcbiq)(NCS)	580 (9.7)	[171]
[M(LLL–A)(X)$_3$]		
Ru (tc-terpy)($NCS)_3$]	620 (6.5)	[175]
[M(LLL–A)(LL)(X)]		
Ru(Hphos-terpy)(Me_2bpy)(NCS)	506 (9.0)	[169,173]

[a] dcbpy, 4,4′-dicarboxy-2,2′-bipyridine; dcbiq = bmipy, 2,6-bis(1-methylbenzimidazol-2-yl)pyridine; tc-terpy, 4,4′,4″-tricarboxy-2,2′:6,2″-terpyridine; phos-terpy, 4-phosphonato-2,2′:6,2″-terpyridine.
[b] ε in water pH 4.85.

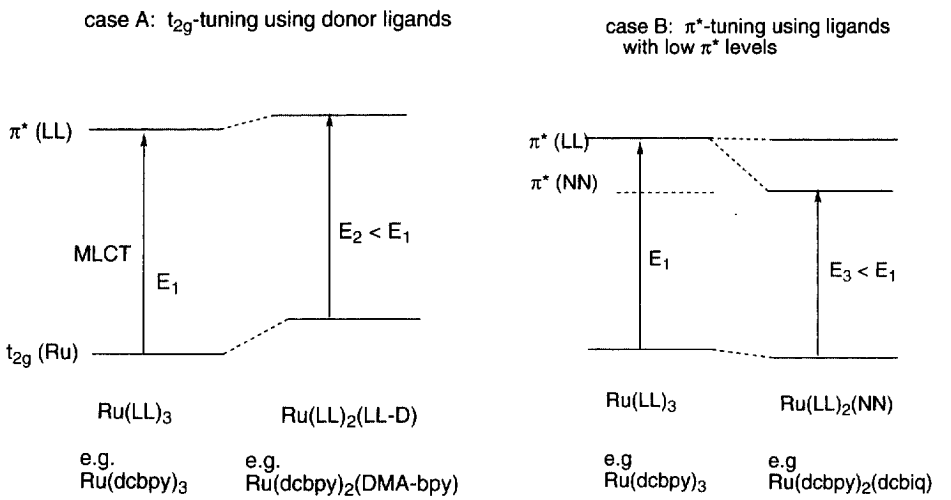

Fig. 9. A schematic representation of t_{2g} and π^* tuning of polypyridine complexes. (A) Replacement of an acceptor group (carboxyl) by a donor group (4,4′-dimethylamino) in one of the bipyridine ligand in [Ru(dcbpy)$_3$]. (B) Replacement of a carboxy–bipyridine ligand by dicarboxy-biquinoline in [Ru-(dcbpy)$_3$].

[Ru(dcbpy)$_2$(DEA-bpy)] and [Ru(dcbpy)$_2$(ph-py)], there is a gradual lowering of the energy of the MLCT state due to the presence of electron-rich ligands 4,4′-diethylamino-bpy (DEA) and an *ortho*-metalating ligand phenylpyridine (ph-py). Fig. 9 shows schematically the shift in the relative energy positions of the metal-centered (t_{2g}) and ligand-centered (π^*) orbitals. The lowering of the energy of the MLCT state is accompanied by a gradual decrease in emission quantum yield and shorter excited state lifetimes. Quantitative analysis for about 20 mixed ligands complexes showed that the enhanced decay of the excited state is due to enhanced radiationless decay. The rate parameters can be quantitatively explained in terms of energy gap law [63,64]. As per the energy gap law, non-radiative decay processes become more important decay channels with lowering of the energy of the lowest excited state. One of the efficient photosensitizers [Ru(dcbpy)$_2$(NCS)$_2$] referred to earlier was identified via this systematic tuning of optical and redox properties of the complexes.

4.3.4. Polynuclear polypyridine complexes as sensitizers

Even though the MLCT transitions of polypyridine complexes have a large bandwidth (> 80 nm), for a single chromophore, the light harvesting capacity is rather limited. One approach for efficient harvesting of sunlight would be to link several graded series of chromophores in a supramolecule using appropriate spacer or bridging units. Higher energy chromophores could transfer the excitation energy to the lowest energy unit and charge injection can take place from this unit. The efficiency of intramolecular energy- and electron-transfer processes in supramolecular assemblies will depend on the extent of electronic coupling between different

chromophoric units as modulated by the bridge. Amphidentate ligands such as cyanide (CN^-) and thiocyanate (NCS^-) are attractive candidates in this context. These ligand-bridged complexes are very stable in multiple oxidation states of the metal centers [19–22,67]. Mixed valence form of these complexes show moderately intense inter-valence (IT) transitions that facilitate study of electronic coupling between the constituent units. The cyano-bridged complex $Ru(dcbpy)_2$-$[Ru(bpy)_2(CN)_2]_2$ is a photosensitizer that belongs to this category. The central unit carrying dcbpy ligands and *N*-bonded cyanides is the lowest energy chromophore. Time-resolved emission, absorption and emission studies have shown that efficient intramolecular energy transfer occurs from the peripheral units to the central unit. Even though it is a trinuclear complex, the MLCT transition energies are similar and hence the overall conversion efficiency of this complex is comparable to that of the mononuclear complexes referred to earlier. There have been systematic studies of cyano-bridged trinuclear complexes of the type $[(X)(LL)_2(M_1-CN-M_2(NN)_2-M_1(LL)_2(X)]$, where M_1, M_2 = Ru, Os, LL, NN = bpy, dcbpy and X = Cl, H_2O, CN, etc. [211]. Depending on the nature of the metal, polypyridine and spectator ligands, the lowest energy chromophore can be placed on the central or peripheral units. Thus, by appropriate design, it is possible to construct supramolecules with a graded series of chromophores linked and follow the energy cascade upon excitation with white light.

In an intriguing experiment, Argazzi et al. [212] examined excited state charge injection in two isomeric Ru–Re complexes $[(dcbpy)(CO)_3Ru-CN-Ru(bpy)_2(CN)]$ and $[(dcbpy)(CO)_3Re-NC-Ru(bpy)_2(CN)]$ where the anchoring carboxyl group placed in the high-energy Re-chromophore. Photocurrent action spectra resembled closely the absorption spectra. Remarkably high monochromatic photocurrent efficiency obtained in these complexes raises questions as to whether a direct covalent linking of the chromophore involved in charge injection is necessary.

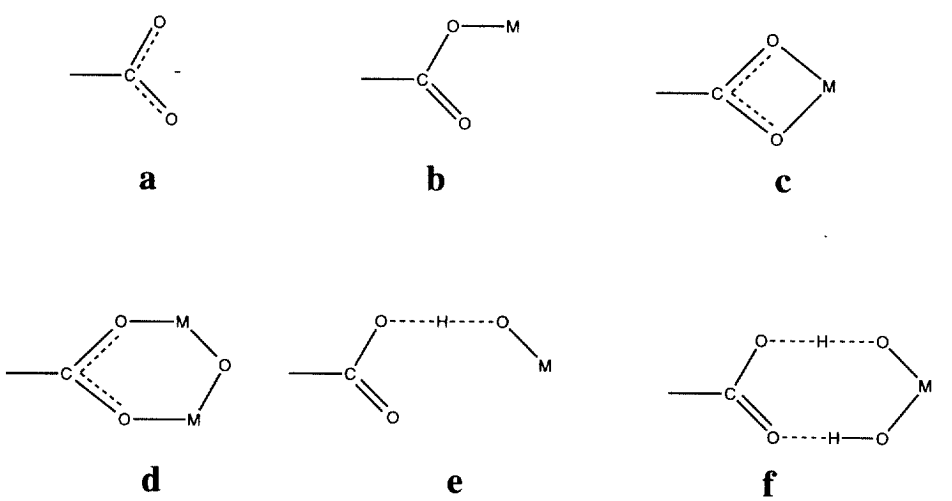

Scheme 1.

4.3.5. Surface chelation/anchoring of dyes

In view of the importance in influencing the performance of the solar cell, the nature of binding of chelates on sol–gel oxide films (TiO_2, SiO_2, ZrO_2, SnO_2, Al_2O_3) has been the subject of several investigations [108,182,213–223]. For oxide semiconductor surfaces, preferred anchoring groups are carboxylate, salicylate and phosphonate on the polypyridine ligand. 4,4′-dicarboxy-2,2′-bipyridine (dcbpy) and 6-phosphonato-terpyridine have been found to be very efficient. These functional groups are known to exhibit a high affinity toward the TiO_2 surface, with $\Delta G°$ ca. 30 kJ for salicylate at pH 5.7. If such affinities are not sufficient, it is possible to render adsorption quasi-reversibly by cross-linking the sub-units after adsorption. The adsorption of aryl and aliphatic carboxylic acids on TiO_2, for example, has been shown to follow Langmuir isotherm and surface chelation is accompanied by a decrease in the point of zero zeta potential (PZZP).

The carboxylic acid groups, while ensuring efficient adsorption of the dye on the surface of the amphoteric oxide TiO_2 promote electronic coupling between the donor levels of the excited dye (a MO which is largely π^* of the ligand in character) and the acceptor levels of the semiconductor (3d wave function/conduction band of TiO_2). Scheme 1 shows some of the possible modes of chelation/derivatization, where M is a surface ion or atom (Si, Sn or Ti).

They can be physical adsorption (perhaps via H-bonding) or chemical bond formation to the surface by unidentate, chelating or bridging mode of attachment. A variety of hydrogen-bonding structures could be drawn involving one or both of the carboxylato groups, two of which are included in Scheme 1.

There have been reports of cases where chelation of dyes on oxide surfaces leads to strong coloration (development of new charge-transfer absorption bands) and the resulting surface-bound complexes act as photosensitizer. Nearly two decades ago, Zollinger et al. [214] observed that certain azo-dyes (e.g *o,o′*-dihydroxyazo derivatives) form 1:1 Zn-complex at the surface of ZnO powders and this affords sensitization of ZnO to visible light. Similarly metallophthalocyanines formed at the surface of CdS by immersing the CdS in a phthlonitrile melt increased the spectral response of the semiconductor. Recent examples of this category are 8-hydroxyquinoline, $Fe(CN)_6^{4-}$, phenyl fluorene and $Ru(bpy)_2(CN)_2$ [215,216] adsorbed onto TiO_2 surfaces. 8-Hydroxyquinoline forms a yellow complex that was effective in sensitizing the visible light induced generation of hydrogen from water. The surface chelate of phenylfluorene on TiO_2 has a distinct absorption band in the visible at 476 nm ($\varepsilon = 3.6 \times 10^4\ s^{-1}$). Electronic excitation in this band leads to extremely rapid and efficient injection of electrons onto the conduction band of the semiconductor. A lower limit for the rate constant of interfacial electron transfer was determined as $10^8\ s^{-1}$ and the back electron transfer was found to occur with a specific rate of $2.8 \times 10^5\ s^{-1}$. The injected electrons in the conduction band readily reduce electron acceptors such as methyl viologen efficiently in the same manner as when they are produced by bandgap excitation of the semiconductor. In the case of $[Ru(bpy)_2(CN)_2]$, surface chelation is indicated by red-shift in the photocurrent action spectra-maximum observed at 515 nm while it is at 493 nm in solution. For

the corresponding bis-chloro complex, the photocurrent action spectrum has a maximum at 566 as compared to 534 nm observed in solution.

Examination of the IR and Raman spectra of the carboxylic acid (–COOH), ester (–COOEt), carboxylato anion (–COO–) with those obtained for surface-bound dyes can provide useful clues on the dominant mode of binding [219–221]. The following IR, Raman active bands can be considered as key markers: C=O stretch of the ester and acid derivatives in the vicinity of 1730 and 1550 cm^{-1}, and O–C–O– asymmetric stretch of carboxylato anion at ca. 1615 cm^{-1}. The similarites between the spectra on SnO_2 and TiO_2 and the ester derivative in solution point to chemical bonding and ester formation to the surface and structure B in Scheme 1. The spectrum on SiO_2 is nearly identical to the spectrum of the carboxylato derivative, which points to either chelate C or bridge bonding mode D. Bonding as per mode B (or ester) plays a minor role on silica surfaces.

Based on a comparison of vibrational and X-ray structural data for a series of acetates and trifluoroacetates, Deacon and Phillips [222] have provided some guidelines regarding carboxylato binding to metal ions. In this approach, the positions and differences between carboxylato frequencies in the complexes and ionic salts are compared. As a unidentate ligand, carboxylato loses the equivalence of the two carbon–oxygen bonds and the peak near 1600 cm^{-1} in the free ion shifts to higher energy. The magnitudes of d for $[\nu_{asym}(COO-) - \nu_{sym}(COO-)]$ or $[\nu(C=O) - \nu(C-O)]$ are greater for ester-type linkages (structure B) than for ionic carboxylates. The data for $[Ru(bpy)_2(dcbpyH_2)]$ bound to TiO_2 and SnO_2 are consistent with this type of attachment. IR and Raman data alone do not allow inference as to whether one or both of the carboxylato groups are bound to the surface. A single carboxylate group and by inference, a single ester link is sufficient to create stable structures on the surface. Based on molecular modelling calculations, Meyer et al. proposed a binding mode where one carboxyl group binds as ester and the other via H-bonding [219]. Based on single ester mode binding and Langmuir adsorption, surface binding constant K has been determined by equilibration to be $8 \pm 6 \times 10^4$ M^{-1} (CH_2Cl_2, 293 K) for $Ru(bpy)_2(dcbpy)_2$ on SnO_2, in the same range reported earlier for cyano-bridged Ru-trinuclear complex. McQuillan and coworkers have elaborated [217,218] on the use of ATR-FTIR spectroscopy in situ to study chelation of small molecules and metal complexes on sol–gel films of TiO_2, ZrO_2 and Al_2O_3.

4.3.6. Porphyrins and phthalocyanines as sensitizers

Along with polypyridines, metalloporphyrins form the second major series of potential photosensitizers. However there have been only very limited number of studies using porphyrins on nanocrystalline semiconductor electrodes [223–227]. A number of naturally occurring porphyrin derivatives carry carboxylic groups as one of the peripheral substituents. The pH-dependence of the surface charge of colloidal particles of TiO_2 can be used to control the adsorption and desorption of dyes on to the semiconductor surfaces. Thus anionic porphyrins such as Zn-tetracarboxyphenyl-porphyrin [223], Zn uroporphyrins [224] bind to cationic surfaces at $pH \leq 5$. Concurrent monitoring of the photophysical properties of the porphyrins

allow monitoring of the excited state quenching (via electron transfer and other ways) in singlet and triplet manifolds. Flash photolysis and microwave absorption studies of copper chlorophyllin [225] in the presence of colloidal TiO_2 indicated possible sensitization by these derivatives. Dabestani et al. [84] examined sensitization of the Zn tetracarboxyphenyl porphyrin (ZnTPPC) on porous, nanocrystalline electrodes and obtained a maximum quantum efficiency of 9.5 and 27% on TiO_2 and $SrTiO_3$ films, respectively.

As part of his Ph.D. work, Kay [226] examined recently the photosensitization efficiency of a number of chlorophyll derivatives and their naturally occuring analogs anchored on to nanocrystalline TiO_2 electrodes. Monochromatic efficiencies in the range 60–83% were obtained in the region of the maxima of Soret and Q-bands for a number of porphyrin derivatives: chlorophyll a, Mg-chlorin-e_6, Cu-chlorin-e_6, pheophorbide a, H_2-chlorin-e_6, Cu-2-a-oxymesoisochlorin-e4, H_2-mesoporphyrin IX, Zn-mesoporphyrin IX and Cu-mesoporphyrin IX. In the case of Cu-mesoporphyrin IX, IPCE values of 83% for the Soret band at 400 nm corresponds to nearly unity quantum efficiency when light reflection losses are taken into account.

For white light, the conversion efficiencies obtained with metalloporphyrins are low, mainly due to poor absorption in the major part of the visible spectrum. While polypyridine complexes show moderately strong absorption in the 400–600 nm region, light absorption of porphyrins in this region is very poor. Comparison of different chlorophyll derivatives indicates that the free carboxyl groups are important for adsorption and sensitization of TiO_2. In limited trials on a solar cell using tetrapropylammonium iodide, iodine mixture in 50:50 ethylene carbonate/acetonitrile, a Cu-2-a-oxymesochlorin sensitized TiO_2 electrode delivered an electrial charge of 200 C cm^{-2} in 18 h illumination, corresponding to a turnover of 105 per dye molecule. There has also been reports [227] of electron trapping in porphyrin-sensitized porous nanocrystalline TiO_2 electrodes.

Another factor that limits the practical utility of metalloporphyrins as photosensitizers is their tendency to aggregate readily. Porphyrins are known to aggregate in solution even at low concentrations (10^{-5} M) via $\pi-\pi$ interactions involving the porphyrin delocalised aromatic ring system. Presence of axial ligands can inhibit this stacking interactions leading to aggregation. It has been found that presence of co-adsorbates such as bile acid derivatives improves significantly the light conversion efficiency. Both photocurrent and voltage can be improved appreciably by addition of cholanic acid derivatives (such as deoxycholic acid) to the ethanolic solution used for dye-uptake. The effect also occurs on pre-adsorption of cholanic acids while post-adsorption on an already colored electrode is less effective. Rather high concentrations (10-fold with respect to the porphyrin) are often employed. These cholic acids are steroid derivatives and it is likely that they adsorb on the TiO_2 surface with their carboxyl and hydroxyl functions.

In her preliminary studies, A. Wiederkher ([228]a) examined the sensitization efficiency of Zn(II) derivative of tetracarboxy-phthalocyanine (ZnTCPc) on nanocrystalline TiO_2 film electrodes. ZnTCPc has a strong tendency to aggregate in solution. A single band at 640 nm observed in DMSO at low concentration is

replaced by a broad absorption with double maxima at 640 and 690 nm. In non-ionic micellar medium of Triton X-100, the relative intensity of the dimer band can be varied by varying the [dye] to [micelle] ratio. On TiO_2 electrodes, the photocurrent action spectrum is very broad in the red region with two distinct maxima at 640 and 690 nm. The maximum IPCE obtained in the 600–750 nm region was 15%. Addition of co-adsorbates such as bile acids (cheno-deoxycholic acid) or axial ligating molecules such as pyridine improves significantly the monochromatic conversion efficiency to ca. 40%.

In recent studies, a Ru(II)-phthalocyanine derivative, [bis(3,4-dicarboxypyridine)(1,4,8,11,15,18,22,25-octamethyl-phthalocyanato)ruthenium(II)] (JM3306) has been found to be an efficient photosensitizer for excited state charge injection in nanocrystalline TiO_2-based solar cells ([228]b). The dye was coated on to TiO_2-electrode using ethanolic solutions containing 40 mM 3α,7α,-dihydroxy-5β-cholic acid as an additive to avoid surface aggregation of the sensitizer. The photocurrent action spectrum obtained on nanocrystalline TiO_2 is relatively broad with IPCE values in the vicinity of 60% obtained around 660 nm. The surface attachment of the dye is presumably through the axial dicarboxypyridine ligands. Despite the fact that the pyridyl orbitals are not directly involved in the $\pi-\pi^*$ excitation which is responsible for the 650 nm band, electronic coupling of its excited state to the Ti 3d conduction band manifold is strong enough to render charge injection process efficient. Bignozzi and coworkers have reported recently [181,182] efficient sensitization using Ru–polypyridine complexes where the coupling of the MLCT excited state to the conduction band manifold was through space and did not involve the anchoring group.

5. Mechanistic studies of dye-sensitized nanocrystalline solar cells

5.1. An overview of mechanistic studies in model systems

In view of the better conversion efficiency obtained using nanocrystalline electrodes, there have been many mechanistic studies of the details of operation of the solar cell. Early experimental support for the mechanism, shown in Fig. 4, comes from the observed correlation relating the redox potential of the dye, the ionization potential of the dye in the ground and excited state with the semiconductor donor/acceptor levels and the observed spectral sensitizing ability of the dye. Another line of evidence for efficient charge injection occurring from adsorbed dyes comes from model system studies using dye-colloidal semiconductor mixtures [53,229]. The translucent nature of the finely dispersed colloidal semiconductor sols allow direct monitoring of the photoredox processes by fast time-resolved techniques. In aqueous solutions of amphoteric oxide colloids, the nett charge carried by the colloidal particle depends on the pH. Above the isoelectric point (or PZZP), the colloids are negatively charged, while they are positively charged at low pH values. The electrostatic charge-driven movement of these charged particles towards the anode or cathode can be directly monitored in electrophoretic studies and the

mobility can be measured. Using anionic or cationic dyes and controlling the solution pH, it is possible to selectively adsorb/desorb the dyes from the semiconductor surface. Monitoring of the singlet and triplet excited state properties as a function of pH showed that, the quenching of the excited state is intimately linked to the state of adsorption. Efficient quenching of excited state(s) takes place if and only if the dye is adsorbed onto the semiconductor. In the absence of other reagents, the oxidized dye is reduced back to the ground state by the conduction band electrons. Data on the rate constants for excited state quenching and charge injection and reverse electron transfer have been obtained for several dye-colloid combinations [53,229].

Reactions 12–17 below are some of the key reactions that we will consider. For simplicity let us consider the excited state manifold of the dye to consist of a series of singlets and triplets and the charge injection step occurs from the lowest singlet excited state. For metal complexes with heavy transition metal ions such as Ru^{2+} extensive spin–orbit coupling leads to extremely rapid formation of the luminescent MLCT state that is predominantly triplet in character. McCusker et al. recently reported formation of luminescent CT state of $Ru(bpy)_3^{2+}$ on fs timescales [230].

$$S + h\nu \rightarrow S_n \rightarrow S^* \tag{12}$$

$$S^* \rightarrow S_0 + h\nu_1 \text{ (luminescence)} \tag{13}$$

$$S^* \rightarrow S_0 \text{ (internal conversion)} \tag{14}$$

$$S^* \rightarrow T_0 \text{ (inter-system crossing)} \tag{15}$$

$$S^* + SC \rightarrow S^- + e_{cb}^-(SC) \text{ (charge injection)} \tag{16}$$

$$S^* + S \rightarrow 2S \text{ (concentration quenching)}$$

$$e_{cb}^-(SC) \rightarrow e^-(TCO) \text{ (percolation)} \tag{17}$$

Depending on the energy of the absorbed photon, one can populate any of the upper or lower singlet excited state (S_0 or S_n). The optical excitation process itself (Reaction 12) is instantaneous (a few fs or less) followed by ultra-fast internal conversion to the lowest excited state of interest (excited state involved in electron transfer) which we denote simply as S*. The excited singlet state can decay either by electron-transfer to the conduction band of the semiconductor (Reaction 16) or in competitive pathways such as non-radiative decay to the ground state (Reaction 14) or inter-system crossing to the triplet state (T_0) (Reaction 15). Let us consider the excited state quenching via electron-transfer and other pathways. The key questions are (a) how efficient is the excited state quenching? (b) how fast is the charge injection step from the excited state itself? and (c) is electron-transfer to the conduction band of the semiconductor only or the dominant process?

The list (Reactions 12–17) shown above corresponds to the simplest case where the lowest singlet excited state S* alone takes part in the charge injection process. In cases where the inter-system crossing kinetically competes with singlet state quenching, substantial amounts of triplet excited state (T*) can be produced. Energetics permitting, charge injection can take place from the triplet excited state

as well. It was mentioned earlier that in transition metal complexes, the spin–orbit coupling can be very pronounced, leading to formation of mixed/pseudo triplet excited state extremely rapidly and electron-transfer reactions take place from this excited state. Polypyridine complexes of Ru(II) would be a typical example.

Time-resolved monitoring of the luminescence decay is the most direct measure. Transient absorbance changes corresponding to formation of the excited state (S*) and the dye cation (S^+) provide equally direct measurements of rate constants. Experimentally the latter are difficult to execute and also in analysis of the kinetic data due to extensive overlap in the absorption of S* and S^+. Luminescence decay as a function of surface coverage (ϑ) is an elegant way of knowing if the dye aggregation leads to additional quenching pathways. Excited state deactivation processes unrelated to charge injection are best studied using inert surfaces—materials where there are no electron donor or acceptor levels in the vicinity of the redox levels of the dye in the ground and excited state. Muenter [231] used the large decrease in the fluorescence lifetime and quantum yields of two carbocyanine dyes observed upon adsorbing on to AgCl, AgBr single crystals as compared to that seen in a photographically inert medium such as gelatin to deduce rate constants in the range 10^9–10^{10} s^{-1} for the charge injection process.

Measurement of transient photocurrents is another useful technique in this regard. This can be carried out without any external bias (open-circuit) or with the electrode held at a fixed potential using a potentiostat. The nature of the electron-flow (anodic or cathodic) is a direct measure of the direction of electron flow (from the dye to the semiconductor or from the semiconductor to the adsorbed dye or to solution species). The magnitude of the photocurrent however is a complex quantity, at least in the case of nanocrystalline electrodes where it is a measure of the net charge collected at the back TCO electrode. The electrons have to pass through several particles to arrive at the collector electrode and there can be losses on the way by trapping at defect sites. Probably on clean single crystal electrodes the photocurrent intensity is more directly related to excited state charge injection. In fact in early studies a major puzzling question was lack of any correspondence between the excited state decay as monitored by luminescence decay at various dye coverage (ϑ) levels and charges collected in the form of measured photocurrent. It was pointed out earlier that in cyanine dyes extensively used in photography, some of the higher form (J-aggregates) are good sensitizers. In such cases, monomer fluorescence intensity decreases much more drastically with increasing surface coverage while photocurrent decreased much more slowly. Efficient migration of excitation energy in the form of excitons in higher form of J- and H-aggregates to trap sites can also lead to excited state quenching.

There have been a number of studies of luminescence of adsorbed aromatic hydrocarbons on insulating oxide surfaces such as silica (SiO_2), alumina (Al_2O_3), and magnesia (MgO) [232–235]. Oxide surfaces have large number of hydroxyl groups and the nature of the surface depends largely on the pre-treatment history of the sample and subsequent exposure (if any) to atmospheric gases, dust etc. High temperature treatment of the surface can lead to a re-structuring of the surface, leading to valence-deficient trap sites. Adsorption of arenes on these sites leads to

charge-transfer interactions (for pyrene these CT states can be detected spectroscopically) and efficient quenching of excited states. Thomas and coworkers [235] recently have provided quantitative data on the luminescence and quantum yields for singlet and triplet excited state on insulating oxides and how they vary with surface treatment. van der Waals surfaces of layered semiconductors such as WSe_2, $MoSe_2$, WS_2 and SnS_2 are chemically inert due to saturation of bonding. Parkinson and Spitler [236,237] have shown that by using defect-free surfaces it is possible to obtain high IPCE values. In view of the low bandgap of these materials, the authors used a number of IR light absorbing dyes as sensitizers. IPCE of >0.8 (and $\eta > 4\%$) were obtained with pentathiacyanine dyes adsorbed on WSe_2.

Excited state charge injection of xanthene and cyanine group dyes on oxide surfaces has been extensively examined [238–245]. Itoh et al. [238] measured fluorescence spectra, lifetimes and intensity of rhodamine B adsorbed on to SnO_2, TiO_2 and glass substrates as a function of the surface coverage. On a glass surface, the fluorescence intensity increased linearly for low ϑ. It has been estimated that $>90\%$ of the adsorbed dye exists in monomer state form when $\vartheta < 0.7$. Thus aggregation is rather small even at high coverages. The rate of charge injection to the conduction band was estimated to be $7.4 \times 10^8\ s^{-1}$ for SnO_2 and $< 3 \times 10^7\ s^{-1}$ for TiO_2. In a related study of rhodamine B on TiO_2 and ZrO_2, Hashimoto et al. found a weak temperature dependence of fluorescence intensity and decay, indicating the excited state electron transfer to be almost activationless. Nakashima, Willig et al. [239] analyzed the florescence decay of rhodamine B adsorbed on to aromatic hydrocarbon crystals and obtained rate of hole injection from excited RhB as 10^{10} s^{-1}.

Anfinrud et al. [240] followed bleaching recovery of rhodamine 640, 3B dyes on ZnO, fused silica as a function of surface coverage. On ZnO, the kinetics can be fitted to two exponentials of 9.3–13.3 and 61–87 ps. On silica much longer lifetimes (290–540 and 19.7–23.0 ps) were obtained. Liang [241] studied the emission decay of rhodamine B, eosin on SnO_2, transparent conducting oxide (TCO) and quartz glass surfaces. The dye was adsorbed directly from the solution. The lifetime was nearly the same (47–55 ps), in all cases irrespective of the nature of the surface (semiconductor or insulator). Crackel and Struve [242] examined cresyl violet decay on TiO_2 (rutile) surface, diluted with arachidic acid. Without the co-adsorbates, the decay was very fast (≤ 300 ps). With spacers, the decay was fitted to two exponentials (53–72 and 946–2012 ps). Control experiments on quartz glass showed a much longer lifetime of 2200–2400 ps indicating absence of any surface energy transfer. In their study of charge injection from adsorbed oxazine dye on SnS_2 electrodes, Lanzafame et al. [243] found the excited state electron transfer to occur in < 100 fs, followed by recombination with biphasic kinetics of 10 ps and a variable component in the hundreds of ps range. These components were assigned to direct recombination (electron recombining at the same dye molecule from which it was injected) and indirect recombination (electron relaxation/diffusion to another recombination center or dye cation). Hashimoto et al. [244,245] followed the luminescence decay of $Ru(bpy)_3^{2+}$ adsorbed on to TiO_2 particles and found the emission to decay rapidly but in a complex manner. A four-component fit was used.

Table 4
Time-resolved measurements data on the rates of excited state charge injection of adsorbed dyes and back electron transfer in semiconductor colloids and nanocrystalline films

Dye[a]	τ_o (EtOH) (ns)	Semiconductor[b]	k_{inj} (s^{-1})	τ_{back}	References
$[Ru(bpy)_3]^{2+}$	620	TiO_2 coll	2×10^5		[162,163]
$[Ru(dcbpy)_3]$	600	TiO_2 nc	3×10^7	0.33 μs	[263]
Anthracene-9-COOH	9.1	TiO_2 coll	5.9×10^8		[226]
Chlorin-e_6	5.3	TiO_2 nc	2.5×10^9		[26]
Cu-chlorophyllin		TiO_2	4.2×10^9		[229]
Cresyl violet	3.0	TiO_2 sc	3×10^{11}		[242]
$[Ru(dcbpy)_2(H_2O)_2]$		TiO_2	$>1.4\times10^{11}$		[246]
Perylene derivative		TiO_2 nc	5×10^{13}		[251]
Coumarin-343	10	TiO_2 sols	5×10^{13}	0.5 μs	[248]
$[Ru(dcbpy)_2(NCS)_2]$	50	TiO_2 nc	$>4\times10^{14}$		[250]
$[Ru(dcbpy)_2(NCS)_2]$	50	TiO_2 nc	$>8\times10^{13}$		[247,249]
$[Ru(dpbpy)_3]$	500	TiO_2 nc	$>1\times10^{12}$	20 ns	[258]
9-Anthracene-COOH	9.1	TiO_2 sol/EtOH	$\geq3\times10^{13}$	33 ± 2 ps	[259]
Anthocyanin	2.6	TiO_2 sol/EtOH	$\geq1\times10^{13}$	0.52, 67 ps	[254]
$[Ru(bpy)_2(dcbpy)]$	230	SnO_2 nc	4×10^8		[33]
$Ru(bpy)_3^{2+}$	620	SnO_2 coll	$\approx1\times10^8$		[101]
Pd-Chlorophyll		SnO_2	1.6×10^9		[238]b
Chlorophyll-b	4	SnO_2	$>4\times10^8$		[193]
Cresyl violet	3.0	n-SnS_2 sc	$>1\times10^8$		[246]b
Rhodamine B	2.5	n-SnO_2	$>1\times10^8$		[246]
Rhodamine B	2.5	SnO_2	2×10^{10}		[244]b
Rhodamine B	2.5	SnO_2	2×10^{10}		[241]a
Oxazine-1		n-SnS_2 sc	2.5×10^{13}	10 ps	[243]a
Thiacarbocyanine		AgBr	2×10^{10}		[246]c,d

[a] dcbpy, di(carboxy)-bipyridine; dpbpy, di(phosphonato)-bipyridine.
[b] nc, nanocrystalline film; coll, colloids; sc, single crystal.

The behavior was different in vacuo and upon introduction of water vapor. The accelerated decay of the emission on TiO_2 as compared to that seen on SiO_2 and porous vycor glass (PVG) is attributed to electron transfer.

5.2. Recent studies of excited state charge injection in nanocrystalline films

Muenter's time-resolved fluorescence decay study [231] of dyes adsorbed on to silver halides in 1976 was probably the first (with ns time resolution) direct probing of dye sensitization mechanisms. The time resolution was increased to the ps range

in 1980 with measurements by Nakashima, Yoshihara and Willig [239] on fluorescence decay kinetics of rhodamine B on aromatic hydrocarbon crystals. In the last few years there have been many direct kinetic measurements of the key processes taking place on nanocrystalline films by spectroscopic and electrochemical techniques [246–262], the former with fs time-resolution. A quantitative picture is slowly beginning to emerge. To assist a clear picture, the functional details fo the solar cell will be described in the form of several questions and possible answers as inferred with the available experimental data.

If we assume that the observed decrease in the luminescence lifetime on the oxide surfaces is entirely due to charge injection and that the other radiative and non-radiative decay processes of the dye on surface occur at the same rate as in a neat solvent, the charge injection rate can be deduced from the expression:

$$(1/\tau_{ads}) = (1/\tau_{solv}) + k_{inj} \tag{18}$$

where τ_{ads} and τ_{solv} refer to the excited state lifetime in the adsorbed state on the oxide semiconductor and in a neat solvent, respectively and k_{inj} is the specific rate constant for the charge injection process. Clearly when extensive quenching takes place, $\tau_{ads} \ll \tau_{solv}$ and $(1/\tau_{ads}) \approx k_{inj}$).

Recent studies with different sensitizers anchored on to nanocrystalline TiO_2 and other semiconductors have shown that the forward electron transfer (injection of electrons into the conduction band by the electronically excited state of the dye) is extremely rapid (a few ps or much less). Table 4 presents a collection of time-resolved measurements on the kinetics of charge injection and back electron transfer involving semiconductors as acceptors. In majority of the cases ultra-fast decay of the excited state is directly linked to charge injection. The dye cation radical is formed with a yield of nearly 100%. The subsequent recombination reactions occur over a much longer timescale (several μs or longer). Thus the conditions are ideal for light induced electron transfer to occur with high quantum efficiency. But it should be emphasized that, observing ultra-fast decay (< ps) of excited state of the sensitizer on semiconductor itself is not a direct proof that the quenching process is only via electron-transfer. There are many documented cases where the measured photocurrent yield is quite negligible yet the excited state decay is extremely rapid. Only in very few cases the yield of redox products (sensitizer cation) has been measured directly in fast transient absorbance studies.

Ultra-fast charge injection rates (in the fs range) measured recently for several sensitizers adsorbed on to TiO_2 raises fundamental questions as to whether the electron transfer does take place from unrelaxed excited states. Ultra fast electron transfer implies ultra-fast charge separation and a slow back reaction. In a number of cases, the excited state charge injection process has been found to be independent of temperature down to 4 K, indicating that the electron-transfer is an activationless process and hence not subject to the kind of dynamical picture that would emerge from classical treatments using the Marcus–Levich equation. Fig. 10 shows schematically one possible scenario for such ultra-fast electron transfer involving anchored dyes. In classical electron transfer quantitatively treated under Marcus–Levich–Jortner–Gerischer type formalism, optical excitation is followed by rapid

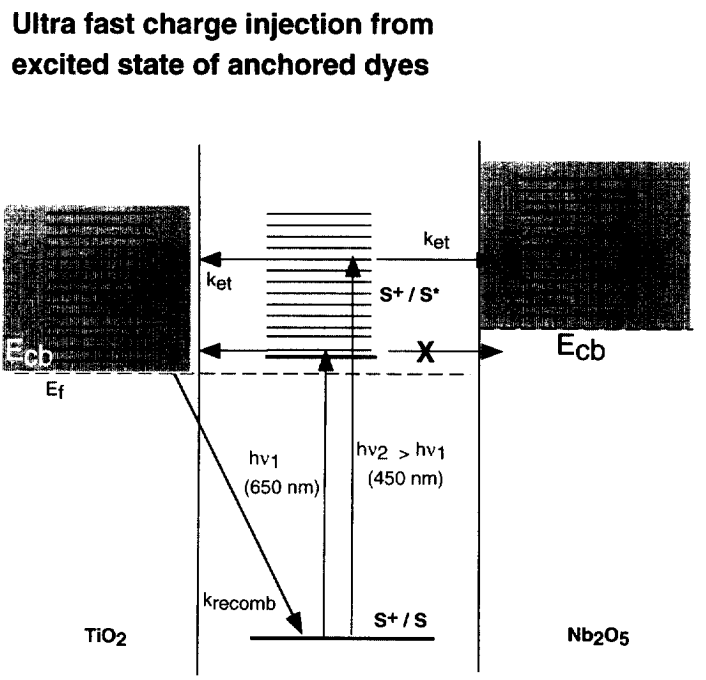

Fig. 10. Schematic representation of excited state charge injection into a continuum of acceptor states (conduction band) of the semiconductor in dye-sensitized solar cell for excitation at two different excitation wavelengths (450 and 650 nm). Shown on the left are possible excited state electron transfer processes for the case of TiO_2. On the right are shown possible charge injection processes with Nb_2O_5 as the semiconductor.

vibrational relaxation (fast redistribution of vibrational energy amongst the sensitizer molecules). In a situation where the photoexcited dye is strongly coupled to the surface, the level matching (in Marcus theory) that ensures energy conservation during electron transfer involves not simply molecular (vibrational) energy level as in solution reactions, but rather a continuum of electronic energy levels that exist in the semiconductor. In such a case, when the donor system is coupled to an electronic continuum and nuclear degrees of freedom are neglected, the rate constant for transfer is given by the golden rule expression:

$$k_{inj} = (2\pi/h)|V|^2\rho \tag{19}$$

where $|V|$ is the electron coupling matrix element and ρ is the density of electronic acceptor states in the semiconductor. The subsequent dephasing which traps the electron can occur on an ultra-fast timescale if the electronic states is high (i.e. above the band-edge) and the electronic coupling between the dye and the semiconductor is large. Thus the injection efficiency is primarily attributed to strong electronic coupling.

Willig [250] has described the ultra-fast charge injection process as electron transfer by electron tunneling but with a finite reaction time. The finite reaction

time allows for the motion of the vibrational wave packet in the time span between the generation of the excited reactant state and the appearance of product states. The reverse electron transfer of the electronic wave packet representing the initially formed hot electron in the semiconductor is considered virtually impossible, since this wave packet spreads in time and moves away from the reaction distance. After a series of inelastic and elastic events, the injected electron can return to the interface; however, the wave packet representing the electron will now be completely different; it will have lost energy, changed momentum, etc.

It is instructive to compare the measured rate constants (k_{inj}) and measured quantum yields with values for the electronic coupling matrix element $|V|$ calculated using the golden rule expression (Eq. (19)) for various sensitizers adsorbed onto colloidal or nanocrystalline TiO_2. Ultra-fast quenching and high injection yields are always accompanied by a substantial increase in the electronic coupling matrix element $|V|$. In the case of complexes bound via carboxylic group, there is strong coupling between the π^* orbital of the dye excited state and the empty Ti(IV) 3d orbital manifold of the semiconductor. Representative values of $|V|$ (in cm^{-1}) are: 0.04 for $[Ru(bpy)_3]^{2+}$; 0.3 for $[Ru(dcbpy)_3]$ in water; 100 for coumarin-343; 130 for $[Ru(dcbpy)_2(NCS)_2]$. In the case of alizarin, which forms a strong colored complex on the surface, optical excitation correspond to excitation into the LMCT band itself where the role of the metal is played by surface Ti^{4+} ions.

One question that has not been investigated until recently is wavelength dependence—if any—of the monochromatic injection efficiency for the excited state charge injection process. In the simple picture (Fig. 4), only those dyes whose redox potential for the lowest excited state is above the conduction band-edge can participate in photo-induced electron transfer. If injection from hot or vibrationally unrelaxed state is feasible, then, for those dyes whose excited state redox potential is just below the conduction band-edge, there exists the possibility for charge injection for high-energy excitation but not for low energy photons. Moser has recently examined ([247]d) the wavelength dependence of the standard dye $[Ru(dcbpy)_2(NCS)_2]$ on two oxides surfaces (TiO_2 and Nb_2O_5) and [Ru(bmip)(dcbiq)(NCS)] on TiO_2 (dcbiq, 4,4′-dicarboxy,2,2′-bipyridine; bmip, 2,6-bis(1-methylbenzimidazol-2yl)pyridine):

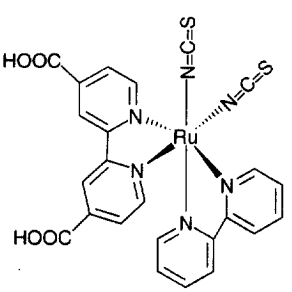

$[Ru(dcbpyH_2)_2(NCS)_2]$

$Eo(S^+/S^*) = +1.10V$ vs NHE

$\Delta E_{0,0} = 1.75$ eV

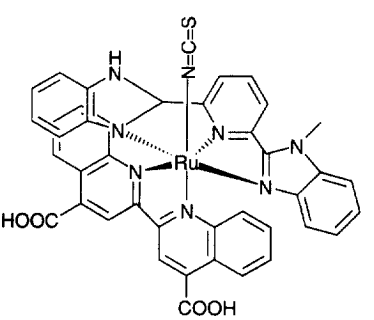

$[Ru(dmipH_2)(dcbiq)(NCS)]$

$Eo(S^+/S^*) = +1.60V$ vs NHE

$\Delta E_{0,0} = 1.60$ eV

Nb_2O_5 has the same bandgap energy as TiO_2 (3.2 eV) but has its conduction band located 0.2–0.3 eV more negative with respect to that of TiO_2. For excitation with 650 nm photons, photo-induced charge injection from bis(thiocyanato) complex can occur on TiO_2 (due to its more favorable location of E_{cb} with respect to E(S*) but not on Nb_2O_5 (see Fig. 10). For excitation at 450 nm, charge injection can take place on both these oxide semiconductors. Analogous situation is present when one compares the photo-induced charge injection on TiO_2 for the two Ru dyes cited above. For the fixed acceptor (TiO_2), the donor levels are differentiated by nearly 0.5 V. The excited state redox potential of the 4,4′-dicarboxy-2,2′-biquinoline dye is located just below the conduction band-edge of TiO_2. Optical excitation of the dcbiq complex with a low energy photon (650 nm) can lead to charge injection while similar excitation of the dcbpy complex yields negligible yields. Thus there are now preliminary indications that charge injection indeed can take place from hot, vibrationally un-relaxed excited state and this in turn, in select cases, results in a wavelength dependence of injection yields (IPCE).

5.3. Dynamics of reverse electron transfer and its implications for overall sensitization efficiency

A key feature of the nanocrystalline TiO_2 solar cells with Ru–carboxy bipyridine based sensitizers is relatively slow back electron transfer (≤ 100 ns) after forward electron injection. Several orders of magnitude difference in the forward and reverse electron transfer rates allow processing of the charge separated products very efficiently: reduction of the oxidized form of the dye by the redox mediators and percolation of the injected charges in the mesoporous layer to arrive at the back contact. In nanocrystalline films, there is hardly any space charge layer and the reverse electron transfer is a thermodynamically well-defined process. For Ru–bpy complexes, with $E(Ru^{3+/2+})$ located between 0.8 and 1.2 V and an $E_{cb}(TiO_2)$ of ca. -0.8 V, the driving force for the back electron transfer exceeds 1.6 eV. Such a large driving force should make the reaction kinetics fall deep in the inverted region in the classical Marcus description. Measurements of rate constants for the reverse electron transfer in question by Moser and Grätzel ([247]c) over a wide range of temperature range indicated it be invariant.

Yan and Hupp [258] recently extended these studies by studying the pH-dependence in a related nanocrystalline TiO_2 system using a Ru–bpy complex with six peripheral phosphanate groups (three of 4,4′-di-substituted bpy ligands). The anchoring ligand [4,4′-$(CH_2PO(OEt)_2)_2$-2,2-bpy] was prepared by reflux of bis-4,4′-bromomethyl-2,2′-bpy with triethylphosphite. As an amphoteric oxide, the TiO_2 surface is dominated by protonatable sites. Protonation of these surface hydroxyl groups alter the fermi levels. The flat-band potential of TiO_2 has been shown to vary by 59 mV for each pH unit changes by a number of techniques. The first order rate constant for the reverse electron transfer has been found to be invariant over a 19 pH unit range, corresponding to a >1 eV change in the apparent free energy of the semiconductor-bound electron. For conventional electron transfer (ET)

processes such large variation in the driving force would have resulted in several order of magnitude variation in the rate constants. Two possibilities were discussed: (a) back ET from special surface states that are induced by dye binding and that are somehow decoupled from the energetic effects and (b) the interfacial ET is a proton-coupled process. If the rate-determining ET preceded the associated proton transfer, then the kinetically relevant driving force would differ from the overall driving force and could conceivably lack a pH-dependence.

O'Regan et al. [262] examined the bias potential dependence of the recombination rate. In the case of carboxylated bpy sensitizer, the decay of about two-thirds of the initial concentration of S^+ formed in a laser pulse was found to be potential dependent. The last one-third of the signal follows a first order kinetics with a rate constant of $3 \times 10^6\ s^{-1}$, essentially independent of the applied bias and identical to that observed with colloidal dispersions of the oxide. This peculiarity of the sintered mesoscopic membranes can be rationalized in terms of trapping of injected electrons at grain-boundaries and at sites that are absent in the dispersed colloidal particles, where the reaction of surface-complexing dyes is believed to involve free cb electrons or carriers that are poorly localized in shallow traps.

Salafsky et al. [256] recently used Transient microwave reflectivity on a dye–TiO_2 nanocrystal system to monitor the dynamics of photoinjected charge in the semiconductor. The electron decay from the nanocrystals is monitored following photoinjection by a dye and reduction of the dye cation by an electron donor. In an I^-/I_3^- ethylene carbonate:propylene carbonate electrolyte like that used in dye–TiO_2 photoelectrochemical cells, this decay rate occurs on a time scale of hundreds of ms to s. Since the decay process represents a short-circuit pathway in the cell, the long lifetime for injected charge could explain the high efficiency of charge collection in such devices.

5.4. Effect of protons/cations on charge injection and recombination

While there is practically no depletion layer within the oxide due to the small size of the particles and their low doping level, a surface charge is rapidly established spontaneously by proton transfer from the protonated carboxylate or phosphonate groups of the Ru complex to the oxide surface producing a charged double layer. When a TiO_2 film is placed in contact with a protic solvent the latter can also act as a proton donor. In aprotic media, Li^+ or Mg^{2+} are potential-determining ions for TiO_2 [263] and they may be used to charge the surface positively. The local potential gradient from the negatively charged sensitizer to the positively charged oxide drives the injection in the desired direction. The same field also inhibits the electrons from leaving the solid after injection has taken place.

Gregg and coworkers [264] measured the pH-dependence of redox potentials of phosphonated–terpy complexes of Ru adsorbed on TiO_2. Upon adsorption onto TiO_2, the redox potential becomes pH-dependent, changing by 53 mV per pH unit, even though the potential of the dye in solution was pH-independent. In amphoteric oxides, the surface charge is strongly dependent on the preparation history of the surface and the degree of protonation of surface hydroxyl groups. In aqueous

solution the latter groups can be readily protonated or depronated upon change of solution pH. Changes in surface charges arising from this varying degree of protonation are reflected in the flat-potential level. The pH-sensitivity of the redox potential induced by adsorption onto TiO_2 is of similar magnitude (59 mV per pH unit in the case of flat-band potential).

In an extension of this study, these authors [265] examined the pH-dependence of redox potential of eight different adsorbed dyes on TiO_2 and Al_2O_3. Depending on the structure of the dye, the pH-dependence varied between 21 and 53 mV per pH unit upon adsorption to these oxide surface. In the case of the Ru complex where the anchoring phosphonate group is linked to the bipyridine ring via a methylene spacer unit and Mg(II), Fe(III)-tetracarboxyphthalocyanines, the pH-dependence of redox potential is much weaker (nearly half), clearly due to weaker electronic coupling. An alternate, but equivalent explanation is to state that the charge density at the polypyridine ring is more effectively reduced (transferred to the semiconductor acceptor) through directly linked phosphanates. It should be pointed out that the electrolytes commonly used in the solar cells are aprotic ones (nitriles) while the above studies of redox potentials of adsorbed dyes are in aqueous media. When aprotic solvents are used as electrolytes, the modulation of the redox potential of dyes upon adsorption can come only through the nature of the oxide surface and its subsequent re-structuring if any through the derivatization process, degree of protonation of the dye and added water (intentional or otherwise).

5.5. Regeneration of the oxidized dye

On thermodynamic grounds, the preferred process for the injected electron in the conduction band is to return to the oxidized sensitizer. Naturally this reaction is undesirable, since such back reactions generate only heat and not electrical current. For efficient processing of charge separated products, it is of interest to develop systems where there is orders of magnitude difference in the forward and back electron transfer rates. Fortunately, in the present case, these rates differ by more than a million. In contrast to the charge injection step which occurs in few ps or less, the back reaction of the electrons of TiO_2 with the oxidized Ru complex is extremely slow, occurring typically in the μs time domain. The process involves a d-orbital localized on the Ru metal whose electronic overlap with the TiO_2 conduction band is small. This together with the fact that the driving force for the back electron transfer is large enough to place it in the inverted Marcus region explains the relatively slow back electron transfer. Thus, in analogy to natural photosynthesis, light induced charge separation is achieved on kinetic grounds, the forward electron transfer being orders of magnitude faster than the back reaction. As a consequence, the presence of a local electrostatic field is not required to achieve good efficiencies for the process. This distinguishes nanocrystalline devises from conventional photovoltaic cells in that the successful operation of the latter is contingent upon the presence of a potential gradient within the p–n junction.

For stable operation of the solar cell and maximal power output, the oxidized dye must be reduced back to the ground state as rapidly as possible by a suitable

electron donor. Since the maximum photovoltage obtainable is related to the position of the mediator redox potential, it is preferable to choose a couple whose potential is as close to the $E(S^+/S)$ as possible. As with the charge injection step, the choice of the mediator should be such that, there is enough driving force (≥ 250 mV) for the dye reduction step to have optimal rate. Thirdly, for stable performance of the solar cell for months, the redox couple must be fully reversible, no significant absorption of the visible light region and stability in the oxidized, reduced forms. The I^-/I_3^- couple is currently being used as the redox mediator of choice. The electrolyte containing the mediator could be replaced by a p-type semiconductor, e.g. cuprous thiocyanate, CuSCN [266,267] and cuprous iodide CuI [54] or a hole-transmitting solid, such as the amorphous organic compounds used in electroluminescence devices. Murakoshi et al. [268] have reported on the possibility of using polypyrrole as a hole-transport layer for dye-sensitized TiO_2 solar cell.

5.6. Electron percolation within the film

As mentioned earlier, electron percolation refers to the process by which the injected electrons hop through the colloidal oxide particles and arrive at the collector conducting glass electrode [269]. An ideal description of the film would be as a collection of large number of particles interconnected with large pores in between—that electrons injected onto any of the constituent particle can traverse through the network and reach the collector/back electrode. High IPCE values ($> 85\%$) indicate that the electron percolation in the nanoporous films can be a very efficient process. From a fundamental point of view, this is one of the most intriguing process amongst many that takes places in the solar cell.

The description elaborated below possibly applies to dye-sensitized case. In these nanocrystalline porous films, the electrolyte penetrates the whole colloidal film up to the surface of the back contact and a semiconductor | electrolyte junction thus occurs at each nanocrystal, much like a normal colloidal system. During illumination, light absorption in any individual colloidal particle will generate an electron-hole pair. Assuming that the kinetics of charge transfer to the electrolyte is much faster for one of the charges (holes for TiO_2) than the recombination processes, the other charge (electrons) can create a gradient in the electrochemical potential between the particle and the back contact. In this gradient, the electrons (for TiO_2) can be transported through the interconnected colloidal particles to the back contact, where they are withdrawn as a current.

The charge separation in a nanocrystalline semiconductor does therefore not depend on a built-in electric field, i.e. a Schottky barrier, but is mainly determined by kinetics at the semiconductor | electrolyte interface. The creation of light induced electrochemical potential for the electrons in TiO_2 also explains the building up of a photovoltage. There will be an increased probability of recombination with increased film thickness, as the electron has, on average, to be transported across an increasing number of colloidal particles and grain boundaries. This indeed has been observed experimentally. Thus there exists an optimal thickness to obtain maximum photocurrent. Another loss mechanism due to increasing film thickness is a resistance loss leading to a decrease in photovoltage and fill factor.

5.7. Dark current

Dark currents significantly reduce the maximum cell voltage obtainable. The oxide layer is an inter-connected network of particles with high porous interior. The dyes can penetrate everywhere and adsorb over a large surface area. Surface concentration of Ru complexes as high as 10^{-7} mol cm^{-2} on 10 μm thick films are achieved, generally indicating a very dense packing of the sensitizer. However, there still exists enough naked sites. The redox mediator also must penetrate the same domain so as to be present in the immediate vicinity of the photosensitizer. If the redox mediator gets to the back contact, dark currents arise from the reduction of the redox mediator by the collector electrode with the oxide layer:

$$2e^- + I_3^- \rightarrow 3I^- \tag{20}$$

In principle, this charge recombination can occur at surfaces other than that of TiO_2. Due to the porous nature of the TiO_2 film, it can also occur at the back conducting glass (ITO) electrode. In reality, the reaction occurs at the TiO_2 particle | redox electrolyte interface due to the relatively large surface area of the nanocrystalline film.

Dark currents can be suppressed by co-adsorption of saturated hydrocarbons with anchoring groups that isolate the uncovered oxide surfaces from interactions with I_3^-, for example, chenodeoxycholic acid. The concentrations of sensitizer and the additives in the coating solution have to be adjusted for high sensitizer loading and at the same time complete isolation (coverage) of non-accessible surface sites—a catch-22 situation for optimization. Several alternate approaches to co-adsorption of additives are also being examined. In one approach, long alkyl chain substituents are introduced at the polypyridine units (not carrying the anchoring groups). Lateral interactions of the alkyl chains and formation of a hydrophobic interface stabilizes the adsorbate from water-induced desorption. A variant of this is use of bulky, sterically hindering groups such as *t*-butylphenyl. Another approach is to introduce electropolymerizable groups such as pyrrolic units at the polypyridine ligands. The corresponding Ru complexes can be adsorbed on to TiO_2 and then photopolymerizsed in the presence of free pyrrole at electrode potentials positive of the flat-band.

In order to reduce the dark current, an oxide underlayer is deposited. Alternatively, exposure of the dye-coated electrode to a solution of a pyridine derivative (donor) such as 4-*t*-butylpyridine was found to improve dramatically the fill factor (ff) and the open-circuit voltage (V_{oc}) of the device without affecting the short-circuit photocurrent (i_{sc}) in a significant fashion. For example, the untreated electrode gave $i_{sc} = 17.8$ mA cm^{-2}, $V_{oc} = 0.38$ V and ff = 0.48, corresponding to an overall conversion efficiency (η) of 3.7%. After the electrode is dipped in 4-*t*-butylpyridine, V_{oc} increases to 0.66, ff to 0.63 and η to 8.5%. The increase in the open circuit voltage and the fill factor is due to the suppression of the dark current at the semiconductor | electrolyte junction. The effect of the substituted pyridine can be rationalized in terms of its adsorption at the TiO_2 surface, blocking the surface states that are active intermediates in the heterogeneous charge transfer.

5.8. Counter electrode performance

Solar cell studies employ usually a F-doped SnO_2 as the conducting glass electrode(s). Such electrodes are known to be poor choice for efficient reduction of triiodide. To reduce the overvoltage losses, a very fine Pt-layer or islands of Pt is deposited on to the conducting glass electrode. This ensures high exchange current densities at the counter-electrode and thus the processes at the counter electrode do not become rate limiting in the light energy harvesting process. By developing a new mode of Pt deposition, we have engineered an extremely active electrocatalyst attaining exchange current densities of > 0.1 A cm^{-2} at very low Pt-loading. This electrocatalyst is very stable and does not show long-term anodic corrosion as was observed in the case of Pt deposits produced by conventional sputtering or galvanic methods.

5.9. A short summary of kinetic studies

On the basis of different measurements, it is possible to indicate the orders of magnitude for the rate constants of electron transfer steps involved:

1. Electron injection into TiO_2: following the light absorption of the Ru complex, the electron injection into the conduction band is in the sub-ps to ps range.
2. Back electron transfer: the rate constant for the back electron transfer (dark reduction in the absence of externally added electron donors) however is much smaller for several reasons, typically τ ca. 1 μs.
3. Reduction of triiodide by e_{cb}^-: another important recombination process is reduction of I_3^- in the electrolyte by conduction band electrons. The exchange current density, j_o of the reverse saturation current of this process has been measured in the range 10^{-11}–10^{-9} A cm^{-2}, depending on the electrolyte. Surface treatment of the electrode can alter these values drastically.
4. The electron movement (percolation) in the nanocrystalline TiO_2 electrode to the back contact is significantly slower than in single crystal TiO_2. Studies have shown that the photocurrent transients, following UV excitation of TiO_2 particles from a ns pulsed laser, decay in the ms to s range.
5. The exchange current density for the reduction of triiodide at the counter electrode ITO coated with a catalytic amount of Pt, has been measured to be $0.01–2 \times 10^{-1}$ A cm^{-2}.
6. Reduction of the oxidized dye by iodide occurs on a timescale of 10^{-8} s.

6. Other optoelectronic systems based on nanocrystalline films

Nanocrystalline films of semiconductors derived using monodispersed colloids are attractive candidates for use as hosts in the design of electrochromic, optical display devices. High surface area and porosity of these films allow for fairly high local concentrations of redox mediators without running into the risk of forming aggregates. Transparency of the host/electrode is another stringent requirement for

optical display and this is easily met in preparations using monodispersed colloids. Ability to control the flat-band potentials of these semiconductors is another positive point as compared to glass electrodes coated with conducting oxides.

Semiconducting nanoporous oxide electrodes can be used to study electrochemical processes of anchored molecules in an efficient manner. In view of the forbidden bandgap, no oxidation process is possible at potentials that are within the band-edge positions. When a semiconductor is made negative with respect to the solution, more electrons move to the surface, the electric field in the semiconductor points towards the interface and the band bend downward. An *accumulation layer* is formed. When the density of the majority carriers at the surface approaches the density of states in the material, the surface becomes degenerate. This occurs when the potential of a moderately doped n-type semiconductor is made slightly more negative of the flat-band potential. From this point, the electrode approaches metallic behavior and electrochemical reductions can be carried out. The electrons that accumulate during the forward bias at potentials at or more negative of -0.8 V are good reducing agents and can reduce redox species surface-bound or even those present in the solution.

6.1. Electrochromic display using surface bound molecules

There exists a whole variety of electron-rich (donor) and electron-deficient (acceptor) molecules with large difference in the absorption properties between the oxidized and reduced forms. The term *electrochromism* is used to refer to the process of reversible switching on and off colors by electrochemical means [270]. Most often the color changes are from transparent (or bleached) state to a colored state or between two colored states. There are also known polyelectrochromic systems where distinct color changes occur in more than two redox states. When redox-active molecules are confined to an electronically conducting substrate, they can be switched between different oxidation/reduction stages by controlling the electrochemical potential of the substrate electrode. Practical applications require electrochromic materials with high contrast ratio, coloration efficiency (absorbance change per charge injected per unit area), cycle life and write-erase efficiency. Prussian Blue and Tungsten Bronzes are the classic text-book examples of electrochromic materials where distinct color changes comes about from inter-valence transitions involving the same metal center in two different oxidation states [271]. Quaternary, bipyridinium salts (viologens) are another group of molecules where distinct color changes occur between reduced and oxidized forms. In the oxidized form, the molecules are nearly colorless but the reduced form have strong absorption in the visible light region.

By controlling the electrochemical potential, it is possible to transform electrochromic systems to be light-transmissive or light-reflective and such devices find practical applications in areas such as optical information storage, anti-glare rear view mirrors for cars, glare-reduction system for offices and smart windows for use in cars and in buildings. Gentex's *Night Vision Safety* mirror technology is one such typical application of electrochromism already commercialized in motor vehicles.

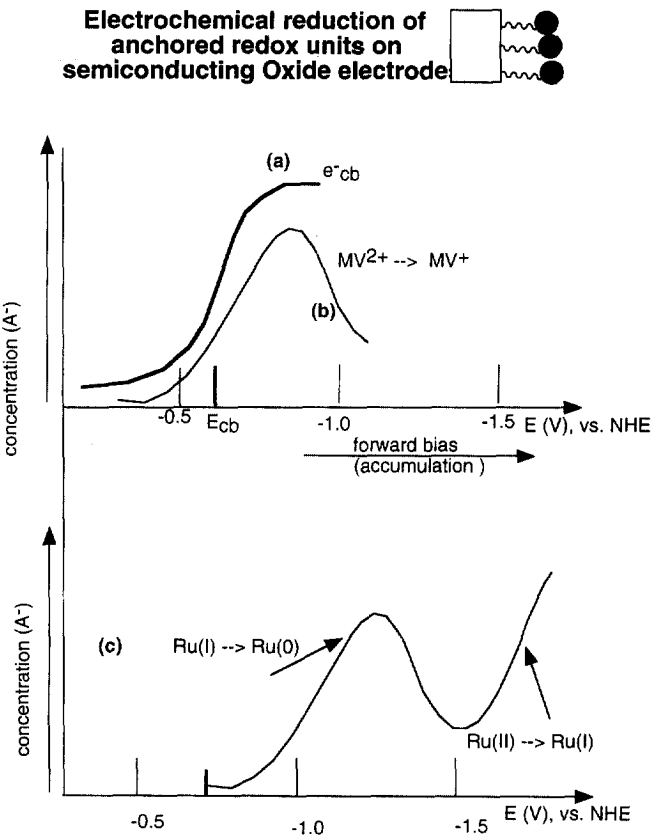

Fig. 11. Schematic presentation of redox processes that occur on anchored redox molecules during potentiostatic control of nanocrystalline oxide electrodes such as TiO_2. (a) Accumulation of electrons in the conduction band of TiO_2 under forward bias conditions. (b) Electrochromical reduction of viologen anchored onto TiO_2 under forward bias. (c) Electrochemical reduction of phosphanato–bpy complex of Ru(II) anchored on TiO_2.

With application of small applied potential, it is possible to reduce considerably glare from headlights of cars in the opposite direction. *Smart windows* is another application where the light transmittance of windows can be varied in a controlled way to reduce power requirements of the building during summer and winter (less forced heating in winter with more sunlight in and less forced cooling with less sunlight coming through). Pilkington has already developed smart windows where visible light transmission can be varied up to a factor of four. Optical display systems require fast response times while applications such as smart windows can accommodate response time extending to several minutes.

Fig. 11 illustrates the principles of electrochemical reduction of anchored redox molecules on a nanocrystalline oxide such as TiO_2. Cathodic polarization of naked electrode more negative of the conduction band-egde leads to accumulation of

electrons (Fig. 11a). On transparent TiO_2, this can be seen by the development of a distinct blue coloration and growth of absorption in the red and near-IR region due to accumulation of conduction band electrons [272,273]. The existence of a distinct maximum (850 and 969 nm at pH 3.0 and 11.6, respectively) clearly indicate that the charge carriers are trapped.

In principle, electron acceptors in the immediate vicinity of the electrode will be reduced at potentials more negative than the V_{fb} of the conduction band (-0.58 V). Absorbance changes measured as a function of applied bias do conform this type of rectified electron transfer at the interface. There have been a number of studies of electrochromism involving viologens anchored to various surfaces. The reduction of surface-bound viologens can be monitored spectroscopically in real time by monitoring the absorbance changes. Methyl viologen reduction is possible at potentials more negative of -0.68 V. For optical display applications, it is useful to employ a surface-bound viologen. Fitzmaurice and co-workers [274] have used the salicylic acid derivatives of methyl viologen to covalently bind them on to the surface of a nanocrystalline TiO_2 film. Application of a negative bias to the nanocrystalline TiO_2 electrode leads to efficient reduction of viologen up to applied potentials of -0.80 V. Fig. 11(b) is an example of increasing concentration of reduced acceptor during the cathodic sweep of a typical cyclic voltammetric scan.

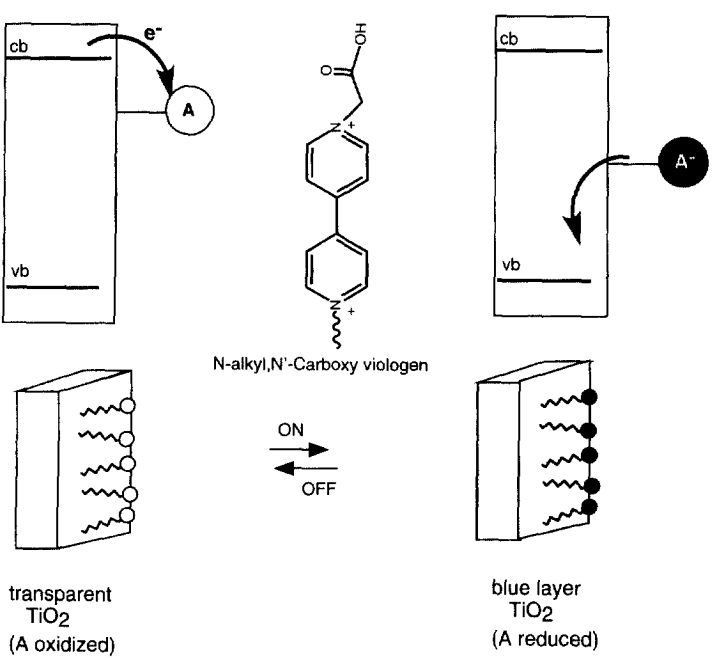

Fig. 12. Electrochemical reduction and associated electrochromism involving anchored viologens on nanocrystalline films of TiO_2. A refers to the surface bound viologen moiety and the bold arrow represents the switching on/off processes.

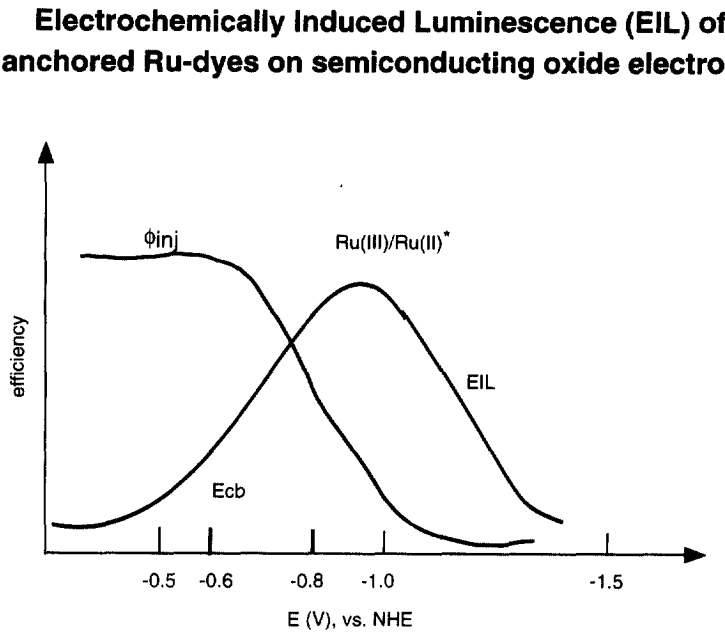

Fig. 13. Schematic presentation of the applied potential dependence of luminescence (EIL) and excited state charge injection (ϕ_{inj}) of Ru–polypyridine complexes bound to nanocrystalline TiO_2 electrode.

Kelly and coworkers have also extended studies of redox reactions involving methyl viologen at semiconductor single crystal electrodes [275].

As part of his doctoral thesis work, Campus [103] has examined the electrochromism of several surface-bound viologen derivatives anchored on to nanocrystalline TiO_2 membrane films. By attaching donor or acceptor groups to the bipyridinium moiety, it is possible to vary the redox potentials of the viologen. Most often this tuning of redox potential is accompanied by a shift in the absorption spectrum of the associated singly and doubly reduced forms. When the potential of a TiO_2 layer modified by a monolayer of a viologen with phosphonate as anchoring group ($E_o = -0.18$ V vs. NHE, $\varepsilon = 9000\ M^{-1}\ cm^{-1}$) is stepped up to -1 V, the electrode turned from colorless to deep blue in < 1 s (see Fig. 12). The related absorption change at 522 nm was as high as 2. Owing to the position of the conduction band of TiO_2 (more negative than the redox potential of the viologen), in this case re-oxidation of the reduced viologen is not feasible unless protons or Li^+ ions are added to the electrolyte. In the presence of such strongly adsorbing cations, the conduction band can be lowered to 0 V. Under these conditions, these derivatized viologens exhibit reversible electrochemistry. Electrochromic windows up to 10×10 cm and small displays were built, using a counter-electrode made of Prussian Blue on conducting glass. Very sharp color changes are achieved in 0.5–3 s.

The electrochemical reduction of surface-bound phosphanato–bipyridine complex of Ru, [Ru(phos–bpy)$_3$], has been studied recently on nanoporous TiO_2 electrodes

[276]. Fig. 11(c) illustrates schematically the accumulation of reduced form of the sensitizer during the cathodic sweep of a cyclic voltammetric scan. Reduction of a Ru(II) complex to the Ru(I) state can be seen at potentials close to -1.2 V and even to Ru(0) state at potentials more negative of -1.5 V.

6.2. Electroluminescence and photoelectroluminescence of anchored dyes

Electroluminescence arising from redox reactions of chromophores present in the solution or anchored to the semiconductor surface have been observed recently. Fig. 13 illustrates the principles that govern luminescence of polypyridine complexes of Ru during potentiostatic control of semiconducting oxide electrodes such as TiO_2. In forward bias experiments (where the oxide electrode is polarized to cathodic potentials beyond the conduction band-edge), the accumulated electrons can be used to reduce the oxidized form of the Ru–bpy complex [Ru(III)$(bpy)_3^{3+}$] present in the electrolyte. Interestingly, Gleria and Memming [277] found that the reduced product was the luminescent MLCT excited state of Ru, $[Ru(bpy)_3]^{2+}$*:

$$Ru(bpy)_3^{3+} + e_{cb}^- \rightarrow Ru(bpy)_3^{2+}* \tag{21}$$

This result can be understood in terms of the redox potential for the relevant state [$Ru^{3+/2+}$*] which is located at ca. -0.8 V. Thus, electrochemical biasing of TiO_2 electrode at potentials ≤ -0.8 V in the presence of $Ru(bpy)_3^{3+}$ leads to electroinduced luminescence (EIL). Gleria and Memming [277] observed CT luminescence upon electron-transfer from n-SiC to $Ru(bpy)_3^{3+}$. Yeh and Bard [278] observed similar kind of luminescence with rubrene radical cations at ZnO electrodes.

Fig. 12(b) illustrates a variation of the above experiment, carried out recently by Athanassov et al. [276] using anchored Ru complexes with phosphonato-bpy ligands. Electrochemically induced luminescence (EIL) of an anchored Ru(II) complex was observed in the presence of oxidants such as peroxydisulphate. The potential dependence of EIL is very similar to that elaborated earlier for experiments done in the dark using $Ru(bpy)_3^{3+}$. The proposed mechanism involve (i) reduction of persulphate ions by the conduction band electrons, leading to formation of strong oxidant SO_4^-, (ii) oxidation of Ru(II) complex to Ru(III) by SO_4^- ions, and (iii) reduction of Ru(III)-phos-bpy complex by conduction band electrons to generate directly the luminescent CT state Ru^{2+}*:

$$S_2O_8^{2-} + e_{cb}^- \rightarrow SO_4^- + SO_4^{2-} \tag{22}$$

$$SO_4^- + Ru(II) \rightarrow SO_4^{2-} + Ru(III) \tag{23}$$

$$e_{cb}^- + Ru(III) \rightarrow Ru(II)* \tag{24}$$

Potential dependence of the luminescence of anchored Ru complexes has been studied (in the absence of electron acceptors such as persulphate) on nanoporous TiO_2 [263] and SnO_2 electrodes. In the absence of external bias, optical excitation

of the anchored Ru complex leads to injection of electrons in the conduction band and oxidation of the Ru(II) complex to the Ru(II) state. However, when the nanoporous electrode is held at more cathodic potentials (forward bias at potentials more negative of -0.6 V), the driving force for excited state quenching decreases and eventually the process stops when the fermi level of the semiconductor is more negative with respect to the excited state potential of the anchored Ru dye (dotted line marked ϕ_{inj}). The CT luminescence of the excited state follows an inverse behavior. The luminescence is totally quenched at positive potentials (e.g. at -0.2 V). With increasing forward bias, as the photo-induced electron transfer looses its efficiency, luminescence recovers. At -0.52 V for TiO_2, the luminescence of the anchored dye is recovered quantitatively. Recovery of luminescence under forward bias was first indicated by Memming et al. [277] in their studies of Ru complexes on SnO_2. The luminescence intensity goes through maximum and decreases at very negative potentials, due to direct direction of the Ru(II) complex to the Ru(I) state (see Section 6.1).

6.3. Photochromism (optical switching) and photoelectrochromism

Switching between two different redox states brought about by electrochemical means can also be effected in photosensitive materials using electron-donors and acceptors to add or remove electrons. Thus photoredox reactions of anchored molecules is one potential pathway in the design of photochromic systems. Optical excitation in the form of photons of a given energy (wavelength) can be used to turn-on or -off the color changes (*optical switches*). While the write (color development) and erase (bleaching) steps are carried out by applying potentials in electrochemical systems, in photo-electrochemical systems, the erase part alone is done electrochemically.

There have been a number of reports [279] where viologen derivatives have been attached to the surface of Q-particles of semiconductors such as CdS using protective/coupling agents such as poly(vinylpyridine), dimethylaminated nylon and polyethylenediamine and thiols. Irradiation of such hetero-dyads with bandgap light in the presence of electron donors leads to development of blue color corresponding to formation of singly reduced viologen cation radical. The reduced viologen, in turn can be used to reduce other molecules present in the solution such as protons to H_2 with Pt catalysts, nitrates to nitrites mediated by enzymes. In the case of viologen–TiO_2 heterodyad mentioned earlier, reduction of surface bound viologen can be seen upon illumination with near-UV photons. It may be mentioned here that, in early eighties, DeBerry and Viehbeck [280] demonstrated UV-induced photochromism of Prussian Blue on a flat TiO_2.

Bonhôte et al. [281] have demonstrated the operation of photochromic and photoelectrochromic systems based on anchored Ru–polypyridyl complexes on nanocrystalline TiO_2 electrodes. In a bis(terpyridine)Ru(II) complex, a phosphonate anchoring group has been used to derivatize the Ru complex on to TiO_2 electrode and an electron-donor triarylamine attached directly to the other terpyridine as shown below:

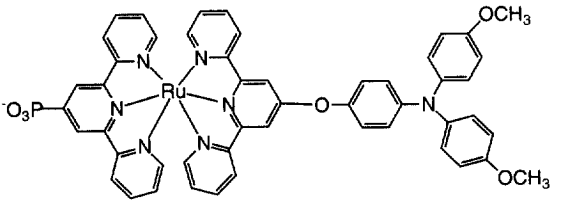

Optical excitation of the surface-bound sensitizer-donor dyad with visible light can lead to either of the following sequence of reactions (see Fig. 14):

(i) charge injection into TiO_2 followed by reduction of S^+ by the donor

$$D-S-TiO_2 \rightarrow D-S^+-(e^-)TiO_2 \quad (25)$$

$$D-S^+-(e^-)TiO_2 \rightarrow D^+-S-(e^-)TiO_2 \quad (26)$$

(ii) reductive quenching of S followed by electron injection to TiO_2 by reduced dye

$$D-S-TiO_2 \rightarrow D^+-S^--TiO_2 \rightarrow D^+-S-(e^-)TiO_2. \quad (27)$$

Both lead to formation of oxidized donor (D^+) and electron in the conduction band of TiO_2. This is followed by back electron-transfer, regenerating the starting materials:

$$D^+-S-(e^-)TiO_2 \rightarrow D-S-TiO_2 \quad (28)$$

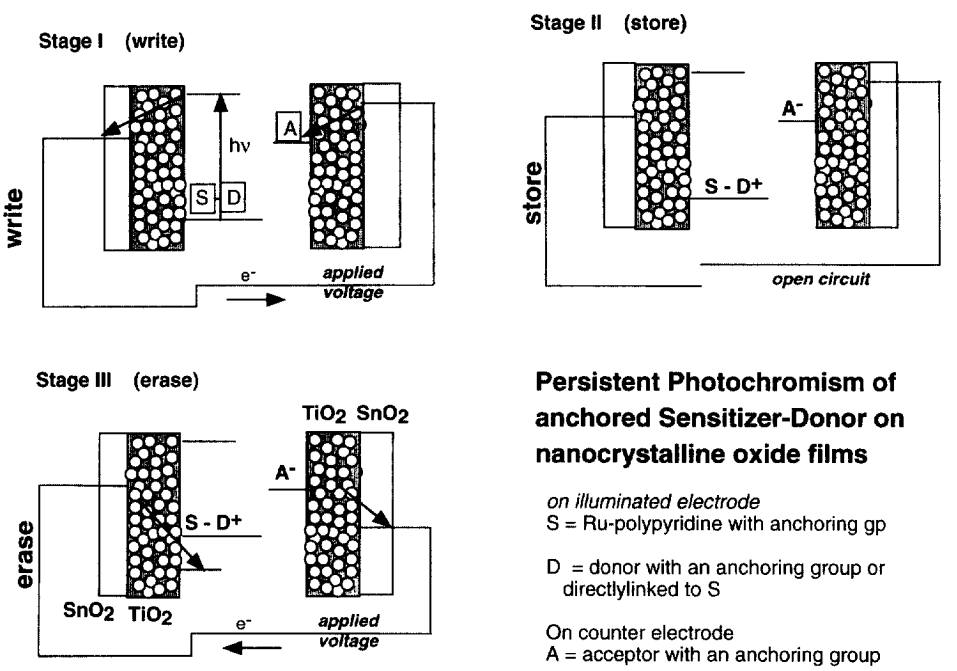

Fig. 14. Principles of operation of photo- and photoelectrochromism using surface-bound polypyridyl complexes of Ru. Stages I, II and III correspond to the writing, storage and erasing processes, respectively.

The last recombination step can be prevented by positive polarization of the supporting TiO_2 anode. In fact, the chelated triad nanocrystalline electrode kept at +0.55 V and illuminated with white light leads to development of an absorption maximum at 750 nm corresponding to D^+. The initial condition was re-generated by applying a potential of −0.3 V and several cycles were realized without modification of the respective spectra.

6.4. Devices based on cation intercalation

The ion migration/diffusion within the pores of nanocrystalline films is quite fast that it is possible to take advantage of this to design electrochromic systems and rechargeable batteries. Electrochemical studies have shown that it is possible to rapidly and reversibly insert protons and Li^+ ions by forward biasing of nanocrystalline TiO_2 films as indicated by the equation:

$$TiO_2 + xe^- + xM^{n+} \rightarrow xMTiO_2 \text{ (insertion) (where } M^{n+} = Li^+, H^+) \quad (29)$$

The films are transparent. Upon a potential sweep from −0.64 to −1.64 V vs. Ag | AgCl the TiO_2 electrode turns blue within 14 s (absorbance change from 0.2 to 2.2 at 780 nm) due to the electrons in the conduction band and formation of Ti^{3+} ions [282–284]. Absorption changes of >90% light throughout the visible and near IR can be switched on and off within a few seconds. The process can be reversed at a similar rate if it is polarized again at −0.64 V.

In one form of rechargeable batteries (*rocking chair batteries*), power generation is linked to migration of Li^+ ions from an anode host lattice of TiO_2 to the cathode consisting of mixed oxides NiO_2/CoO_2 or MnO_2.

$$TiO_2 + xe^- + xLi^+ \rightarrow Li_xTiO_2 \text{ (insertion)} \quad (30)$$

$$LiCoO_2 - xe^- \rightarrow Li_{1-x}CoO_2 + xLi^+ \text{ (extraction)} \quad (31)$$

$$\text{Net: } TiO_2 + LiCoO_2 \rightarrow Li_xTiO_2 + Li_{1-x}CoO_2 \quad (32)$$

In the conventional design, the materials are used in the form of micron-sized particles compressed pellets mixed with carbon and a polymeric binder. The morphology of the electrodes are such that large pores/channels present therein allow reversible insertion of Li and extraction into and from the lattice. Alternate versions employing nanocrystalline films of TiO_2 with faster ion transport have been developed supplying 4–4.5 mA h corresponding to 50 mA h g^{-1} capacity which compares well with the rocking chair battery having a carbon anode.

7. Conclusions

A broad overview of current efforts to utilize porous, high surface area membrane type films of semiconducting oxides as a key component in the design of various photonic and optoelectronic devices. Major coverage has been on dye-sensitized solar cell based on nanocrystalline films of TiO_2, reflecting current emphasis on these cells.

The nanocrystalline solar cells serve as a useful role model in the design of various optoelectronic devices because many of the required functions are there to be optimized. In view of its significant potential for practical deployment in electronic devices that require low power and operate at ambient light, several companies are getting actively involved in building prototypes and modules. Optical display units based on nanocrystalline films is another area that is likely to see significant advances in the near future. As sol–gel science matures, there will certainly be more devices based on other oxides and non-oxide semiconductors.

Acknowledgements

For nearly two decades the photochemistry group in Lausanne has been involved in studying light-induced processes involving finely dispersed colloids and nanocrystalline films of semiconductors. Progress in this area has been due to coordinated and dedicated efforts on the part of several collaborators, many of them are cited in the references listed. We would like to express our sincere thanks to them for their enthusiastic collaboration. Our thanks also go to numerous governmental and industrial agencies for financial support of our work. Acknowledgments are made particularly to Swiss National Science Foundation (FNRS), COST program of the Federal Office for Education and Science (OFES), Federal Office for Energy (OFEN) and the Commission for Technology and Innovation (CTI), and also the Cell Research section of the National Institute for Applied Photovoltaics (INAP), Gelsenkirchen, Germany.

References

[1] F.L. Carter, R.E. Siatkowski, H. Wohltjen (Eds.), Molecular Electronic Devices, North Holland, Amsterdam, 1988.
[2] D. Mendenhall, A. Greensberg, J. Liebman (Eds.), Mesomolecules: from Molecules to Materials, Chapman and Hall, London, 1995.
[3] V. Ramamurthy (Ed.), Photochemistry in Organized and Constrained Media, VCH, New York, 1991.
[4] K. Kalyanasundaram, Photochemistry in Microheterogeneous Systems, Academic Press, New York, 1985.
[5] (a) T. Matsuura, M. Anpo (Eds.), Photochemistry on Solid Surfaces (Studies on Surface Science and Catalysis), vol. 47, Elsevier, Amsterdam, 1989. (b) K. Honda (Ed.), Photochemical Processes in Organized Molecular Systems, Elsevier, Amsterdam, 1991.
[6] V. Ramamurthy, R.G. Weiss, G. Hammond, Adv. Photochem. 18 (1993) 67.
[7] J.K. Thomas, Chem. Rev. 93 (1993) 301.
[8] A.J. Bard, Integrated Chemical Systems: a Chemical Approach to Nanotechnology, Wiley, New York, 1994.
[9] (a) J. Deisenhofer, H. Michel, Ann. Rev. Biophys. Biophys. Chem. 20 (1991) 247. (b) J. Deisenhofer, H. Michel, Angew. Chem. Int. Edn. Engl. 29 (1989) 829.
[10] (a) J. Barber (Ed.), Molecular Processes of Photosynthesis, JAI Press, Greenwich, CT, 1994. (b) J. Barber (Ed.), Photosynthesis in Relation to Model Systems (Topics in Photosynthesis Ser. vol. 3), Elsevier, Amsterdam, 1979.

[11] (a) G.R. Fleming, P.L. Knight, J.P. Simons (Eds.), Ultrafast Processes in Chemistry and Biology, Royal Society, London, 1998. (b) G.R. Fleming, Chemical Applications of Ultrafast Spectroscopy, Oxford University Press, New York, 1986. (c) M.A. El-Sayed, I. Tanaka, Y. Molin (Eds.), Ultrafast Processes in Chemistry and Photobiology, Blackwell Science, Oxford, 1995.
[12] M.A. Fox, M. Chanon (Eds.), Photoinduced Electron Transfer, Elsevier, Amsterdam, 1988 (in three volumes).
[13] M. Grätzel, Heterogeneous Photochemical Electron Transfer, CRC Press, Boca Raton, FL, 1989.
[14] J. Mattay (Ed.), Photoinduced Electron Transfer (Topics in Current Chemistry), Springer Verlag, New York, 1990.
[15] G.J. Kavarnos, Fundamentals of Photoinduced Electron Transfer, VCH, New York, 1993.
[16] F.C. Anson, F. Ciardelli, K. Yamamoto (Eds.), Multi-electron Transfer Processes for Molecular Conversion, Wiley, Chicester, UK, 1995.
[17] R.D. Miller, G.L. McLendon, A.J. Nozik, W. Schmickler, F. Willig (Eds.), Surface Electron Transfer Processes, VCH, New York, 1995.
[18] S.S. Isied (Ed.), Electron Transfer Reactions: Inorganic, Organometallic and Biological Applications (Advances in Chemistry Ser. vol. 253), American Chemical Society, Washington, DC, 1997.
[19] V. Balzani, A. Juris, M. Venturi, S. Campagna, S. Serroni, Chem. Rev. 96 (1996) 759.
[20] J-P. Sauvage, J-P. Collin, J-C. Chambron, et al., Chem. Rev. 94 (1994) 993.
[21] J-P. Collin, A. Harriman, V. Heitz, F. Odobel, J-P. Sauvage, Coord. Chem. Rev. 148 (1996) 63.
[22] J.-P. Collin, P. Gavina, V. Heitz, J.-P. Sauvage, Eur. J. Inorg. Chem. (1998) 1.
[23] V. Balzani, F. Scandola, Supramolecular Photochemistry, Horwood, Chicester, UK, 1991.
[24] V. Balzani, L. De Cola, (Eds.), Supramolecular Chemistry, Kluwer, Dordrecht, 1992.
[25] J-M. Lehn, Supramolecular Chemistry, VCH, Weinheim, 1995.
[26] F. Vögtle, Supramolecular Chemistry, Wiley, Chicester, UK, 1993.
[27] There is already a European Commission supported TMR Research Project called "Hetero-supramolecular Chemistry: an approach to modulating the function of molecular devices" where several European research groups are involved in development of molecular photonic and electronic devices.
[28] A. Kay, R. Humphry-Baker, M. Grätzel, J. Phys. Chem. 98 (1994) 952.
[29] P.A Connor, K.D. Dobson, A.J. McQuillan, Langmuir 11 (1995) 4193.
[30] K.D Dobson, A.J. McQuillan, Langmuir 13 (1997) 3392.
[31] I. Bedja, S. Hotchandani, P.V Kamat, 98 (1994) 4133.
[32] I. Bedja, S. Hotchandani, R Carpentier, R.W. Fessenden, P.V. Kamat, J. Appl. Phys. 75 (1994) 5444.
[33] P.V. Kamat, I. Bedja, S. Hotchandani, L.K. Patterson, J. Phys. Chem. 100 (1996) 4900.
[34] S. Ferrare, A. Zaban, B.A. Gregg, J. Phys. Chem. 101 (1997) 4490.
[35] L. Hu, M. Wolf, M. Grätzel, Z Jiang, J. Sol-Gel Sci. 5 (1995) 219.
[36] R.R. Bacsa, M. Grätzel, J. Am. Ceram. Soc. 79 (1996) 2185.
[37] A. Kay, M. Grätzel, Sol. Energy Mat. Sol. Cells (1996) 1494.
[38] G. Redmond, A. O'Keefe, C Burgess, C. MacHale, D. Fitzmaurice, J. Phys. Chem. 97 (1993) 11081.
[39] L. Spanhel, M.A. Anderson, J. Am. Chem. Soc. 113 (1991) 2826.
[40] (a) H. Rensmo, K Keis, S. Lindström, et al., J. Phys. Chem. 101 (1997) 2598. (b) M.A. Martinez, J. Herraro, M.T. Gutierrez, Sol. Energy Mater. Sol. Cells 45 (1997) 75.
[41] I. Bedja, S. Hotchandani, R. Carpentier, K. Vinodgopal, P.V. Kamat, Thin Solid Films 247 (1994) 195.
[42] U. Björksten, J. Moser, M. Grätzel, Chem. Mater 6 (1994) 858.
[43] C.J. Brinker, C.W. Scherer, Sol-Gel Science: the Physics and Chemistry of Sol-Gel Processing, Academic Press, San Diego, CA, 1990.
[44] L.C. Klein, Sol-Gel Optics-Processing and Applications, Kluwer, Boston, MA, 1994.
[45] H.D. Gesser, P.C. Goswami, Chem. Rev. 89 (1989) 765.
[46] L.C. Klein (Ed.), Sol-Gel Technology for Thin Films, Fibres, Preforms, Electronics and Speciality Shapes, Noyes, New Jersey, 1988.
[47] (a) E. Matijevic, Mater. Res. Soc. Bull. 4 (1989) 18. (b) E. Matijevic, Mater. Res. Soc. Bull. 5 (1990) 16.

[48] (a) E. Matijevic, Chem. Mater. 5 (1993) 412. (b) E. Matijevic, Chem. Mater. 15 (1985) 485.
[49] (a) E. Matijevic, Langmuir 2 (1986) 12. (b) E. Matijevic, Langmuir 10 (1994) 8.
[50] T. Gerfin, M. Grätzel, L. Walder, Progr. Inorg. Chem. 44 (1997) 345.
[51] C.A. Bignozzi, J.R. Schoonover, F. Scandola, Progr. Inrog. Chem 44 (1997) 1.
[52] A. Hagfeldt, M. Grätzel, Chem. Rev. 95 (1995) 49.
[53] M. Grätzel, K. Kalyanasundaram, Photosensitization and Photocatalysis using Inorganic and Organometallic Compounds, Kluwer, Dordrecht, 1993.
[54] K. Kalyanasundaram, Photochemistry of Polypyridine and Porphyrin Complexes, Academic Press, London, 1992.
[55] D.M. Roundhill, Photochemistry and Photophysics of Metal Complexes, Plenum, New York, 1994.
[56] D. Dolphin (Ed.), The Porphyrins, Academic Press, New York, 1978–1979 (in 7 vols.).
[57] M. Gouterman, P.M. Rentzepis, K.D. Straub (Eds.), Porphyrins: Excited States and Dynamics, ACS Symp. Ser., American Chemical Society, Washington, DC, 1986.
[58] L.R. Milgrom, The Colors of Life: an Introduction to the Chemistry of Porphyrins and Related Compounds, Oxford University Press, Oxford, 1997.
[59] K.M. Smith (Ed.), Porphyrins and Metalloporphyrins, Elsevier, Amsterdam, 1975.
[60] C.C. Leznoff, A.B.P. Lever (Eds.), Phthalocyanines: Properties and Applications, VCH, New York, 1989.
[61] K. Kalyanasundaram, Coord. Chem. Rev. 46 (1982) 159.
[62] J.R. Darwent, P. Walters, A. Mills, G. Porter, A. Harriman, Coord. Chem. Rev. 44 (1982) 83.
[63] (a) T.J. Meyer, Acc. Chem. Res. 22 (1989) 163. (b) T.J. Meyer, Pure Appl. Chem. 58 (1986) 1193.
[64] T.J. Meyer, Progr. Inorg. Chem. 30 (1983) 389.
[65] (a) A. Juris, V. Balzani, F. Barigelletti, S. Campagan, P. Belser, A. von Zelewsky, Coord. Chem. Rev. 84 (1988) 85. (b) V. Balzani, F. Boletta, M.T. Gandolfi, M. Maestri, Top. Curr. Chem. 75 (1978) 1. (c) V. Balzani, A. Juris, M. Venturi, S. Campagna, S. Serroni, Chem. Rev. 96 (1996) 759.
[66] V. Balzani, F. Barigelletti, L. De Cola, Top. Curr. Chem. 158 (1990) 31.
[67] V. Scandola, M.T. Indelli, C. Chiorboli, C.A. Bignozzi, Top. Curr. Chem. 158 (1990) 73.
[68] (a) E.C. Constable, A.M.W. Cargill Thompson, New J. Chem. 29 (1996) 65. (b) E.C. Constable, Pure Appl. Chem. 68 (1996) 253. (c) E.C. Constable, Progr. Inorg. Chem. 42 (1994) 67.
[69] (a) H. Kuhn, Pure Appl. Chem. 51 (1979) 341; 53 (1981) 2105. (b) H. Kuhn, Thin Solid Films 178 (1989) 1. (c) D. Möbius, Acc. Chem. Res. 14 (1981) 63. (d) H. Kuhn, D. Möbius, Angew. Chem. Int. Ed. Engl. 10 (1971) 620. (e) G. Roberts (Ed.), Langmuir–Blodgett Films, Plenum, New York, 1990.
[70] (a) M. Fujihira, Mol. Cryst. Liq. Cryst. 183 (1990) 59. (b) M. Fujihira, K. Nishiyama, K. Aoki, Thin Solid Films 160 (1988) 317. (c) M. Fujihira, H. Yamada, Thin Solid Films 160 (1988) 125. (d) T. Kondo, H. Yamada, K. Nishiyama, K. Suga, M. Fujihira, Thin Solid Films 179 (1989) 463. (e) M. Fujihira, M. Sakomura, Thin Solid Films 180 (1989) 43.
[71] (a) W. Arden, P. Fromherz, Ber. Bunsenges. Phys. Chem. 82 (1978) 868. (b) W. Arden, P. Fromherz, J. Electrochem. Soc. 127 (1980) 370. (c) H. Hada, Y. Yonezawa, H. Inaba, Ber. Bunsenges. Phys. Chem. 85 (1981) 425.
[72] (a) Z.Y. Li, T.E. Mallouk, C.W. Lai, Inorg. Chem. 28 (1989) 178. (b) J.S. Krueger, T.E. Mallouk, J.E. Meyer, J. Am. Chem. Soc. 110 (1988) 8232.
[73] (a) C.C. Christ, J. Yu, X. Zhao, G.T.R. Palmore, M.S. Wrighton, Inorg. Chem. 32 (1992) 4439. (b) S.R. Wasserman, G.M. Whitesides, I.M. Tidswell, B.M. Ocko, P.S. Pershan, J.D. Axe, J. Am. Chem. Soc. 111 (1989) 5852.
[74] P.K. Ghosh, T.G. Spiro, J. Am. Chem. Soc. 102 (1980) 5543.
[75] H.O. Finklea, H. Abruna, R.W. Murray, Adv. Chem. Ser. 184 (1980) 253.
[76] S.M. Baxter, W.E. Jones, E. Danielson, L. Worl, G. Strouse, J. Younathan, T.J. Meyer, Coord. Chem. Rev. 111 (1991) 47. (a) J.M. Calvert, R.H. Schmehl, B.P. Sullivan, J.S. Facci, T.J. Meyer, R.W. Murray, Inorg. Chem. 22 (1983) 2151. (b) C.M. Elliot, C.J. Baldy, L. Nuwaysir, C.L. Wilkins, Inorg. Chem. 29 (1990) 389; L. Della Ciana, I. Hamachi, T.J. Meyer, J. Org. Chem. 54 (1989) 1731; W.E. Jones, S.M. Baxter, G.F. Strouse, T.J. Meyer, J. Am. Chem. Soc. 115 (1993) 7363; R.M. Leasure, W. Ou, J.A. Moss, R.W. Linton, T.J. Meyer, Chem. Mater. 8 (1996) 264; R.M. Leasure, T. Kajita, T.J. Meyer, Inorg. Chem. 35 (1996) 5962; L.M. Dupray, T.J. Meyer, Inorg. Chem. 35 (1996) 6299.

[77] P.K. Ghosh, T.G. Spiro, J. Electrochem. Soc. 128 (1981) 1281.
[78] (a) A. Deronzier, M. Essakalli, J. Chem. Soc. Chem. Commun. (1990) 242. (b) S. Cosnier, A. Deronzier, J.C. Moutet, J. Phys. Chem. 89 (1985) 4895. (c) A. Deronzier, J.C. Montet, Acc. Chem. Res. 22 (1989) 249. (d) A.J. Downard, N.A. Surridge, T.J. Meyer, S. Cosnier, A. Deronzier, J.C. Moutet, J. Electroanal. Chem. 246 (1988) 321.
[79] C.E.D. Chidsey, D.N. Loiacono, Langmuir 6 (1990) 682. (b) C.D. Bain, E.B. Troughton, Y.-T. Tao, J. Evall, G.M. Whitesides, J. Am. Chem. Soc. 111 (1989) 321. (c) C.D. Bain, G.M. Whitesides, Science 240 (1988) 62. (d) A. Ullman, J.E. Eilers, N. Tilman, Langmuir 5 (1989) 1147.
[80] S.L. Mecklenberg, D.G. McCafferty, J.R. Schoonover, B.M. Peck, B.W. Erickson, T.J. Meyer, Inorg. Chem. 338 (1994) 2974.
[81] M.A. Fox, F.J. Nobs, T.A. Voynick, J. Am. Chem. Soc. 103 (1980) 4029.
[82] G. Sprintschnik, H.W. Sprintschnik, P.P. Kirsch, D.G. Whitten, J. Am. Chem. Soc. 99 (1977) 4947.
[83] P. Liska, N. Vlachopoulos, M.K. Nazeeruddin, P. Comte, M. Grätzel, J. Am. Chem. Soc. 110 (1988) 3686.
[84] R. Dabestani, A.J. Bard, A. Campion, M.A. Fox, T.E. Mallouk, S.E. Webber, J.M. White, J. Phys. Chem. 92 (1988) 1872.
[85] V. Shklover, Md.K. Nazeeruddin, S.M. Zakeeruddin, et al., Chem. Mater. 9 (1997) 430.
[86] Kalyanasundaram, Md.K. Nazeeruddin, M. Grätzel, G. Viscardi, P. Savarino, E. Barni, Inorg. Chim. Acta 198–200 (1992) 831.
[87] R. Memming, F. Schröppel, U. Bringman, J. Electroanal. Chem. 100 (1979) 307.
[88] R. Argazzi, C.A. Bignozzi, T.A. Heimer, F.N. Castellano, G.J. Meyer, J. Phys. Chem. 33 (1994) 5741.
[89] Strouse, Meyer et al. IC(95) 473
[90] T.A. Heimer, S.T. D'Arcangelis, F. Farzad, J.M. Stipkala, G.J. Meyer, Inorg. Chem. 35 (1996) 5319.
[91] Md.K. Nazeeruddin, P. Pechy, M. Grätzel, J. Chem. Soc. Chem. Commun. (1997) 1705.
[92] Md.K. Nazeeruddin, E. Müller, R. Humphry-Baker, N. Vlachopoulos, M. Grätzel, J. Chem. Soc. Dalton Trans. (1997) 4571.
[93] S.G. Yan, J.T. Hupp, J. Phys. Chem. 100 (1996) 6867.
[94] A. Zaban, S. Ferrere, B.A. Gregg, J. Phys. Chem. 102B (1998) 452.
[95] G.B. Saupe, T.E. Mallouk, W. Kim, R.H. Schmehl, J. Phys. Chem. 101B (1997) 2508.
[96] S. Ruile, O. Kohle, P Pechy, M. Grätzel, Inorg. Chim. Acta 261 (1997) 129.
[97] Hirao (81) 56
[98] Y. Athanassov, F.P. Rotzinger, P. Pechy, M. Grätzel, J. Phys. Chem. 101B (1997) 2558.
[99] P. Pechy, F.P. Rotzinger, Md.K. Nazeeruddin, O. Köhle, S.M. Zakeeruddin, R. Humphry-Baker, M. Grätzel, J. Chem. Soc. Chem. Commun. (1995) 65.
[100] S.M. Zakeeruddin, Md.K. Nazeeruddin, P. Pechy, F.P. Rotzinger, R. Humphry-Baker, K. Kalyanasundaram, M. Grätzel, Inorg. Chem. 36 (1997) 5937.
[101] W.E. Ford, M.A.J. Rodgers, J. Phys. Chem. 98 (1994) 3822.
[102] (a) T.J. Meyer, G.J. Meyer, B.W. Pfennig, et al., Inorg. Chem. 33 (1994) 3952. (b) B.W. Pfennig, P. Chen, T.J. Meyer, Inorg. Chem. 35 (1996) 2898.
[103] F. Campus, Ph.D. Dissertation, Ecole Polytechnique Federale de Lausanne, Switzerland, 1997, no. 1697.
[104] S. Ferrare, A. Zaban, B.A. Gregg, J. Phys. Chem 101B (1997) 4490.
[105] B. Burfeindt, T. Hannappel, W. Storck, F. Willig, J. Phys. Chem. 100 (1996) 16463.
[106] P.V. Kamat, J. Phys. Chem. 84 (1980) 859.
[107] I. Martini, J.H. Hodakand, G. Hartland, J. Phys. Chem. 102B (1998) 607.
[108] (a) J. Moser, S. Punchihewa, P.P. Infelta, M. Grätzel, Langmuir 7 (1991) 3012. (b) S. Yamada, H. Kohrogi, T. Matsuo, Chem. Lett. (1995) 639.
[109] C.J. Barbé, F. Arendse, P. Comte, M. Jirousek, F. Lenzmann, V. Shklover, M. Grätzel, J. Am. Ceram. Soc. 80 (1997) 3157.
[110] R.R. Bacsa, M. Grätzel, J. Am. Ceram. Soc. 79 (1996) 2185.
[111] A. Kay, Ph.D Dissertation, Ecole Polytechnique Federale de Lausanne, Switzerland, 1994, no. 1214.

[112] Q Xu, M.A. Anderson, J. Am. Ceram. Soc. 77 (1977) 1939.
[113] L. Kavan, M. Grätzel, J. Rathousky, A. Zukal, J. Electrochem. Soc. 143 (1996) 394.
[114] L. Kavan, M. Grätzel, S.E. Gilbert, G. Klemenz, H.J. Scheel, J. Am. Chem. Soc. 118 (1996) 6716.
[115] L. Kavan, M. Grätzel, Electrochim. Acta 40 (1995) 643.
[116] L. Kavan, K. Kratochvilova, M. Grätzel, J. Electroanal. Chem. 394 (1995) 93.
[117] L. Kavan, A. Kay, B. O'Regan, M. Grätzel, J. Electroanal. Chem. 346 (1993) 291.
[118] L. Kavan, T. Stoto, M. Grätzel, D. Fitzmaurice, V. Shklover, J. Phys. Chem. 97 (1993) 9493.
[119] A. Fujishima, K. Honda, Nature (London) 238 (1972) 37.
[120] M. Grätzel (Ed.), Energy Resouces Through Photochemistry and Catalysis, Academic Press, New York, 1982.
[121] M. Schiavello (Ed.), Photoelectrochemistry, Photocatalysis and Photoreactors: Fundamentals and Developments, NATO ASI Ser. C 146, Reidel, Dordrecht, 1984.
[122] (a) N. Serpone, E. Pelizetti (Eds.), Photocatalysis: Fundamentals and Applications, Wiley, New York, 1989. (b) E. Pelizetti, N. Serpone, Homogeneous and Heterogeneous Photocatalysis, NATO ASI Ser. C 174, Reidel, Dordrecht, 1986.
[123] G. Calzaferri (Ed.), Proceeeings of 10th International Conference on Photochemical Transformations and Storage of Solar Energy, Elsevier, Amsterdam, 1995 (reprint of Sol. Energy Mater. Sol. Cells, 38 (1995) 1).
[124] E. Pelizetti, M. Schiavello, Photochemical Conversion and Storage of Solar Energy, proceedings of 8th International Conference on Photochemical Conversion and Storage of Solar Energy, Kluwer, Dordrecht, 1991.
[125] J.R. Norris, D. Meisel (Eds.), Photochemical Energy Conversion: Proceedings of 7th International Conference on Photochemical Conversion and Storage of Solar Energy, Elsevier, Amsterdam, 1989.
[126] (a) E. Rabinowitch, J. Chem. Phys. 8 (1849) 551, 560. (b) P.D. Wildes, N.N. Lichtin, J. Am. Chem. Soc. 100 (1978) 6568. (c) W.D.K. Clark, J.A. Eckert, Sol. Energy 17 (1975) 147.
[127] W.J. Albery, P.N. Bartlett, J.P. Davies, A.W. Foulds, A.R. Hillman, F.S. Bachiller, Faraday Discuss. Chem. Soc. 70 (19800 341 and refs. cited therein.
[128] (a) M.I.C. Ferreira, A. Harriman, J. Chem. Soc. Faraday Trans. II 75 (1979) 874. (b) C. Creutz, N. Sutin, Inorg. Chem. 15 (1976) 496. (c) W.J. Albery, A.W. Foulds, J.R. Darwent, J. Photochem. 89 (1982) 376.
[129] For a compilation of several hundred papers dealing with photoelectrochemical processes on semiconductor electrodes see: K. Kalyanasundaram, Sol. Cells 15 (1985) 93.
[130] S. Chandra, Photoelectrochemical Solar Cells, Gordon Breach, New York, 1985.
[131] (a) H.W. Vogel, Ber. Dtschl. Chem. Ges. 6 (1873) 1320. (b) H.W. Vogel, Photogr. News 18 (19873) 585. (c) J. Moser, Monatl. Chem. 8 (1887) 373.
[132] E.K. Putziko, A. Terenin, Zhur. Fiz. Khim. 23 (1949) 676.
[133] (a) H. Gerischer, H. Tributsch, Ber. Bunsenges. Phys. Chem. 72 (1968) 437, 562. (b) H. Gerischer, M.E. Michel-Beyerle, F. Rebentrost, H. Tributsch, Electrochim. Acta 13 (1968) 1509. (c) H. Gerischer, Photochem. Photobiol. 16 (1972) 243. (d) H. Tributsch, Photochem. Phtoobiol. 16 (1972) 261. (e) B. Pettinger, H.R. Schröppel, H. Gerischer, Ber. Bunsenges. Phys. Chem. 77 (1973) 960. (f) M. Spitler, M. Lübke, H. Gerischer, Chem. Phys. Lett. 56 (1977) 577. (g) T. Yamase, H. Gerischer, M. Lübke, B. Pettinger, Ber. Bunsenges. Phys. Chem. 82 (1978) 1041. (h) T. Yamase, H. Gerischer, M. Lübke, B. Pettinger, Ber. Bunsenges. Phys. Chem. 83 (1979) 658.
[134] (a) A. Terenin, I.A. Akimov, J. Phys. Chem. 69 (1965) 730. (b) A. Terenin, I.A. Akimov, J. Phys. Chem. USSR 217 (1961) 307.
[135] (a) R. Memming, H. Tributsch, J. Phys. Chem. 75 (1971) 562. (b) R. Memming, in: E. Kay, P. Bagus (Eds.), Topics in Surface Chemistry, Plenum, New York, 1978, p. 19.
[136] (a) K. Hauffe, J. Range, Z. Naturforsch. 23b (1968) 736. (b) K. Hauffe, H.J. Danzmann, H. Pusch, J. Range, H. Volz, J. Electrochem. Soc. 117 (1970) 995. (c) K. Hauffe, U. Bode, Faraday Discuss. Chem. Soc. 58 (1974) 281. (d) K. Hauffe, Photogr. Sci. Eng. 20 (1976) 124.
[137] (a) F. Willig, H. Gerischer, Top. Curr. Chem. 61 (1976) 31. (b) H. Gerischer, Photochem. Photobiol. 16 (1972) 243. (c) M. Grätzel, K. Kalyanasundaram, in: Photochemistry and Photocatalysis using Inorganic and Organometallic Compounds, Kluwer, Dordrecht, 1993, p. 247. (d) B.A. Parkinson, M. Spitler, Electrochim. Acta 37 (1992) 943.

[138] (a) H. Tsubomura, M. Matsumura, Y. Nomura, T. Amamiya, Nature 261 (1976) 462. (b) M. Matsumura, Y. Nomura, H. Tsubomura, Bull. Chem. Soc. Jpn. 50 (1977) 2533. (c) M. Matsumura, S. Matudaira, H. Tsubomura, M. Takata, H. Yanagida, IEC Prod. Res. Dev. 19 (1980) 415. (d) M. Matsumura, K. Mitsuda, N. Yoshizawa, H. Tsubomura, Bull. Chem. Soc. Jpn. 54 (1981) 692 and refs. cited therein.

[139] (a) A. Fujishima, T. Iwase, T. Watanabe, K. Honda, J. Am. Chem. Soc. 97 (1975) 4134. (b) T. Watanabe, A. Fujishima, K. Honda, Ber. Bunsenges. Phys. Chem. 79 (1975) 1213. (c) T. Iwasaki, T. Sawada, H. Kamada, A. Fujishima, K. Honda, J. Phys. Chem. 83 (1979) 2142. (d) T. Watanabe, M. Nakao, A. Fujishima, K. Honda, Ber. Bunsenges. Phys. Chem. 84 (1980) 74. (e) T. Watanabe, T. Takizawa, K. Honda, Ber. Bunsenges. Phys. Chem. 85 (1981) 430.

[140] (a) M. Spitler, M. Calvin, J. Chem. Phys. 66 (1977) 4294. (b) M. Spitler, M. Calvin, J. Chem. Phys. 67 (1977) 5193. (c) R.W. Berriman, P.B. Gilman, Photogr. Sci. Eng. 17 (1973) 235. (d) T. Tani, S. Kikuchi, Photogr. Sci. Eng. 12 (198) 80.

[141] T.H. James (Ed.), Theory of the Photographic Process, 4th ed., Macmillan, New York, 1977.

[142] J.W. Weigl, Angew. Chem. Int. Ed. Engl. 16 (1977) 374.

[143] R. Steiger, H. Hediger, P. Junod, H. Kuhn, D. Möbius, Photogr. Sci. Eng. 24 (1980) 185.

[144] T. Tani, T. Suzumoto, K. Ohzeki, J. Phys. Chem. 94 (1990) 1298.

[145] (a) F Nüesch, M. Grätzel, Chem. Phys. 193 (1995) 1. (b) F. Nüesch, J.E. Moser, V. Shklover, M. Grätzel, J. Am. Chem. Soc. 118 (1996) 5420.

[146] (a) M.T. Spitler, A. Ehret, R. Kietzmann, F. Willig, J. Phys. Chem. 101 (1997) 2552. Fassler et al. (b) Kavassilis, M.T. Spitler, J. Phys. Chem. 87 (1993) 3166. (c) L.M. Natoli, M.A. Ryan, M.T. Spitler, J. Phys. Chem. 89 (1985) 1448.

[147] (a) R. Gleria, R. Memming, Z. Phys. Chem. (Neue Folge) 98 (1976) 303. (b) M. Gleria, R. Memming, Z. Phys. Chem. (Neue Folge) 101 (1976) 171. (c) R. Memming, F. Schröppel, U. Bringmann, J. Electroanal. Chem. 100 (1979) 307. (d) R. Memming, F. Schröppel, Chem. Phys. Lett. 62 (1979) 207.

[148] W.D.K. Clark, N. Sutin, J. Am. Chem. Soc. 99 (1977) 4676.

[149] A. Hamnett, M.P. Dare-Edwards, R.D. Wright, K.R. Seddon, J.B. Goodenough, J. Phys. Chem. 83 (1979) 3280.

[150] N. Alonso, V.M. Beley, P. Chartier, V. Ern, Reuv. Phys. Appl. 16 (1981) 5.

[151] N. Alonso Vante, V. Ern, P. Chartier, C.O. Dietrich-Buchecker, D.R. McMillin, P.A. Marnot, J-P. Sauvage, Nouv. J. Chim. 7 (1983) 3.

[152] C. Creutz, N. Sutin, Proc. Natl. Acad. Sci. USA 72 (1975) 2858.

[153] R. Memming, F. Schröppel, Chem. Phys Lett. 62 (1979) 207.

[154] (a) A. Mackor, J. Schoonman, Rec. Trav. Chim. 99 (1980) 71. (b) A.H.A. Tinnemans, A. Mackor, Rec. Trav. Pays-Bas 100 (1981) 295.

[155] (a) S. Anderson, E.C. Constable, M.P. Dare-Edwards, J.B. Goodenough, A. Hamnett, K.R. Seddon, R.D. Wright, Nature 280 (1979) 571. (b) J.B. Goodenough, A. Hamnett, M.P. Dare-Edwards, G. Campet, R.D. Wright, Surf. Sci. 101 (1980) 531. (c) M.P. Dare-Edwards, J.B. Goodenough, A. Hamnett, K.R. Seddon, R.D. Wright, Faraday Discuss. Chem. Soc. 70 (1981) 285.

[156] P.K. Ghosh, T.G. Spiro, J. Electrochem. Soc. 128 (1981) 1281. (b) P.K. Ghosh, T.G. Spiro, J. Am. Chem. Soc. 102 (1980) 5543.

[157] H.O. Finklea, H. Abruna, R.W. Murray, Adv. Chem. Ser. 184 (1980) 253.

[158] (a) H. Tributsch, M. Calvin, Photochem. Photobiol. 14 (1971) 95. (b) H. Tributsch, M. Calvin, Photochem. Photobiol. 16 (1972) 261.

[159] (a) T. Miyasaka, K. Honda, Surf. Sci. 101 (1980) 541; T. Miyasaka, K. Honda, in: A.J. Nozik (Ed.), Photoeffects at Semiconductor-Electrolyte Interfaces, ACS Symp. Ser. 146 (1981) 231. (b) P.A. Breddels, G. Blasse, Chem. Phys. Lett. 79 (1981) 209. (c) K. Takahashi, S. Nakatani, T. Yamaguchi, T. Komura, S. Ito, K. Murata, Sol. Energy Mater. Sol. Cells 45 (1997) 127.

[160] (a) C.D. Jaeger, F-R. Fan, A.J. Bard, J. Am. Chem. Soc. 101 (1980) 2592. (b) A. Giraudeau, F-R. Fan, A.J. Bard, J. Am. Chem. Soc. 102 (1980) 5137. (c) H. Yanagi, S.Y. Chan, P.A. Lee, K.W. Nebesny, N.R. Armstrong, A. Fujishima, J. Phys. Chem. 100 (1996) 5447. (d) J. Hodak, C. Quinteros, M.I. Litter, E.S. Roman, J. Chem. Soc. Faraday Trans. 92 (1996) 5081.

[161] J. DeSilvestro, M. Grätzel, L. Kavan, J. Moser, J. Augustynski, J. Am. Chem. Soc. 107 (1985) 2988.
[162] P. Liska, N. Vlachopoulos, M.K. Nazeeruddin, P. Comte, M. Grätzel, J. Am. Chem. Soc. 110 (1988) 3686.
[163] N. Vlachopoulos, P. Liska, J. Augustynski, M. Grätzel, J. Am. Chem. Soc. 110 (1988) 1216.
[164] M.K. Nazeeruddin, P. Liska, J. Moser, N. Vlachopoulos, M. Grätzel, Helv. Chim. Acta 73 (1990) 1788.
[165] B. O'Regan, M. Grätzel, Nature (London) 335 (1991) 737.
[166] M.K. Nazeeruddin, A. Kay, I. Rodicio, et al., J. Am. Chem. Soc. 115 (1993) 6382.
[167] K. Kalyanasundaram, Md.K. Nazeeruddin, M. Grätzel, G. Viscardi, P. Savarino, E. Barni, Inorg. Chim. Acta 198–200 (1992) 831.
[168] K. Matsui, Md.K. Nazeeruddin, R. Humphry-Baker, M. Grätzel, K. Kalyanasundaram, J. Phys. Chem. 96 (1992) 10590.
[169] P. Pechy, F.P. Rotzinger, Md.K. Nazeeruddin, O. Köhle, S.M. Zakeeruddin, R. Humphry-Baker, M. Grätzel, J. Chem. Soc. Chem. Commun. (1995) 65.
[170] O. Kohle, S. Ruile, M. Grätzel, Inorg. Chem. 35 (1996) 4779.
[171] Md.K. Nazeeruddin, E. Müller, R. Humphry-Baker, N. Vlachopoulos, M. Grätzel, J. Chem. Soc. Dalton Trans. (1997) 4571.
[172] S. Ruile, O. Kohle, P Pechy, M. Grätzel, Inorg. Chim. Acta 261 (1997) 129.
[173] S.M. Zakeeruddin, Md.K. Nazeeruddin, P. Pechy, F.P. Rotzinger, R. Humphry-Baker, K. Kalyanasundaram, M. Grätzel, Inorg. Chem. 36 (1997) 5937.
[174] V. Shklover, Md.K. Nazeeruddin, S.M. Zakeeruddin, et al., Chem. Mater. 9 (1997) 430.
[175] Md.K. Nazeeruddin, P. Pechy, M. Grätzel, J. Chem. Soc. Chem. Commun. (1997) 1705.
[176] R. Amadelli, R. Argazzi, C.A. Bignozzi, F. Scandola, J. Am. Chem. Soc. 112 (1990) 7099.
[177] T.A. Heimer, C.A. Bignozzi, G.J. Meyer, J. Phys. Chem. 97 (1993) 11987.
[178] R. Argazzi, C.A. Bignozzi, T.A. Heimer, F.N. Castellano, G.J. Meyer, Inorg. Chem. 33 (1994) 5741.
[179] C.A Bignozzi, R. Argazzi, J.R. Schoonover, G.J. Meyer, F. Scandola, Sol. Energy Mater. Sol. Cells 38 (1995) 187.
[180] (a) T.A. Heimer, S.T. D'Arcangelis, F. Farzad, J.M. Stipkala, G.J. Meyer, Inorg. Chem. 35 (1996) 5319. (b) T.A. Heimer, G.J. Meyer, J. Lumin. 70 (1996) 468.
[181] R. Argazzi, C.A. Bignozzi, T.A. Heimer, G.J. Meyer, Inorg. Chem. 36 (1997) 2.
[182] K. Murakoshi, G. Kano, Y. Wada, S. Yanagida, H. Miyazaki, M. Matsumoto, S. Murasawa, J. Electroanal. Chem. 396 (1995) 27.
[183] A. Hagfeldt, S. Lindquist, M. Grätzel, Sol. Energy Mater. Sol. Cells 32 (1993) 245.
[184] A. Hagfeldt, B. Didriksson, T. Palmquist, H. Lindström, S. Sodergren, H. Rensmo, S-E. Lindquist, Sol. Energy Mater. Sol. Cells 31 (1994) 481.
[185] R. Knödler, J. Sopka, F. Harbach, H.W. Grünling, Sol. Energy Mater. Sol. Cells 30 (1993) 277.
[186] G. Smestad, C.A. Bignozzi, R. Argazzi, Sol. Energy Mater. Sol. Cells 32 (1994) 259.
[187] R. Grünwald, H. Tributsch, J. Phys. Chem. 101B (1997) 2564.
[188] O. Köhle, M. Grätzel, A.F. Meyer, T.B. Meyer, Adv. Mater. 9 (1997) 904.
[189] G. Redmond, D. Fitzmaurice, M. Grätzel, Chem. Mater. 6 (1994) 686.
[190] I. Bedja, P.V. Kamat, X. Hua, A.G. Lappin, S. Hotchandani, Langmuir 13 (1997) 2398.
[191] H. Rensmo, K. Keis, H. Lindström, et al., J. Phys. Chem. 101B (1997) 2598.
[192] I. Bedja, S. Hotchandani, P.V. Kamat, J. Phys. Chem. 98 (1994) 4133.
[193] I. Bedja, S. Hotchandani, R. Carpentier, R.W. Fessenden, P.V. Kamat, J. Appl. Phys. 75 (1994) 5444.
[194] D. Liu, G. Hug, P.V. Kamat, J. Phys. Chem. 99 (1995) 16768.
[195] D. Liu, P.V. Kamat, J. Electrochem. Soc. 142 (1995) 835.
[196] C. Nasr, D. Liu, S. Hotchandani, P.V. Kamat, J. Phys. Chem. 100 (1996) 11054.
[197] P.V. Kamat, I. Bedja, S. Hotchandani, L.K. Patterson, J. Phys. Chem. 100 (1996) 4900.
[198] K. Schwarzburg, F. Willig, J. Phys. Chem. 101B (1997) 2451.
[199] B.I. Lemon, J.T. Hupp, J. Phys. Chem. 101 (1996) 14578.
[200] L.A. Lyon, J.T. Hupp, J. Phys. Chem. 99 (1995) 15718.

[201] (a) A. Solbrand, H. Lindström, H. Rensmo, A. Hagfeldt, S.-E. Lindquist, S. Södergren, J. Phys. Chem. 101B (1997) 2514. (b) H. Rensmo, H. Lindström, S. Södergren, A.K. Willstedt, A. Solbrand, A. Hagfeldt, S.-E. Lindquist, J. Electrochem. Soc. 143 (1996) 3173.
[202] (a) S. Södergren, H. Siegbahn, H. Rensmo, H. Lindström, A. Hagfeldt, S.-E. Lindquist, J. Phys. Chem. 101B (1997) 3087. (b) D.W. Bahnemann, M. Hilgendorff, R. Memming, J. Phys. Chem. 101B (1997) 4265.
[203] J.Z. Zhang, Acc. Chem. Res. 30 (1997) 423.
[204] (a) P.E. Dejongh, D. Vanmaekelbergh, Phys. Rev. Lett. 77 (1996) 3427. (b) P.E. Dejongh, D. Vanmaekelbergh, J. Phys. Chem. 101 (1997) 2716.
[205] (a) B. O'Regan, M. Grätzel, D. Fitzmaurice, Chem. Phys. Lett. 183 (1991) 89. (b) B. O'Regan, M. Grätzel, D. Fitzmaurice, J. Phys. Chem. 95 (1991) 10526.
[206] (a) B. Enright, D. Fitzmaurice, J. Phys. Chem. 100 (1996) 1027. (b) R. Flood, B. Enright, M. Allen, S. Barry, A. Dalton, H. Tynan, D. Fitzmaurice, Sol. Energy Mater. Sol. Cells 39 (1995) 83.
[207] N.S. Foster, C.A. Koval, J.G. Sczechowski, R.D. Noble, J. Electroanal. Chem. 406 (1996) 213.
[208] R.U. Flood, D.J. Fitzmaurice, J. Phys. Chem. 99 (1995) 8954.
[209] G.K. Boschloo, A. Goosens, J. Schoonman, J. Electroanal. Chem. 428 (1997) 25.
[210] K. Kalyanasundaram, Md.K. Nazeeruddin, Chem. Phys. Lett. 193 (1992) 292.
[211] K. Matsui, Md.K. Nazeeruddin, R. Humphry-Baker, R.E. Hester, M. Grätzel, K. Kalyanasundaram, submitted for publication.
[212] R. Argazzi, C.A. Bignozzi, T.A. Heimer, G.J. Meyer, Inorg. Chem. 36 (1997) 2.
[213] D.N. Furlong, D. Wells, W.H.F. Sasse, J. Phys. Chem. 90 (1986) 1107.
[214] R. Brändli, P. Rys, H. Zollinger, H.R. Oswald, F. Schweitzer, Helv. Chim. Acta 53 (1970) 1133.
[215] V.H. Houlding, M. Grätzel, J. Am. Chem. Soc. 105 (1983) 5695.
[216] H. Frei, D.J. Fitzmaurice, M. Grätzel, Langmuir 6 (1990) 198.
[217] P.A. Connor, K.D. Dobson, A.J. McQuillan, Langmuir 11 (1995) 4193.
[218] N.W. Duffy, K.D. Dobson, K.C. Gordon, B.H. Robinson, A.J. McQuillan, Chem. Phys. Lett. 266 (1997) 451.
[219] T.J. Meyer, G.J. Meyer, B.W. Pfenning, et al., Inorg. Chem 33 (1994) 3952.
[220] W. Shi, S. Wolfgang, T.C. Strekas, H.D. Gafney, J. Phys. Chem. 89 (1985) 974.
[221] (a) S. Umapathy, A.M. Carter, A.W. Parker, R.E. Hester, J. Phys. Chem. 94 (1990) 8880. (b) S. Umapathy, G. Lee-Soon, R.E. Hester, J. Chem. Soc. Chem. Commun. (1987) 1841.
[222] G.B. Deacon, R.J. Phillips, Coord. Chem. Rev. 33 (1980) 227.
[223] (a) K. Kalyanasundaram, N. Vlachopoulos, V. Krishnan, A. Monnier, M. Grätzel, J. Phys. Chem. 91 (1987) 2342. (b) M. Fujihira, T. Kubota, T. Osa, J. Electroanal. Chem. 81 (1981) 379.
[224] K. Kalyanasundaram, J.A. Shelnutt, M. Grätzel, Inorg. Chem. 27 (1988) 2820.
[225] (a) P.V. Kamat, J.-P. Chauvet, R.W. Fessenden, J. Phys. Chem. 90 (1986) 1389. (b) P.V. Kamat, J.-P. Chauvet, Radiat. Phys. Chem. 37 (1991) 705. (c) I. Bedja, S. Hotchandani, R. Carpentier, R.W. Fessenden, P.V. Kamat, J. Appl. Phys. 75 (1994) 5444.
[226] (a) A. Kay, Ph.D. Dissertation, Ecole Polytechnique Federale de Lausanne, Switzerland, 1994. (b) A. Kay, M. Grätzel, J. Phys. Chem. 97 (1993) 6272. (c) A. Kay, R. Humphry-Baker, M. Grätzel, J. Phys. Chem. 98 (1994) 952.
[227] G.K. Boschloo, A. Goosens, J. Phys. Chem. 100 (1996) 19489.
[228] (a) Ana Wiederkehr, Ph.D Dissertation, Ecole Polytechnique Federale de Lausanne, Switzerland, 1990, no. 872, Ch. 5. (b) Md.K. Nazeeruddin, R. Humphry-Baker, M. Grätzel, B.A. Murrer, J. Chem. Soc. Chem. Commun. (1998) 719.
[229] (a) P.V. Kamat, Progr. React. Kinet. 19 (1994) 277. (b) P.V. Kamat, in: K. Kalyanasundaram, M. Grätzel (Eds.), Kinetics and Catalysis in Microheterogeneous Systems, Surfactant Science Ser. vol. 38, Marcel Dekker, New York, 1991.
[230] N.H. Damrauer, G. Cerullo, A. Yeh, T.R. Boussie, C.V. Shank, J.K. McCusker, Science 275 (1997) 54.
[231] A.A. Muenter, J. Phys. Chem. 80 (1976) 2178.
[232] D. Oelkrug, in: O.S. Wolfbeis (Ed.), Fluorescence Spectroscopy: New Methods and Applications, Springer-Verlag, Heidelberg, 1993, pp. 65–78.

[233] (a) D. Oelkrug, W. Honnen, F. Wilkinson, C.J. Willsher, J. Chem. Soc. Faraday Trans. I 83 (1987) 2081. (b) F. Wilkinson, C.J. Willsher, J. Chem. Soc. Faraday Trans. I 777 (1981) 309.
[234] (a) Y.S. Liu, W.R. Ware, J. Phys. Chem. 97 (1993) 5980. (b) Y.S. Liu, P. de Mayo, W.R. Ware, J. Phys. Chem. 97 (1993) 5987. (c) Y.S. Liu, P. de Mayo, W.R. Ware, J. Phys. Chem. 97 (1993) 5995.
[235] (a) S.A. Ruetten, J.K. Thomas, J. Phys. Chem. 102B (1998) 598. (b) Z. Liu, Y. Mao, S.A. Ruetten, J.K. Thomas, Sol. Energy Mater. Sol. Cells 38 (1995) 199. (c) M.A.T. Marro, J.K. Thomas, J. Photochem. Photobiol. 72 (1993) 251. (d) S. Pankasem, J.K. Thomas, J. Phys. Chem. 95 (1991) 6990. (e) R. Krasnansky, R. Koike, J.K. Thomas, J. Phys. Chem. 94 (1990) 4521.
[236] (a) M. Spitler, B.A. Parkinson, Langmuir 2 (1986) 549. (b) B.A. Parkinson, Langmuir 4 (1988) 967.
[237] R.W. Fessenden, P.V. Kamat, J. Phys. Chem. 99 (1995) 12902.
[238] (a) K. Itoh, Y. Chiyokawa, M. Nakao, K. Honda, J. Am. Chem. Soc. 106 (1984) 1620. (b) T. Watanabe, K. Machida, H. Suzuki, M. Kobayashi, K. Honda, Coord. Chem. Rev. 64 (1985) 207.
[239] N. Nakashima, K. Yoshihara, F. Willig, J. Chem. Phys. 73 (1980) 3553.
[240] P.A. Anfinrud, T.P. Causgrove, W.S. Struve, J. Phys. Chem. 90 (1986) 5887.
[241] (a) Y. Liang, A.M. Ponte Goncalves, D.K. Negus, J. Phys. Chem. 87 (1983) 1. (b) Y. Liang, A.M. Ponte Goncalves, J. Phys. Chem. 89 (1985) 3290.
[242] R.L. Crackel, W.S. Struve, Chem. Phys. Lett. 120 (1985) 473.
[243] (a) J.M. Lanzafame, R.J.D. Miller, A.A. Muenter, B.A. Parkinson, J. Phys. Chem. 96 (1992) 2820. (b) J.M. Lanzafame, L. Min, R.J.D. Miller, A.A. Muenter, B.A. Parkinson, Mol. Cryst. Liq. Cryst. 194 (1991) 287. (c) J. Lanzafame, S. Palese, D. Wang, R.J.D. Miller, A.A. Muenter, J. Phys. Chem. 98 (1994) 11020. (d) B. Trösken, F. Willig, K. Schwarzburg, A. Ehret, M. Spitler, J. Phys. Chem. 99 (1995) 5152.
[244] (a) K. Hashimoto, T. Hiramoto, T. Sakata, J. Phys. Chem. 92 (1988) 4272. (b) K. Kemnitz, N. Nakashima, K. Yoshihara, H. Matsunami, J. Phys. Chem. 93 (1989) 6704.
[245] (a) K. Hashimoto, M. Hiramoto, A.B.P. Lever, T. Sakata, J. Phys. Chem. 92 (1988) 1016. (b) K. Hashimoto, T. Hiramoto, T. Kajiwara, T. Sakata, J. Phys. Chem. 92 (1988) 4636. (c) K. Hashimoto, T. Hiramoto, T. Kajiwara, T. Sakata, Chem. Phys. Lett. 148 (1988) 215.
[246] (a) R. Eichberger, F. Willig, Chem. Phys. 141 (1990) 159. (b) F. Willig, R. Eichberger, N.S. Sundaresan, B.A. Parkinson, J. Am. Chem. Soc. 112 (1990) 2702. (c) R. Kietzmann, R. Ehret, M. Spitler, F. Willig. J. Am. Chem. Soc. 115 (1993) 1930. (d) R. Kietzmann, F. Willig, H. Weller, et al., Mol. Cryst. Liq. Cryst. 194 (1991) 169.
[247] (a) J-E. Moser, M. Grätzel, J.M. Durrant, D.R. Klug, in: (M. Chergui (Ed.), Femtochemistry: Ultrafast Chemical and Physical Processes in Molecular Systems, World Scientific, Singapore, 1996, p. 495. (b) J.-E. Moser, Sol. Energy Mater. Sol. Cells 38 (1995) 343. (c) J.E. Moser, M. Grätzel, Chem. Phys. 176 (1993) 493. (d) J.-E. Moser, M. Grätzel, Chimia 52 (1998) 160.
[248] J.M. Rehm, G.L. McLendon, Y. Nagasawa, K. Yoshihara, J. Moser, M. Grätzel, J. Phys. Chem. 100 (1996) 9577.
[249] Y. Tachibana, J-E. Moser, M. Grätzel, D.R. Klug, J.R. Durrant, J. Phys. Chem. 100 (1996) 20056.
[250] T. Hannappel, B. Burfeindt, W. Storck, F. Willig, J. Phys. Chem 101B (1997) 6799.
[251] B. Burfeindt, T. Hannappel, W. Storck, F. Willig, J. Phys. Chem. 100 (1996) 16463.
[252] K. Schwarzburg, F. Willig, J. Phys. Chem. 101B (1997) 2451.
[253] J. Rabani, K. Ushida, K. Yamashita, J. Stark, S. Gershuni, A. Kira, J. Phys. Chem. 101B (1997) 3136.
[254] N.J. Cherapy, G.P. Smestad, M. Grätzel, J.Z. Zhang, J. Phys. Chem. 101B (1997) 9342.
[255] I. Martini, J.H. Hodak, G.V. Hartland, J. Phys. Chem. 102B (1998) 607.
[256] J.S. Salassky, W.H. Lubberhuizen, E. van Faassen, R.E.I. Schropp, J. Phys. Chem. 101B (1997) 766.
[257] H. Lu, J.N. Prieskorn, J. Hupp, J. Am. Chem. Soc. 115 (1993) 4927.
[258] S.G. Yan, J.T. Hupp, J. Phys. Chem. 100 (1996) 6868.
[259] (a) I. Martini, G.V. Hartland, P.V. Kamat, J. Phy. Chem. 101B (1997) 4826. (b) I. Martini, J.H. Hodak, G.V. Hartland, P.V. Kamat, J. Chem. Phys. 107 (1997) 8064.

[260] (a) P. Bonhôte, A.P. Dias, N. Papageorgiou, K. Kalyanasundaram, M. Grätzel, Inorg. Chem. 35 (1996) 1168. (b) N. Papageorgiou, Y. Athanassov, M. Armand, P. Bonhôte, H. Pettersson, A. Azam, M. Grätzel, J. Electrochem. Soc. 143 (1997) 3099. (c) N. Papageorgiou, W.F. Maier, M. Grätzel, J. Electrochem. Soc. 144 (1997) 876. (d) N. Papageorgiou, M. Grätzel, P.P. Infelta, Sol. Energy Mater. Sol. Cells 44 (1996) 405.
[261] A. Zaban, S. Ferrere, J. Sprague, B.A. Gregg, J. Phys. Chem. 101B (1997) 55.
[262] S. Ferrere, A. Zaban, B.A. Gregg, J. Phys. Chem. 101B (1997) 4490.
[263] (a) B. O'Regan, J. Moser, M.A. Anderson, M. Grätzel, J. Phys. Chem. 94 (1990) 8720. (b) G. Redmond, D. Fitzmaurice, J. Phys. Chem. 97 (1993) 11081.
[264] A. Zaban, S. Ferrere, S. Sprague, B.A. Gregg, J. Phys. Chem. 101 (1997) 55.
[265] A. Zaban, S. Ferrere, B.A. Gregg, J. Phys. Chem. 102B (1998) 452.
[266] B. O'Regan, D.T. Schwartz, Chem. Mater. 7 (1996) 1349.
[267] K. Tennakone, A.R. Kumarasinghe, P.M. Sirimanne, G.R.R. Kumara, Thin Solid Films 261 (1995) 307.
[268] K. Murakoshi, R. Kogure, Y. Wada, S. Yanagida, Chem. Lett. (1997) 471.
[269] H. Tributsch, F. Willig, Sol. Energy Mater. Sol. Cells 38 (1995) 355.
[270] P.M.S. Monk, R.J. Mortimer, D.R. Rosseinsky, Electrochromism: Fundamentals and Applications, VCH, Weinheim, 1995.
[271] C.G. Granvist, Handbook of Inorganic Electrochromic Materials, Elsevier, Amsterdam, 1995.
[272] B. O'Regan, M. Grätzel, D. Fitzmaurice, Chem. Phys. Lett. 183 (1991) 89.
[273] B. O'Regan, M. Grätzel, D. Fitzmaurice, J. Phys. Chem. 95 (1991) 10526.
[274] X. Marguerettaz, R. O'Neill, D. Fitzmaurice, J. Am. Chem. Soc. 116 (1994) 2629.
[275] G.H. Schoenmakers, R. Waagener, J.J. Kelly, Ber. Bunsenges. Phys. Chem. 100 (1996) 1169.
[276] Y. Athanassov, F.P. Rotzinger, M. Grätzel, J. Phys. Chem. 101B (1997).
[277] M. Gleria, R. Memming, Z. Phys. Chem (Neue Folge) 101 (1976) 171.
[278] L.S.R. Yeh, A.J. Bard, Chem. Phys. Lett. 44 (1976) 339.
[279] H. Yoneyama, T. Torimoto, Adv. Mater. 7 (1995) 492.
[280] DeBerry and Viehbeck.
[281] (a) P. Bonhôte, J.E. Moser, N. Vlachopoulos, et al., J. Chem. Soc. Chem. Commun. (1996) 1163. (b) J.E. Moser, P. Bonhôte, L. Walder, M. Grätzel, Chimia 51 (1997) 28.
[282] A Hagfeldt, N Vlachopoulos, M. Grätzel, J. Electrochem. Soc. 141 (1994) 82.
[283] S-Y. Huang, L. Kavan, I. Exnar, M. Grätzel, J. Electrochem. Soc. 142 (1995) L142.
[284] S.-Y. Huang, L. Kavan, A. Kay, M. Grätzel, I. Exnar, Act. Passiv. Electr. Comp. 19 (1995) 23.